ACKNOWLEDGEMENTS

The author wishes to express his gratitude to Dr. M.S. Troitsky, Professor and Chairman of the Civil Engineering Department, for suggesting the topic and for his valuable advice, interest, suggestions and guidance in the course of this investigation.

The assistance provided by Dr. M.M. Douglass and Dr. Z.A. Zielinski in reviewing this paper as well as all the cooperation offered during the author's studies is highly appreciated.

The financial support provided by the National Research Council is gratefully acknowledged.

The writer also wishes to extend his gratitude to Messrs. Edward Heasman and Ernst Haefeli from the machine shop for their suggestions and assistance in the fabrication of the experimental set-up.

Grateful acknowledgement is made to Mr. Louis Stankevicius, Structural Laboratory Technician, for his help during the experimental part of this investigation.

Thanks are also due to Mrs. Julie Strick for the typing of the manuscript.

Oscar M. Valencia

Concordia University
Montreal, Quebec
March 1978

TABLE OF CONTENTS

LIST OF FIGURES

LIST OF TABLES

NOTATION

A	-	Cross-sectional area.
$\bar{A}$	-	Homologous calculated cross-sectional area in model.
$\bar{A}_a$	-	Actual cross-sectional area in model.
c	-	Distance from the neutral axis to any fiber in a cross-section.
$\bar{c}_b$	-	Distance from the neutral axis to the extreme bottom fiber in the model.
$\bar{c}_t$	-	Distance from the neutral axis to the extreme top fiber in the model.
C.E.	-	Coefficient of efficiency equal to the ratio of prestressing moment over length of prestressing cable.
D_{ij}	-	Distribution factor in moment distribution method.
$\bar{d}$	-	Homologous calculated height in cross-section in model.
$\bar{d}_a$	-	Actual height in cross-section in model.
E	-	Modulus of elasticity.
$\bar{E}$	-	Modulus of elasticity in model.
e, e_1, e_2, e_3	-	Eccentricity of the prestressing cable or wire about the neutral axis.
f	-	Stress in a structural element.
$\bar{f}_r$	-	Rupture flexural strength of plexiglass.
I	-	Moment of inertia.

$\bar{I}$	-	Homologous calculated moment of inertia in model.
I_a	-	Actual moment of inertia in model.
k	-	Scale reduction factor for length.
L	-	Length of a span.
M	-	Bending moment due to external loads.
$\bar{M}$	-	Homologous calculated bending moment in model.
m	-	Bending moment produced by a unit force in a structural element.
M_b	-	Basic moment; moment existing in a statically determinate structure that is obtained after removal of necessary supports. The moment is originated by prestressing forces.
M_s	-	Secondary moment, moment introduced by the prestressing in a statically indeterminate structure.
M_p	-	Prestressing moment.
P	-	Prestressing force.
$\bar{P}$	-	Prestressing force in model.
Q	-	A concentrated force.
$\bar{Q}$	-	Homologous calculated concentrated force in model.
R_b	-	Reaction at support b or at central support of a two span girder study in this paper.
S	-	Section modulus.
$\bar{S}$	-	Section modulus in model.
S_b	-	Basic shear; a shear existing in a statically determinate structure that is obtained after removal of necessary supports. The shear is originated by prestressing forces.
w	-	Uniformly distributed load.

$\bar{w}$	-	Uniformly distributed load in model.
Y	-	Slicing factor (explained in Section 3.2.4).
z	-	Prediction factor (explained in Section 3.2.1).
Δ	-	Deflection.
$\bar{\Delta}$	-	Deflection in model.
Δ_{b1}	-	Displacement at b' due to external loads.
δ_{bb}	-	Displacement at b due to a unit force applied at b.
ε	-	Strain.
ε_p	-	Strain in prototype
$\bar{\varepsilon}_1$	-	Reading of strain in model at the extreme top fiber in cross-section.
$\bar{\varepsilon}_2$	-	Reading of strain in model at the extreme bottom fiber in cross-section.
$\bar{\varepsilon}_a$	-	Axial strain in model.
$\bar{\varepsilon}_b$	-	Homologous ideal strain in model at the bottom fiber of cross-section.
$\bar{\varepsilon}_{ba}$	-	Actual strain in model at the bottom fiber of cross-section.
$\bar{\varepsilon}_{be}$	-	Total bending strain in model.
$\bar{\varepsilon}_t$	-	Homologous ideal strain in model at the top fiber of cross section.
$\bar{\varepsilon}_{ta}$	-	Actual strain in model at the top fiber in cross-section.
τ	-	Rotation.
τ_{b1}	-	Relative rotation at b due to external loads.

CHAPTER 1

INTRODUCTION

1.1 HISTORICAL REVIEW

Prestressing of steel structuers is a design concept that has been used mainly as a remedial solution in old structures. The concept has been utilized relatively infrequently in new designs, even though research has been done in the field and some economical and structural advantages have been achieved in those projects carried out until now.

A number of examples of the utilization of this technique are found in Europe, South Africa, and North America, showing the feasibility of this concept.

In Germany[1] a three span continuous girder bridge was built in Montabaur. The girders are prestressed by means of high-strength cables located in the inner face of the girders and having parabolic shape. The girders work in composite action with the post-tensioned precast concrete deck.

In Belgium[2] a prestressed simple-span box type composite steel bridge girder has been patented with the name of Willstres System. The girder is post-tensioned by high-strength tendons and the composite action between the precast deck and the girder is achieved by prestressing cables and high-strength bolts.

In Poland[20] post-tensioning was used in the design of combined steel cable-stayed and concrete deck bridge across Vistula River. Post-tensioning was also used for increasing the capacity of roof girders of industrial buildings, and for the construction of long span steel girders on "Supersam" shopping center[21,22].

In England[3] tests were conducted in two simple-span prestressed steel trusses in order to obtain a design criterion for the construction of an overpass in London.

In South Africa[4] a highway bridge was built near Brits, which employed the Freyssinet system to prestress steel box girders working compositely with a cast-in-place slab.

In the United States[5] a highway bridge was erected near Des Moines, Iowa, using hybrid steel beams pre-tensioned by welding high-strength cover-plates onto a beam deflected under concentrated loading. This loading is not released until completion of welding.

In the United States[6] again, a single span highway bridge was constructed near Bellingham, Washington. The bridge consisted of two delta girders, prestressed by strands embedded in concrete in a box which lies along their tension flanges. A precast concrete deck was used but it does not work in composite action with the girders.

In Mexico[7], on the Chihuahua-Pacifico railroad, five bridges were constructed using prestressed steel girders working compositely with the concrete deck.

1.2 Types of Prestressed Steel Girders

Prestressed steel is a construction technique in which a steel member is subjected to a predetermined concentric or eccentric force, so that stresses opposite to those produced by the external loads are intro-

duced in the member in order to counteract the external loading. As it is seen, the concept of prestressing steel elements differ from prestressed concrete in the point that in prestressed concrete the prestressing force is mainly used to overcome the lack of tensile strength in the concrete, whereas in steel, the prestressing is used to increase the bearing capacity of the member or to achieve a smaller member size and thereby a reduction in weight.

Basically, there are three general ways of prestressing steel girders. One method is to use end-anchored high-strength wires or rods. Another, called Hybrid, consists in stressing components of the girder in order to introduce stresses in the unstressed components. The third method consists in casting concrete elements into the flanges of a deflected steel girder.

In the method of prestressing by using high-strength cables or rods some variations exist. They are illustrated in Fig. 1, 2 and 3.

The system shown in Fig. 1 has been used to reinforce old bridges. It consists of a trussed beam with a steel or wrought iron rod and turnbuckle. The rod is fastened to each end of the beam, and exerts a negative moment by means of the inclined struts located near the third points.

Fig. 2 is a variation of the previous example, but is not as efficient as that in which the cables are located outside the beam.

Fig. 3 shows sectional and elevation views of a wide-flange beam which has been prestressed by two straight high-strength rods acting against the end bearing block. For simple span beams, straight cables are more advantageous than draped cables.

Stressing components of Hybrid beams is a second method of prestressing steel members. One version of this second method is similar to the principle used in pre-tensioning concrete members (Fig. 4).

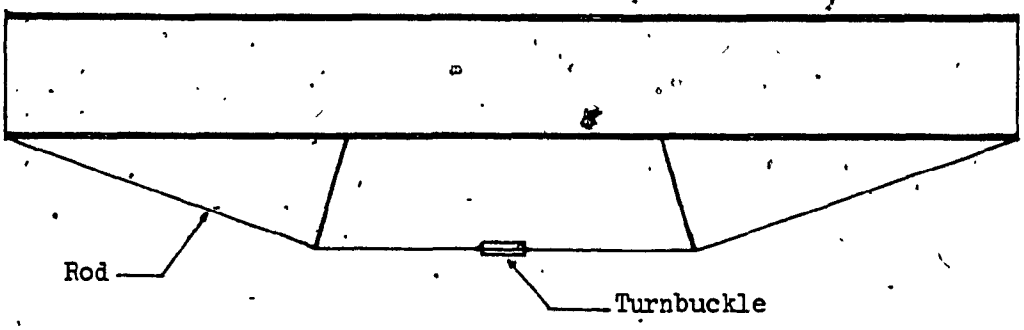

Fig. 1 — Girder with Tensioned Rod.

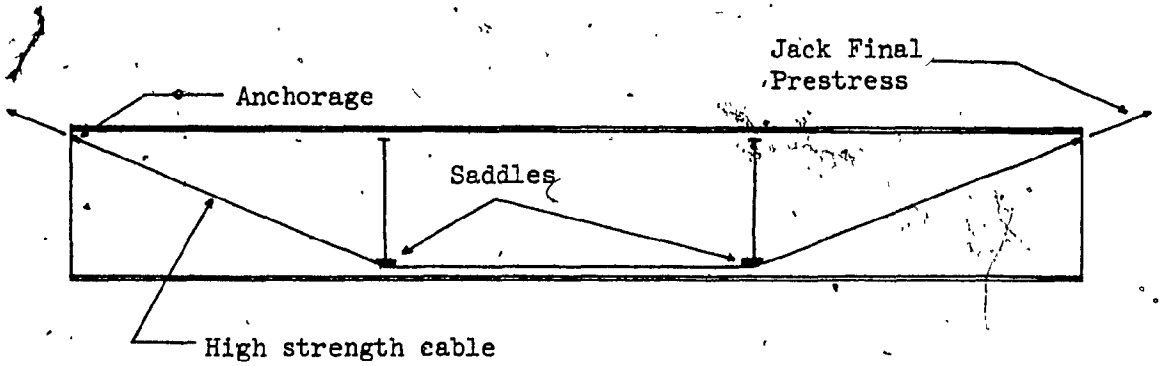

Fig. 2 — Prestressed Girder with Draped Cable.

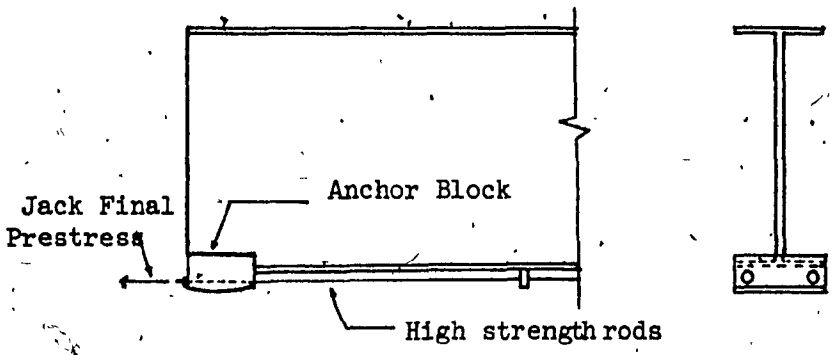

Fig. 3 — Elevation and Sectional Views of Prestressed Girder with Straight Rods.

In this method, a direct tensile force is applied to a high strength plate, and while tension is maintained, the plate is welded to an unstressed "T" or "I" section of structural steel. When welding is completed, the force in the plate is released, thereby achieving the prestressing.

Fig. 5 shows another alternative solution for Hybrid beams, in which a steel I-beam is deflected in loose contact with one or more high-strength cover-plates. While the system is maintained in a deflected position, the cover plates are welded to the flanges of the girder. Subsequent release of the jack load yields the desired prestress.

Fig. 6 illustrates a method of prestressing, where a steel beam is first deflected, then a concrete element is cast into the flange of the girder.

This method is called the "Preflex Technique".[19] In the top view, the jacking forces are applied in a downward direction to a steel beam which has been cambered upward. In the bottom view, a concrete element is cast in a composite manner with the lower portion of the beam, and following the strengthening of the concrete, jacking forces are removed, thereby inducing compressive forces in the concrete.

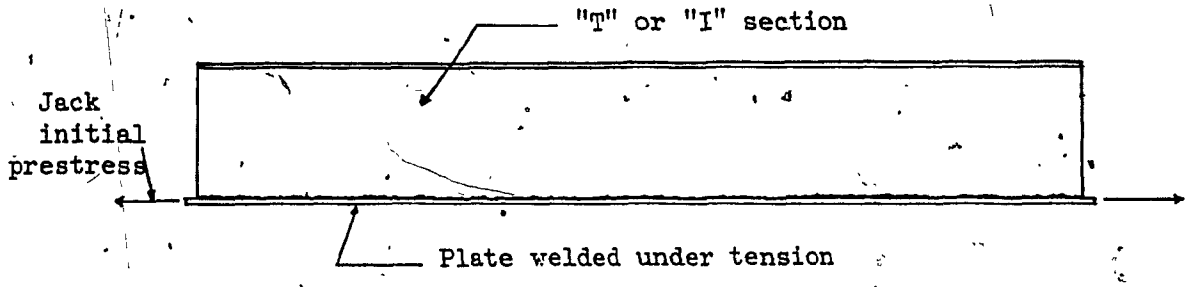

Fig. 4 — Prestressing by Applying Direct Tension to a High Strength Plate.

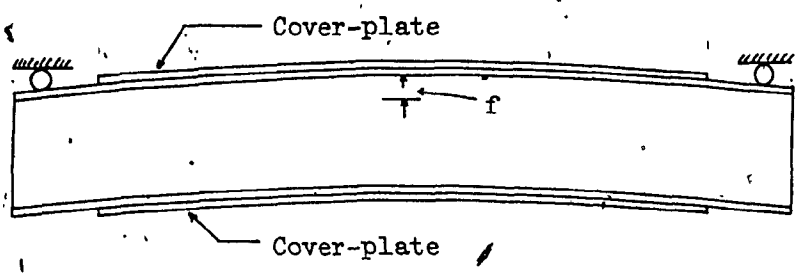

Fig. 5 — Prestressing by Deflecting a Beam and Attaching Cover-Plates.

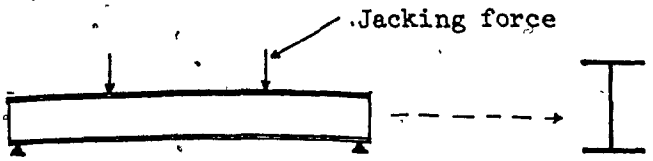

Step 1 — Jack forces are applied to girder furnished by mill with predetermined camber.

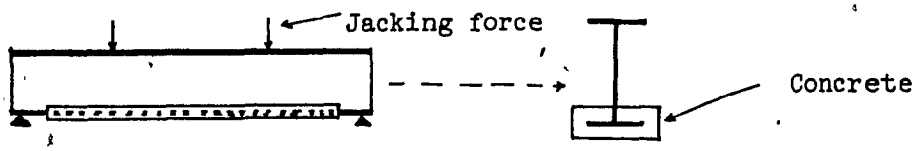

Step 2 — Concrete is cast while jacking forces are maintained.

Fig. 6 — Diagrams Showing "Preflex Technique".

CHAPTER 2

THEORETICAL APPROACH

2.1 INTRODUCTION

By prestressing structural elements stresses opposite to those due to external loading are introduced in the element, so that stresses in the element will be reduced by the addition of the prestressing force.

In the case of trusses, where there is only axial stresses, compressive forces are applied to the members in tension by means of high strength cables, thereby increasing the capacity of such members to carry greater tensile forces. In beams, where bending stresses are of prime importance, the introduction of eccentric prestressing forces originates stresses of opposite sign to those stresses produced by externally applied loads. In this manner the capacity of the beam is increased considerably. It can be said that the greater the eccentricity with respect to the centroid of the section, the greater the capacity of the beam to carry loads in bending.

Stresses in a prestressed beam may be compared with those in a beam-column with eccentric load, where the bending stress becomes more significant than the axial stress when the eccentricity of the load is increased.

In an eccentrically loaded column or in a prestressed girder stresses are given by the expression:

$$f = \frac{P}{A} \pm \frac{Pe}{I} c$$

(Note: eccentricity exists only with respect to x-x axis),

where the first term gives the axial component and the second the bending component, with the tension in the opposite side to the applied force.

The stress distribution is shown in Fig. 7. It can be noted that different stress distributions can be achieved by varying either the applied force or the eccentricity. When a beam is overloaded and stresses exceed the allowable, the introduction of prestressing cables provides a means of keeping stresses within the allowable limits. This is the case for an old structure where the bending capacity needs to be increased.

In the case of new bridge design reduction of structural steel is achieved by using prestressing cables.

In Fig. 8, it can be seen in the stress diagrams how the prestressing counteracts the stresses due to the dead load and live load acting in the beam, in zones where the allowable stress is exceeded.

2.2 Prestressing Moment in Simply Supported Girders

Different moment diagrams can be obtained by varying the eccentricity and the location of the prestressing cables along the beam. For simply supported beams, straight cables along the tension flange provide the most simple solution. However, some advantages can be achieved by draping the cables.

When a straight cable along the bottom flange is used, the prestressing moment is constant along the beam and might cause reversal of

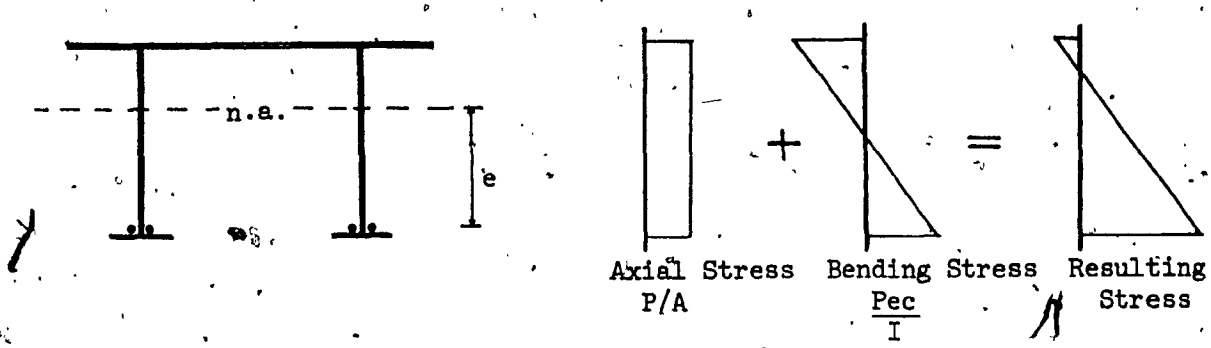

Fig. 7 — Stresses due to Prestressing.

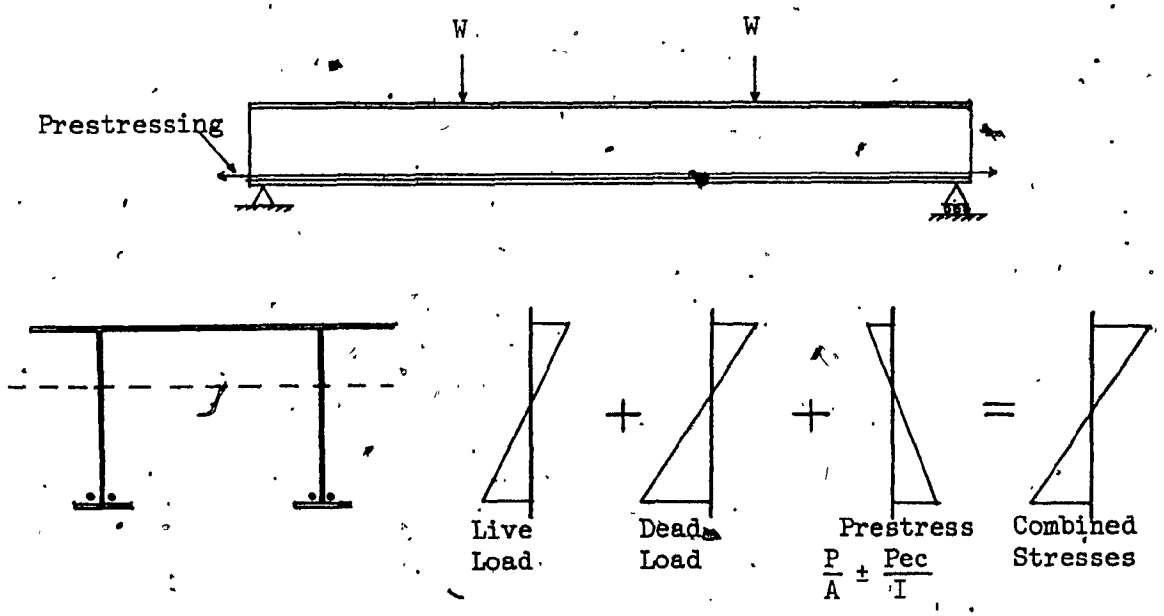

Fig. 8 — Stress Superposition in a Prestressed Girder Design.

stresses at some points in the beam. In the case of draped or parabolic-bent cables, the moment diagram is more rational, with a maximum moment at the center where load moments are greater and zero or very small moment at the supports, where stress due to loading are very low.

In Fig. 9 the prestressing moment diagram for both straight and draped cables is shown.

Another advantage of the draped cable is the contribution with opposite shear forces to those of the external loading. In cases where the shear is critical these cable locations may prove to be advantageous.

Fig. 10 shows the shear diagram due to the prestressing cables as well as the equivalent load for this cable shape (It will be shown later that this approach is very useful in computing the prestressing moments in continuous girders).

2.3 Prestressing Moment in Continuous Girders

As it was shown previously, computing of prestressing moments was accomplished simply by multiplying the prestressing force by the corresponding eccentricity ($M = Pe$). However, for continuous spans this is not true because a secondary moment is introduced in the system by the prestressing forces. This idea is easy to visualize if we study the illustration in Fig. 11. Let us consider a two span continuous bridge with a straight cable along the bottom flange. (It should be noted that this is not a convenient location and it is chosen just to illustrate the method).

If the central support is removed (Fig. 12) the girder will bend upwards, producing a deflection Δ_{b1} at the central support due to a

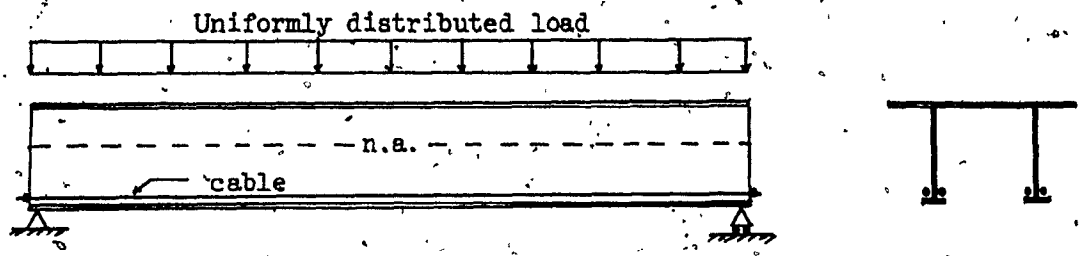

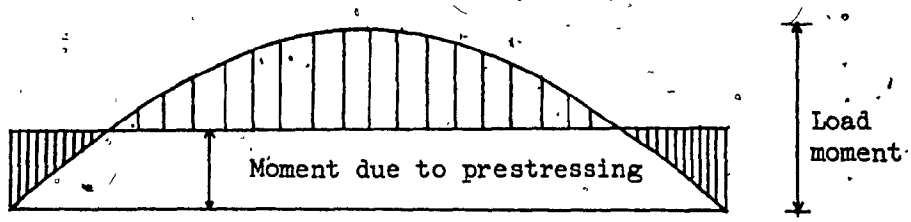

Combined moment diagram

a) Constant eccentric prestressing force

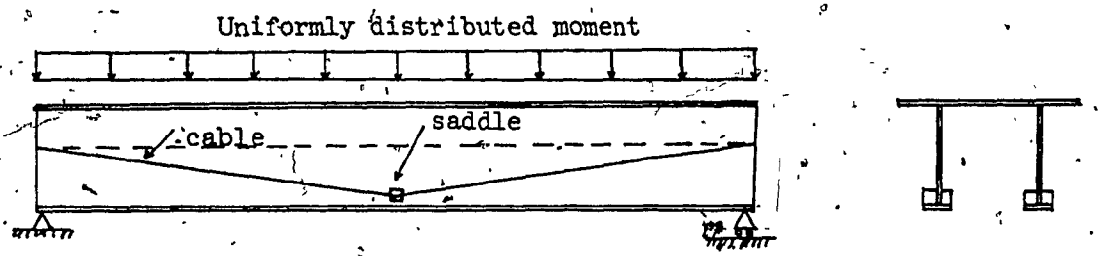

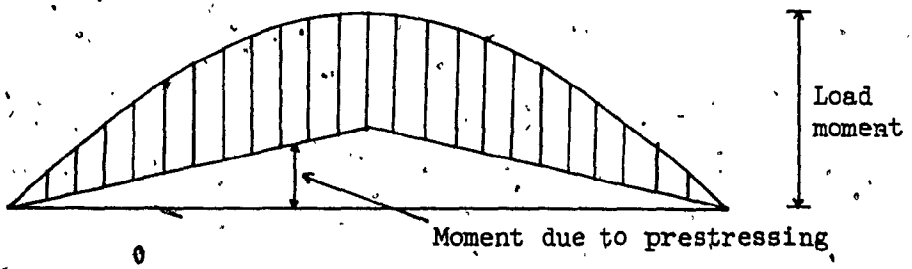

Combined moment diagram

b) Variable eccentric prestressing force

Fig. 9 — Moment Diagrams for Two Basic Prestressing Systems.

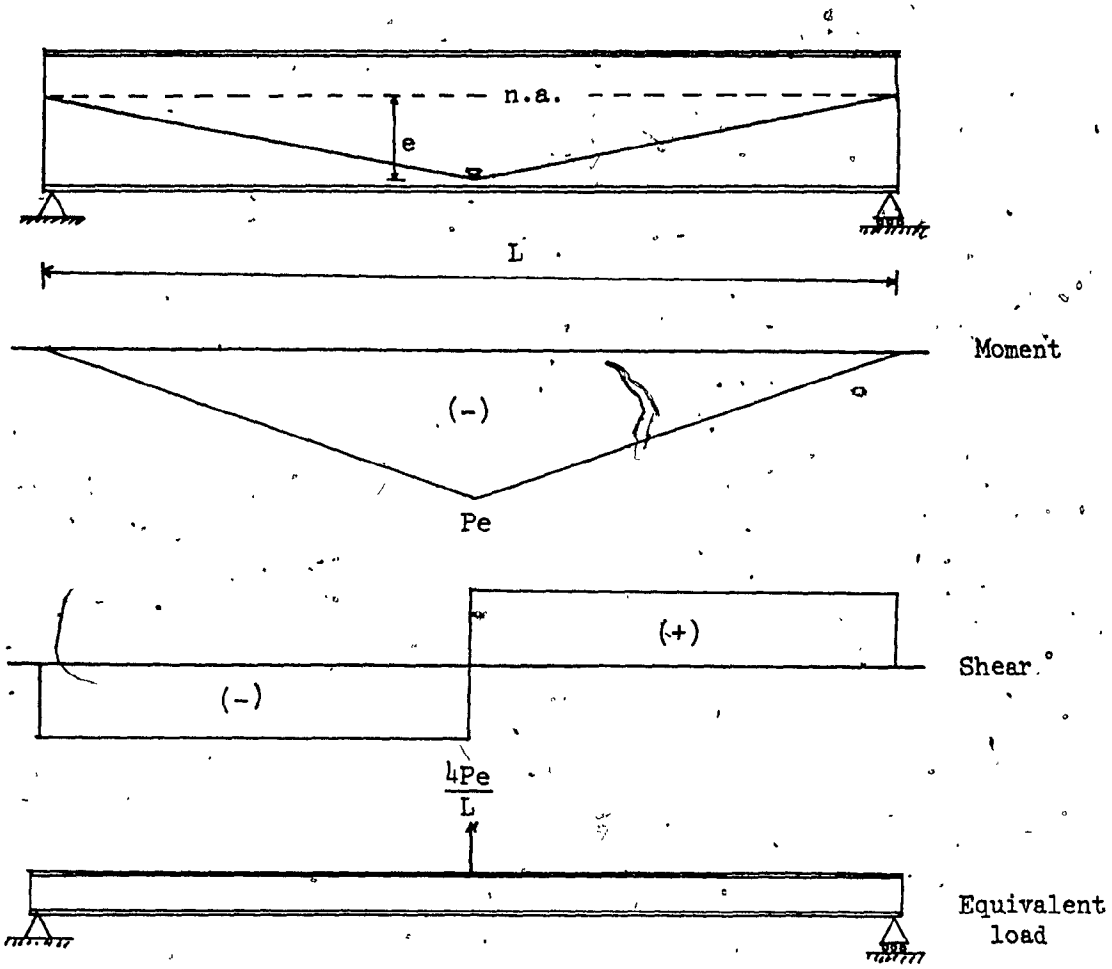

Fig. 10 — Moment and Shear Diagrams and Equivalent Load for the Draped Cable System.

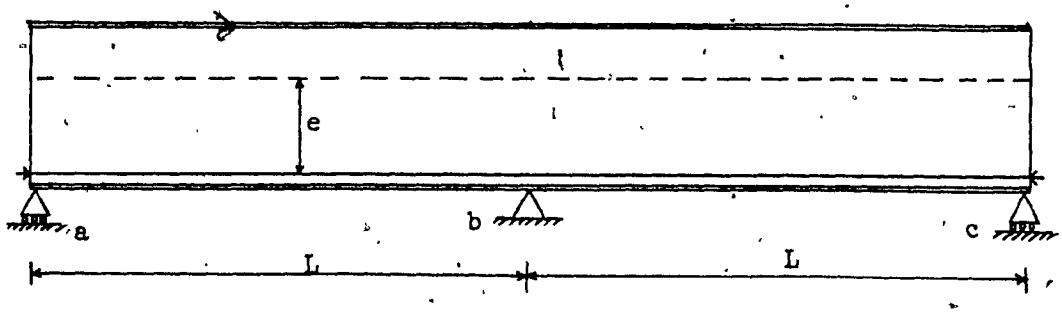

Fig. 11 — Geometry of a Two-Span Continuous Girder.

constant bending moment along the girder (basic moment M_b).

In order to prevent this uplift a force R_b in the central support is required. This force produces a bending moment (secondary moment M_s) of opposite sign of that of the Basic Moment and the final prestressing moment (M_p) is the superposition of both moments (Fig. 13).

The evaluation of the secondary moment is performed in this case easily by the consistent deformation method, from the condition that the vertical displacement at the central support should be zero. In this way we establish the compatibility condition for the central support and find the value of the redundant R_b (Fig. 14).

$0 = \Delta_{b1} - \delta_{bb} R_b \longrightarrow R_b = \frac{\Delta_{b1}}{\delta_{bb}}$, where Δ_{b1} is the vertical displacement at b in the basic structure due to the prestressing forces.

δ_{bb} is the vertical displacement at b due to a unit load applied at b.

From any manual we get:

$$\Delta_{b1} = \frac{ML^2}{8EI} = \frac{Pe(2L)^2}{8EI}, \quad \delta_{bb} = \frac{PL^3}{48EI} = \frac{(2L)^3}{48EI}$$

substituting

$$R_b = \frac{\Delta_{c1}}{\delta_{bb}} = \frac{Pe(2L)^2}{8EI} \times \frac{-48EI}{(2L)^3} = \frac{-3Pe}{L}$$

Then, we get the secondary moment at b to be $M_s = 3/2\ Pe$ and by superimposing both the basic moment and the secondary moment we get the final prestressing moment (Fig. 15).

Discussion of results: As we can see in Fig. 15 the maximum secondary moment (M_s) is 1 1/2 times the basic moment (M_b) and the final prestressing moment is quite different as expected, with a positive moment at the central support and negative moment at the ends.

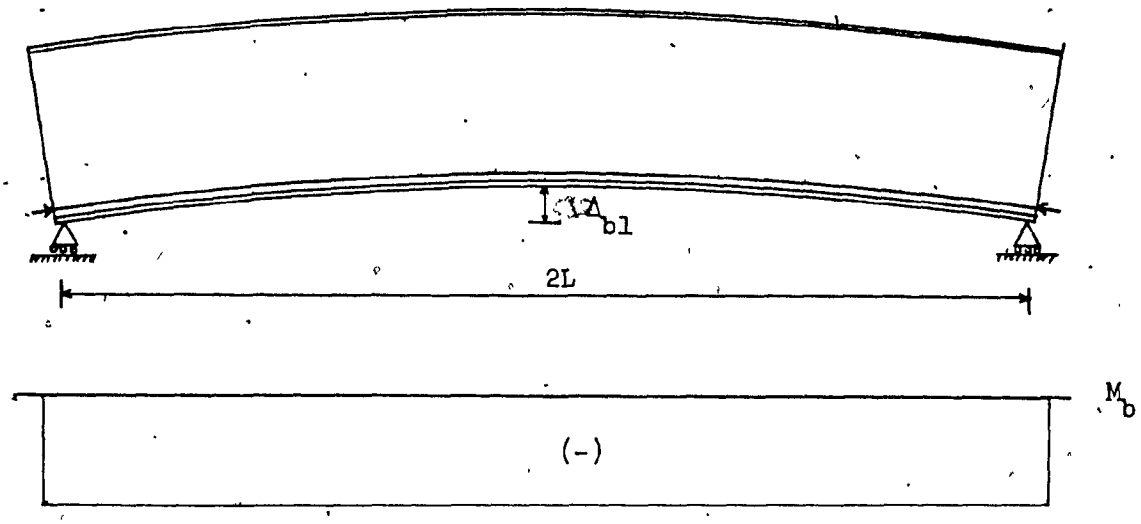

Fig. 12 — Uplift in the Beam After Removal of Central Support and the Basic Moment Diagram.

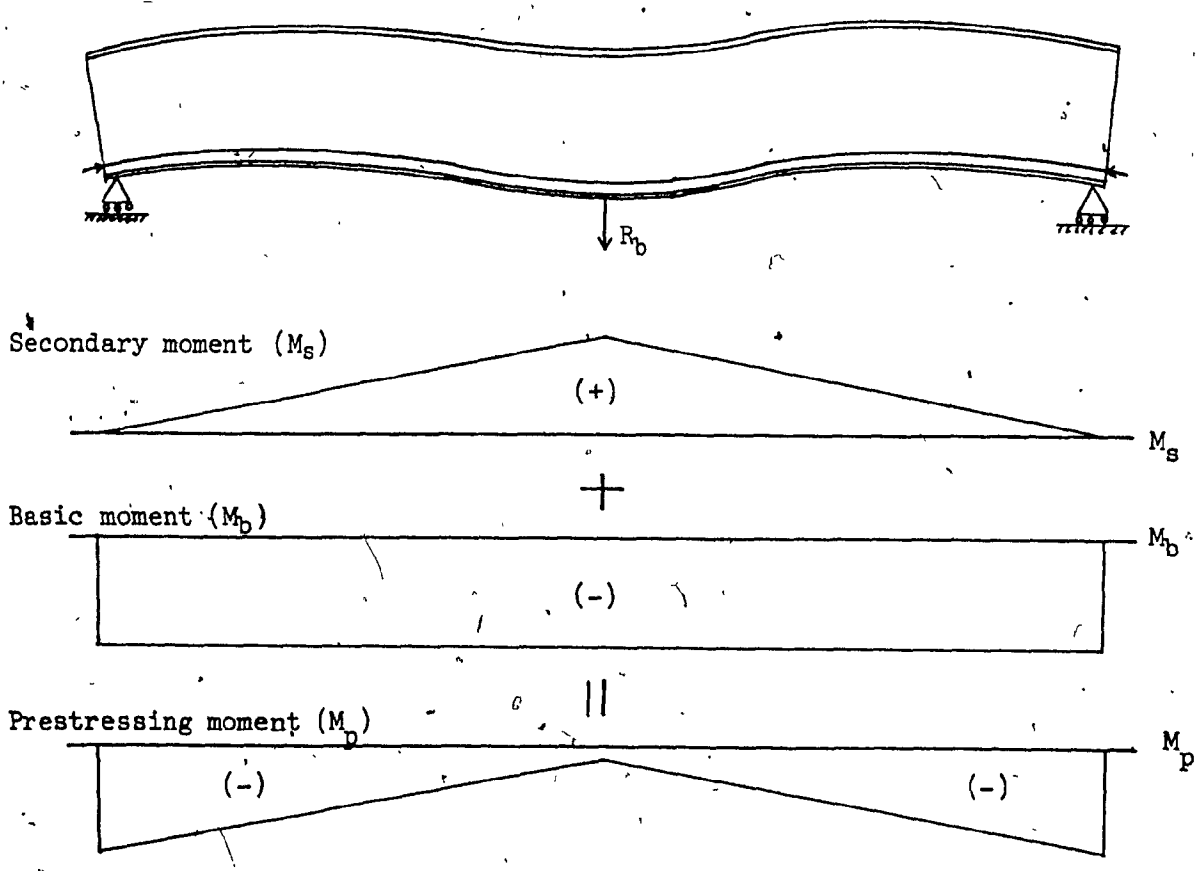

Fig. 13 — Determination of Final Prestressing Moment.

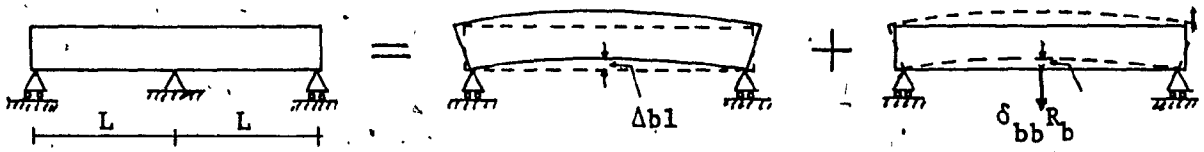

$$0 = \Delta b1 - \delta_{bb} R_b \longrightarrow R_b = \frac{\Delta b1}{\delta_{bb}}$$

Fig. 14 — Compatibility Conditions.

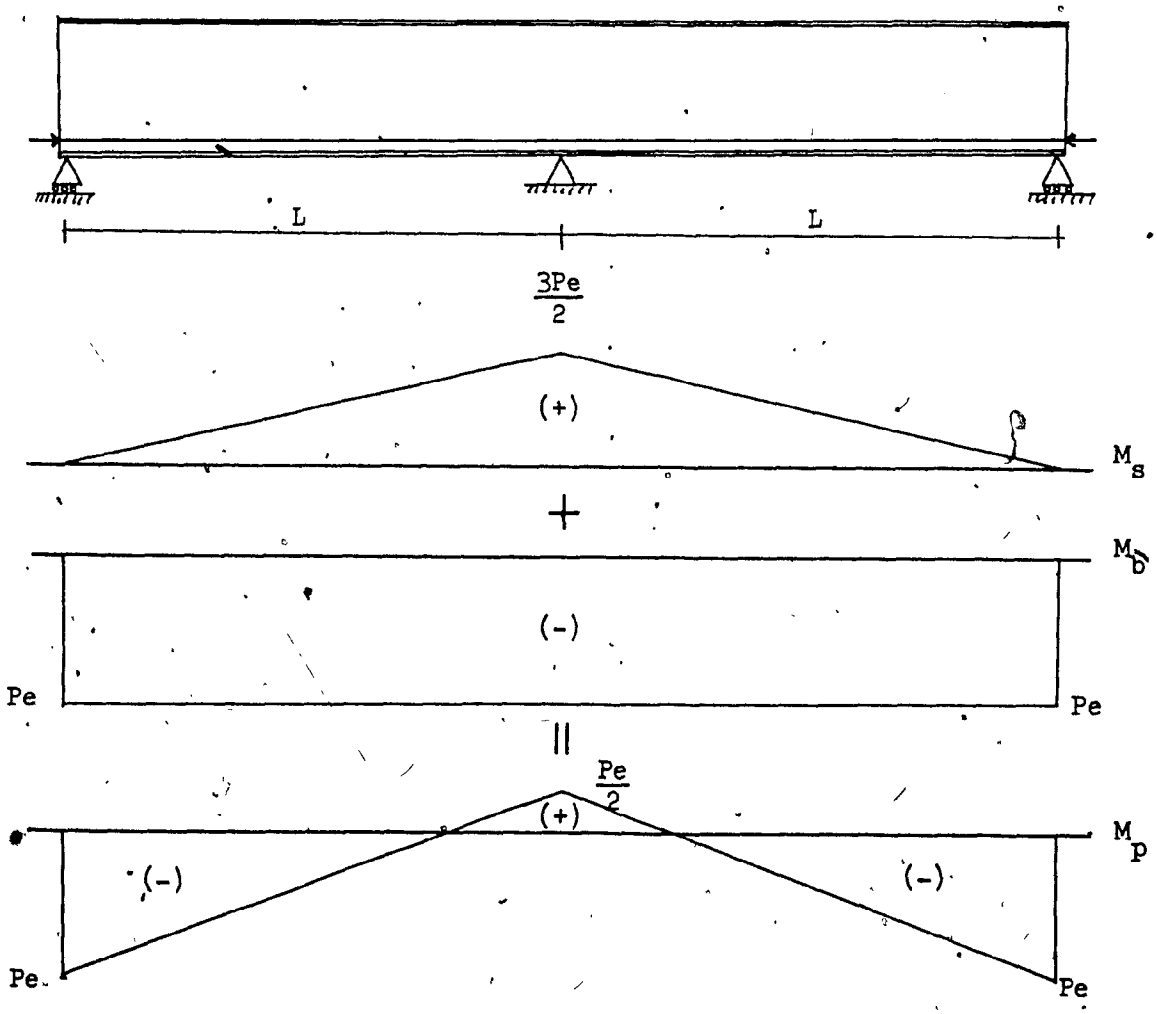

Fig. 15 — Final Prestressing Moment (M_p).

Likewise, we know that for a two span girder loaded uniformly along both spans we have maximum negative moment over the central support and maximum positive moment at the midspans. By observing diagrams in Fig. 16, we can see that the prestressing in the girder produces favorable moments only at the central support, thus counteracting the negative moment of the uniformly distributed load.

It can be seen from the former discussion that the resulting prestressing moment is not quite efficient, especially in zones of maximum positive moment and at the ends where the moment due to external loads is zero but the prestressing moments have a significant value.

Therefore, the ideal prestressing moment diagram is the one that follows, to some extent, the moment diagram due to external loads but with opposite sign.

It should be also sought in a rational design that the secondary moment produces favorable stresses in the most critical zone of the structure, as in the case of previous discussion where the secondary moment produced a considerable positive moment at the central support thus counteracting very efficiently the negative moment due to external loads.

Now, in this part of the discussion, a concordant moment diagram will be aimed for, in other words a moment diagram with a shape close to the moment diagram due to the external loads but with opposite sign.

It is known that, in a design of a bridge, stresses due to self weight are generally greater than stresses due to live loads. Also, the dead load moment diagram is unchangeable during the life of the bridge, whereas the live load diagram is constantly changing with the action of the moving loads. Therefore, in design of a prestressed bridge, it

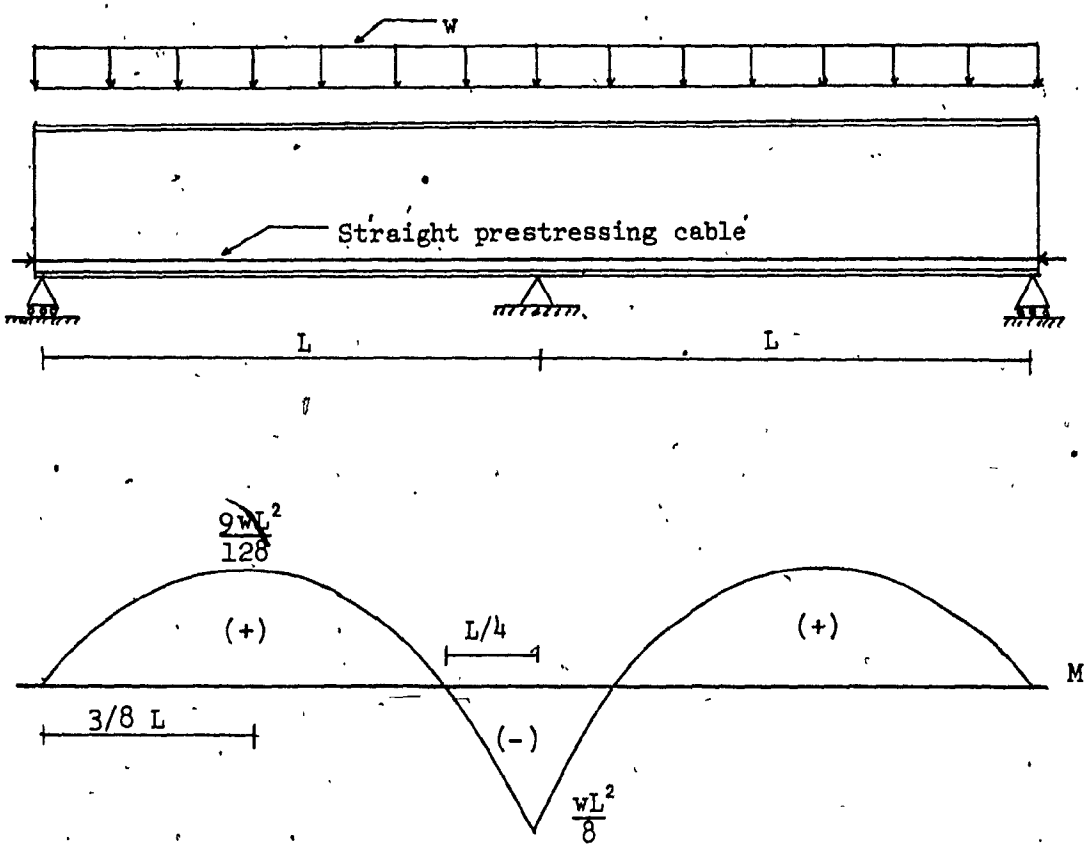

a) Moment diagram for a uniformly distributed load.

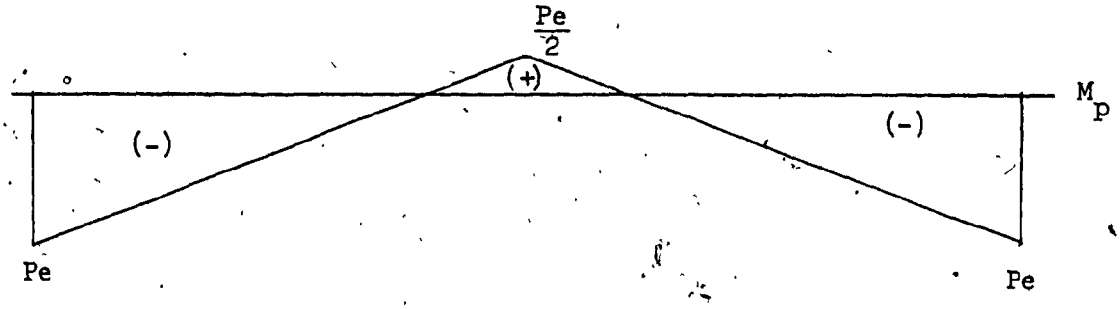

b) Prestressing moment diagram for a straight cable along the bottom flange.

Fig. 16 — Moment Diagrams for a Prestressed Continuous Girder.

is preferable to counteract the action of the dead load that has an unchangeable moment diagram.

According to this criterion the ideal concordant prestressing moment diagram is that one with a parabolic shape, since the shape of moment diagram for uniformly distributed dead load is a parabola.

It is possible to create this concordant prestressing moment by means of a parabolically bent cable. However, parabolical cable configuration will be treated in later discussion using a faster and more powerful method of analysis. In this case, for the sake of clarity and to understand the concepts of concordant moment diagram and secondary moment, straight draped prestressing cables will be considered (Fig. 17).

Again, the method of consistent deformation will be employed and the central support will be chosen as a redundant. The basic structure is then a simply supported beam having as a load the prestressing cables. The basic structure bends under the influence of the load, giving a vertical deflection (Δ_{b1}) assumed upward. The bending moment diagram of this basic structure (M_b) corresponds to the shape of the cable and is expressed in terms of P, e_1, e_2 (Fig. 18).

To find the deflection Δ_{b1} the virtual work method is used. Axial and shear deformations are neglected since they produce small deformations compared with those deformations due to bending.

Then, the general expression for deformation at any point is —

$$\Delta = \int_0^{2L} \frac{m\,M\,dx}{EI}$$

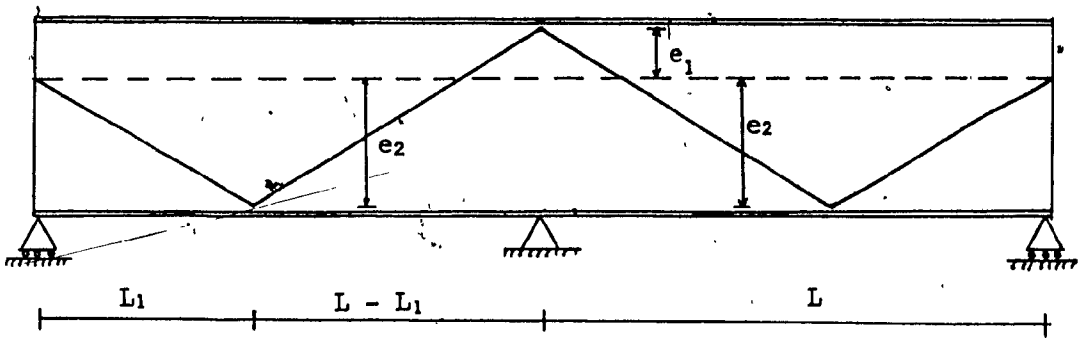

Fig. 17 — Geometry of the Straight Draped Cable Arrangement.

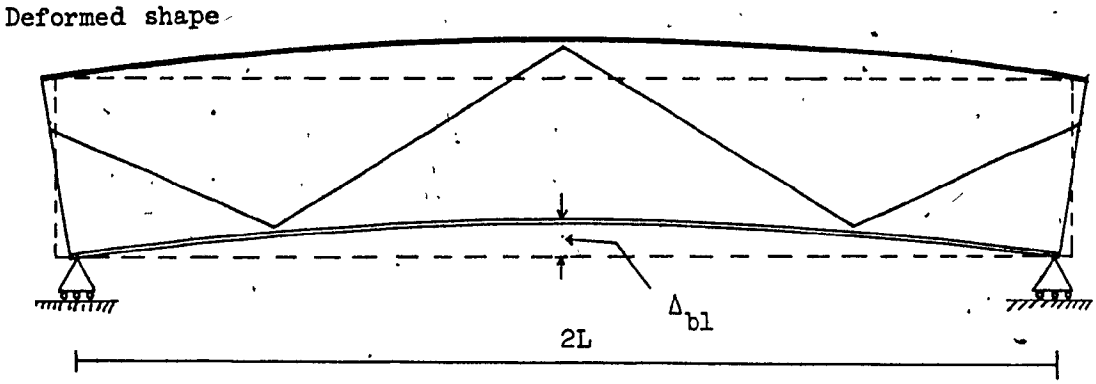

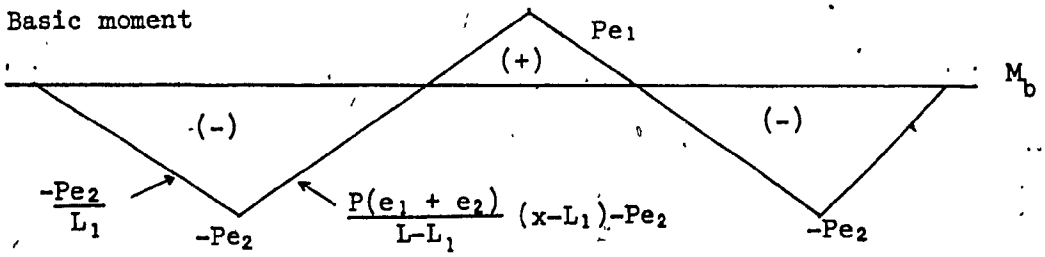

Fig. 18 — Basic Moment Diagram for Draped Cable Arrangement.

where M is the moment due to the actual loading in the basic structure, m is the moment due to the unit load applied at the point and in the direction of the desired deformation.

In this particular example the unit load is a vertical unit force applied at the point where the central support is removed (Fig. 19). Taking advantage of the symmetry the integration is only taken over half the length. Substituting values at EI constant, the integral becomes:

$$\Delta_{bL} = \frac{2}{EI}\left[\int_0^{L_1}\left(\frac{-x}{2}\right)\left(-\frac{Pe_2x}{L}\right)dx + \int_{L_1}^{L}\left(\frac{-x}{2}\right)\left(P\,\frac{xe_1 + e_2}{L - L_1}(x-L_1) - Pe_2\right)dx\right]$$

$$= \frac{2}{EI}\left[\frac{Pe_2}{6L_1}x^3\Big|_0^{L_1} - \frac{P}{6}\frac{(e_1 + e_2)}{(L - L_1)}x^2\Big|_{L_1}^{L} + \frac{P(e_1 + e_2)L_1x^2}{4(L - L_1)}\Big|_{L_1}^{L_2} + \frac{Pe_2}{4}x^2\Big|_{L_1}^{L}\right]$$

$$= \frac{2}{EI}\left[\frac{Pe_2}{6L}L_1^3 - \frac{P(e_1 + e_2)}{6(L - L_1)}(L^3 - L_1^3) + \frac{P(e_1 + e_2)L_1(L^2 - L_1^2)}{4(L-L_1)} + \frac{Pe_2}{4}(L^2 - L_1^2)\right]$$

$$= \frac{2}{EI}\left[\frac{Pe_2L_1^2}{6} - \frac{P(e_1+e_2)}{6}(L^2 + LL_1 + L_1^2) + \frac{P(e_1+e_2)}{4}(L_1L + L_1^2) + \frac{Pe}{4}(L^2 - L_1^2)\right]$$

$$= \frac{2}{EI}\left[\frac{Pe_2}{2}\left(\frac{L_1^2}{3} - \frac{L^2}{3} - \frac{LL_1}{3} - \frac{L_1^2}{3} + \frac{LL_1}{2} + \frac{L_1^2}{2} + \frac{L^2}{2} + \frac{L_1^2}{2}\right) + \frac{Pe_1}{2}\left(\right.\right.$$

$$\left.\left. - \frac{L^2}{3} - \frac{LL_1}{3} - \frac{L_1^2}{3} + \frac{LL_1}{2} + \frac{L_1^2}{2}\right)\right]$$

$$\Delta_{bc} = \frac{P}{6EI}\left[e_2(L^2 + LL_1) + e_1(-2L^2 + LL_1 + L_1^2)\right] \quad \ldots\ldots\ldots 2.1$$

Now we set the compatibility equation for the central support to satisfy the condition that the displacement in the actual structure is zero (Fig. 20).

$$0 = \Delta_{b1} - \delta_{bb} R_b \longrightarrow R_b = \frac{\Delta_{b1}}{\delta_{bb}} \quad \ldots\ldots\ldots\ldots (2.2)$$

where δ_{bb} is the displacement at b due to a vertical unit load applied at b.

Solution for δ_{bb} is given by:

$$\delta_{bb} = \frac{PL^3}{48EI} = -\frac{(2L)^3}{48EI} = -\frac{L^3}{6EI} \quad \ldots\ldots\ldots\ldots\ldots\ldots (2.3)$$

Then, by substituting expression (2.1) and (2.3) into (2.2) the value of R_b is obtained:

$$R_b = \frac{P}{L^3}\left[e_2(L^2 + LL_1) + e_1(-2L^2 + LL_1 + L_1^2)\right] \ldots\ldots (2.4)$$

Once the reaction at point b is known the secondary moment at b is found by statics:

$$M_s = -\frac{R_c}{2} \times L = \frac{P}{2L^2}\left[e_2(L^2 + LL_1) + e_1(-2L^2 + LL_1 + L_1^2)\right] \ldots\ldots (2.5)$$

Now the final prestressing moment is found by superimposing the basic moment with the secondary moment. Computing the prestressing moment at the middle support we get:

$$M_p = M_b + M_s = Pe_1 + \frac{P}{2L^2}\left[e_2(L^2 + LL_1) + e_1(-2L^2 + LL_1 + L_1^2)\right]$$

$$M_p = \frac{P}{2L^2}\left[e_2(L^2 + LL_1) + e_1(LL_1 + L_1^2)\right] \quad \ldots\ldots\ldots\ldots (2.6)$$

Fig. 21 shows the resulting prestressing moment diagram.

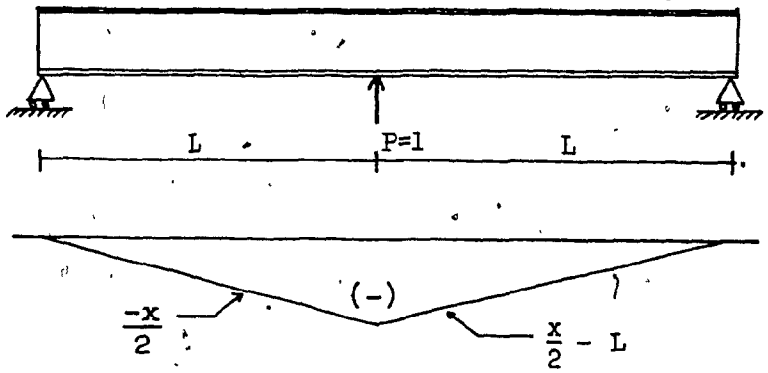

Fig. 19 — Moment Due to a Unit Load.

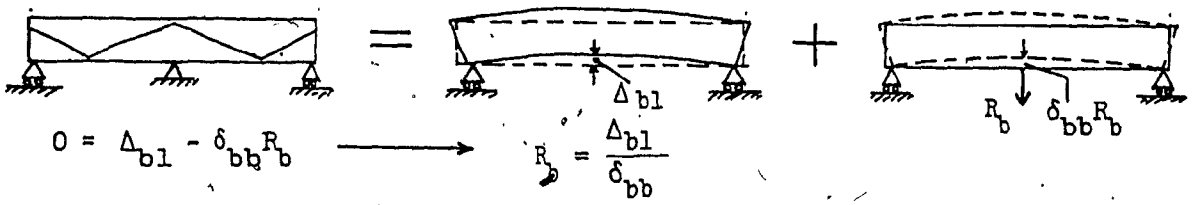

$$0 = \Delta_{b1} - \delta_{bb}R_b \longrightarrow R_b = \frac{\Delta_{b1}}{\delta_{bb}}$$

Fig. 20 — Compatibility Conditions

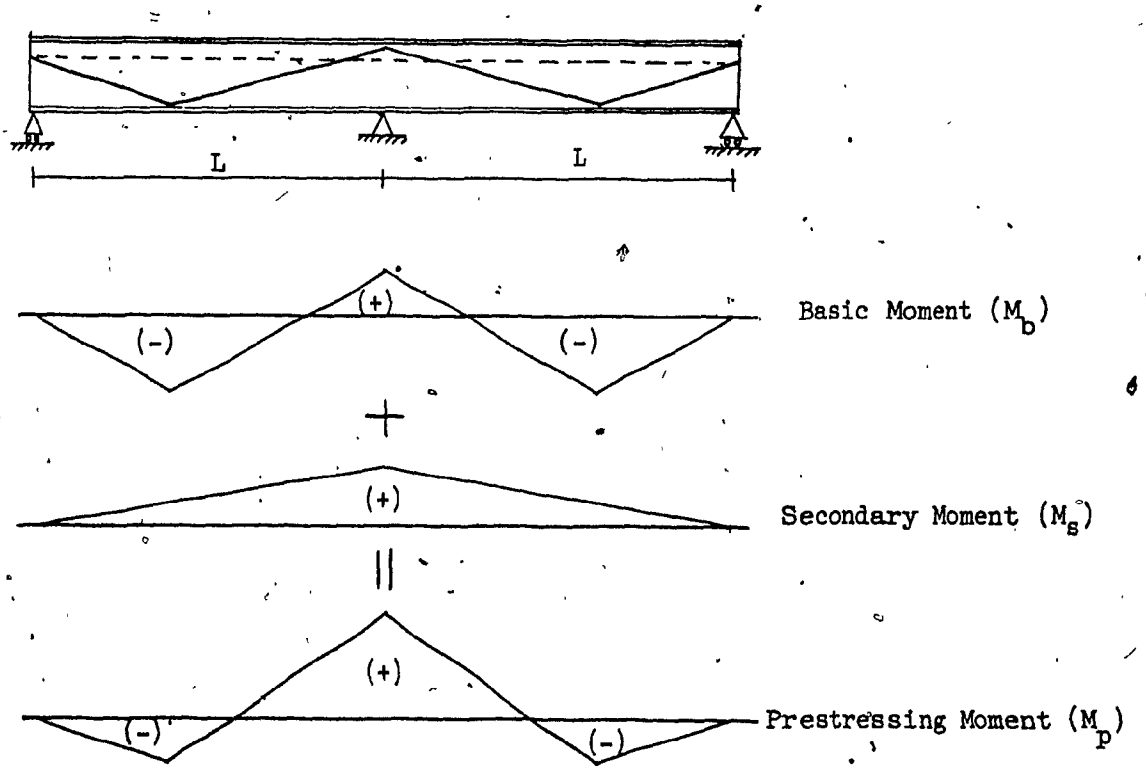

Fig. 21- Final Prestressing Moment for the Draped Cable Configuration.

Giving numerical values to expression 2.5 for secondary moment it was found that the secondary monent is most of the time positive, unless the value of e_2 is very small compared to e_1. This means that in this cable configuration the secondary moment makes the prestressing moment at the middle support bigger, so that the prestressing moment counteracts very efficiently the maximum negative moment existing in the middle support due to the uniformly distributed dead load.

As a conclusion it can be said that this draped cable configuration is more effective than the straight cable along the bottom flange because the final prestressing moment yields a moment diagram with a shape closer to the dead load moment diagram but with opposite sign (Fig. 21).

2.4 Equivalent Load Method

In the previous discussion the traditional approach of consistent deformations method was successfully applied in deriving expressions for the prestressing moment of various cable configurations in continuous girders under prestressing. In this part, the Equivalent Load Method will be treated.

This method of analysis is a more versatile, general and simplified method because it can be used automatically and easily to analyze prestressed continuous bridges having any type of prestressing cable configuration. It also may be applied in analyzing frames under prestressing.

In order to illustrate the equivalent load method the final prestressing moment for a two-span continuous prestressed bridge will be found. The shape of the prestressing cable is shown in Fig. 22. This shape is the most general cable configuration and it encompasses all the

examples previously discussed.

The method consists in determining equivalent externally applied forces that produce the same effects in the structure as those forces induced by the prestressing cables. This method of analysis is explained in Khachaturian's book[8] and the sequence of calculations is as follows:

The first step is to determine the statically determinate prestressing moment or basic moment (M_b). This is an idealized bending moment that the prestressing cables would produce in the actual structure if no secondary moment existed in the system. In other words, it is the prestressing moment that would exist in a simply supported beam having the same overall dimensions and the same prestressing forces of the actual statically indeterminate structure under analysis. Fig. 23 shows the basic moment of the continuous bridge under consideration. Once the basic moment is found its corresponding statically determinate shear (S_b) should be derived. This is done in a reversed procedure than in the usual way. For our continuous bridge the shear is shown in Fig. 24.

From the statically determinate shear diagram we can go back to find the corresponding equivalent loading for the continuous bridge. In finding the equivalent loading it is assumed that the horizontal component of the prestressing cable is equal to the prestressing force. Carrying out the computation in a reversed manner, the equivalent loading is obtained (Fig. 25).

As a verification it is recommended to carry out the calculations starting now from the equivalent load in order to arrive to the basic moment and check whether the same basic moment diagram is obtained.

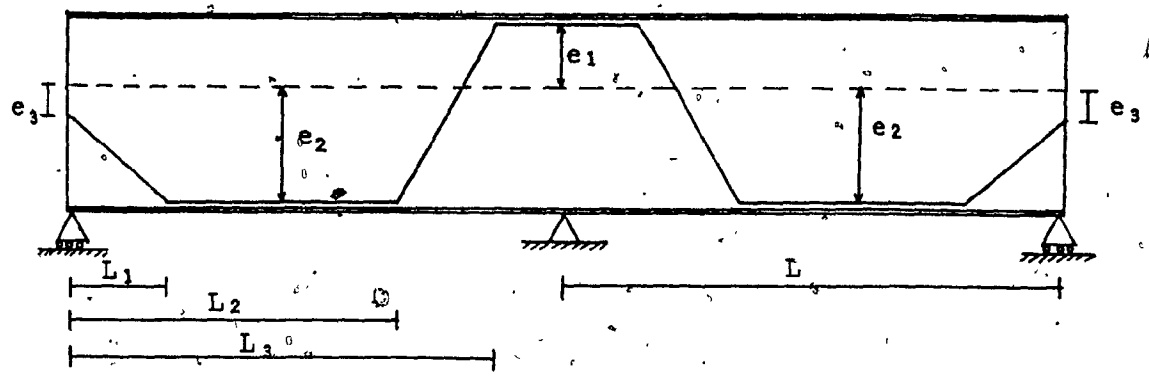

Fig. 22 — General Draped Cable Configuration.

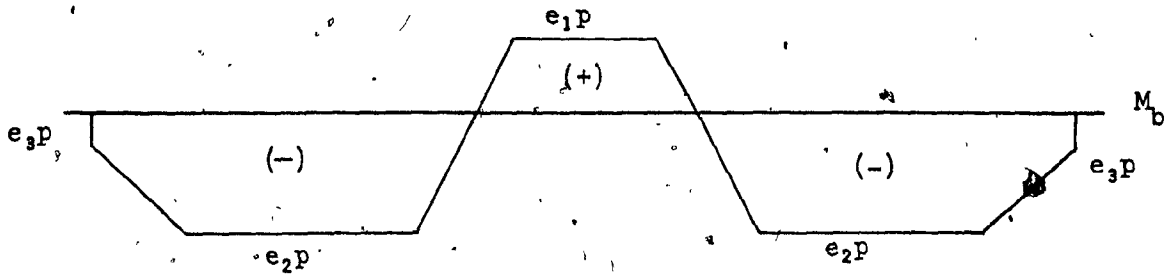

Fig. 23 — Basic Moment Diagram (Statically Determinate Moment).

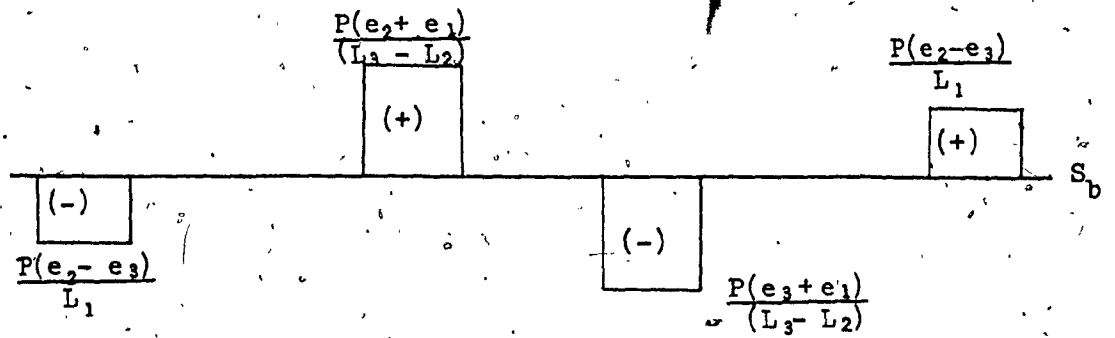

Fig. 24 — Basic Shear Diagram (Statically Determinate Shear)

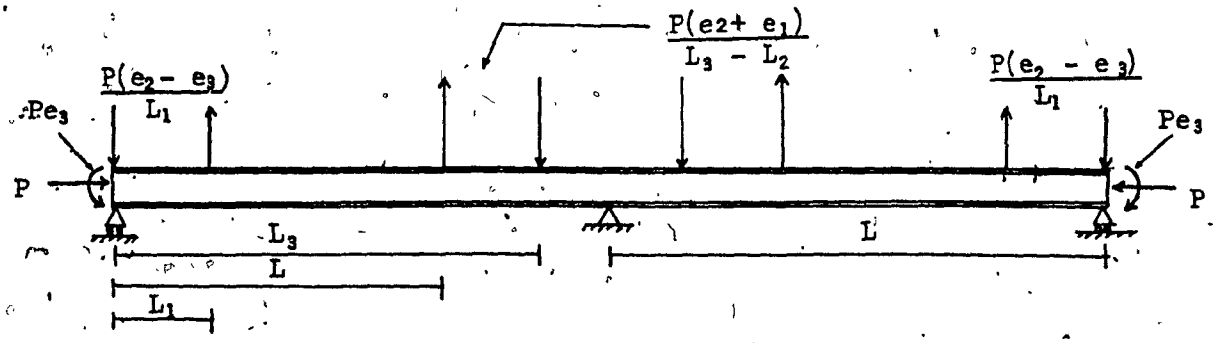

Fig. 25 — Equivalent Load System.

We can see in diagram Fig. 25 that the 3 conditions of static equilibrium $\Sigma Fx = 0$, $\Sigma Fy = 0$, $\Sigma M = 0$ are not satisfied for the continuous girder yet. They are only satisfied for a simply supported beam.

Next step is to solve our continuous girder with a system of loads equal to the equivalent loading (Fig. 25) already found.

For the case of constant moment of inertia in the continuous girder the most suitable tool of analysis is the moment distribution method since end moments for the type of loads existing in the equivalent loading system are given in handbooks.

Now we proceed to compute the end moments. Because of the symmetry in the structure we only need to find the end moments in one span. Also due to symmetry, the relative stiffness for each of the two spans is the same and therefore the distribution factor (Dij) at the central support has the same value.

The equivalent loading system is split into its component loads, then the fixed-end forces are calculated separately for the various concentrated loads. Fig. 26 shows the calculation of the fixed-end moments.

By superposition the total fixed-end moment is found:

$$M_t = \frac{P}{2L^2}\left[e_3 2L^2 - (e_2-e_3)(L^2-L_1^2) - \frac{L_2}{(L_3-L_2)}(e_2+e_1)(L^2-L_3^2) + \frac{L_3}{(L_3-L_2)}(e_2+e_1)(L^2-L_3^2)\right]$$

Because of the symmetry of the girder the fixed-end moment in the span on the right is equal to the fixed end moment in the span on the left but with opposite sign; therefore, there is no unbalanced moment to distribute in the central joint and the total fixed-end moment already found is the final prestressing moment at the central support.

The fixed-end moment for a fixed-pinned beam is given by next expression:

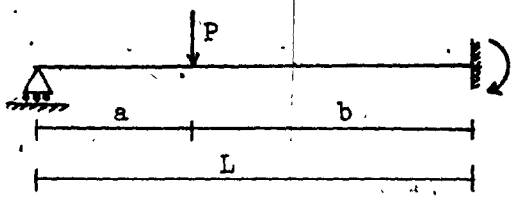

$$M = \frac{Pab}{2L^2}(L + a)$$

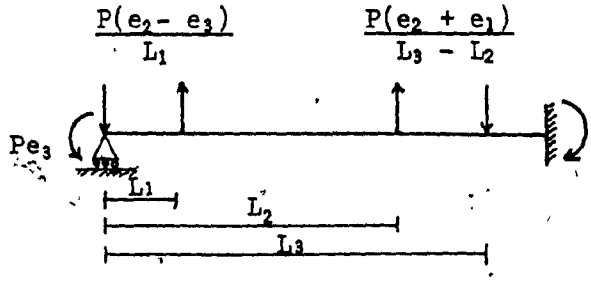

M_t

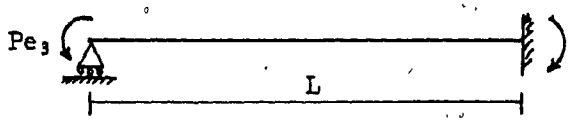

$$M = Pe_3$$

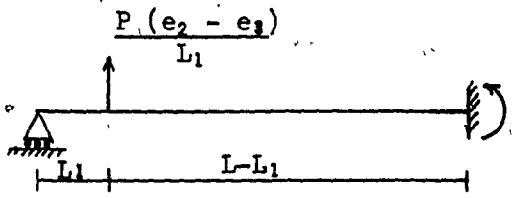

$$M = \frac{P}{2L^2}(e_2 - e_3)(L^2 - L^2)$$

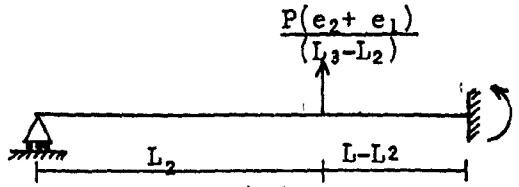

$$M = \frac{PL_2(e_2 + e_1)(L^2 - L_2^2)}{2L^2(L_3 - L_2)}$$

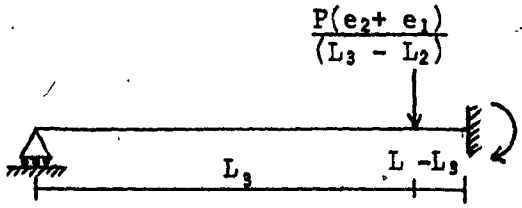

$$M = \frac{PL_3(e_2 + e_1)(L^2 - L_3^2)}{2L^2(L_3 - L_2)}$$

Fig. 26 — Calculation of Fixed-end Moments.

Rearranging the expression for the prestressing moment at the central support we get:

$$M_p = \frac{P}{2L^2}\left[e_3 2L^2 - e_2(L^2 - L_1^2) + e_3(L^2 - L_1^2) + (-L^2L_2 + L_2^3 + L^2L_3 - L_3^3)\frac{e_2 + e_1}{L_3 - L_2}\right]$$

$$M_p = \frac{P}{2L^2}\left[e_3(3L^2 - L_1^2) - e_2(L^2 - L_1^2) + \left(L^2(L_3 - L_2) + L_2^3 - L_3^3\right)\frac{e_2 + e_1}{L_3 - L_2}\right] \quad \ldots\ldots\ldots\ldots (2.7)$$

and this expression is the general formula for the moment at the central support in our two-span continuous prestressed girder under study (Fig. 22).

As it can be seen, the method of equivalent load, compared with the method of consistent deformation explained at the beginning of the chapter is faster and more powerful since it can be applied automatically to a continuous beam with any number of spans. It can also be applied to certain types of rigid frames.

We can summarize the method in two simple steps. First, from the basic prestressing moment diagram determine the equivalent loading in the structure. And second, solve the statically indeterminate structure under the action of the equivalent load system using moment distribution or any other suitable method of analysis.

From the general expression already found it is possible to derive formulas for more simple cable configurations. It only suffices to make certain parameters in the general formula (expression 2.7) equal to zero.

If e_3 in expression 2.7 is made equal to zero the cable configur-

ation shown in Fig. 27 is obtained. It can be noticed that the end cable anchorage is now located exactly at the neutral axis of the girder. In this way, the prestressing moment at the ends of the girder is eliminated.

Making $e_3 = 0$, expression 2.7 becomes:

$$M_p = \frac{P}{2L^2}\left[-(L^2 - L_1^2)e_2 + \frac{L^2(L_3-L_2)+L_2^3-L_3^3}{L_3-L_2}(e_2+e_1)\right] \quad \ldots\ldots (2.8)$$

For the case shown in Fig. 28 the horizontal bottom portions of the cable in both spans is deleted. Hence, $L_2 = L_1$ and $e_3 = 0$ in the general expression. Now the formula for the moment at the central support becomes:

$$M_c = \frac{P}{2L^2}\left[-(L^2 - L_1^2)e_2 + \frac{L^2(L_3-L_1)+L_1^3-L_3^3}{L_3-L_1}(e_2+e_1)\right] \quad \ldots\ldots (2.9)$$

Now as a last variation and also as a check of the method, the formula for the case previously developed by the consistent deformation method at the beginning of the chapter (Fig. 17) will be derived.

For this cable configuration there is no portion of the cable that is horizontal; all cable components are inclined as shown in Fig. 28a. In this cable configuration $L_1 = L_2$, $L_3 = L$ and $e_3 = 0$.

Then:

$$M_p = \frac{P}{2L^2}\left[-(L^2 - L_1^2)e_2 + \frac{L^2(L-L_1)+L_1^3-L^3}{L-L_1}(e_2+e_1)\right]$$

$$M_p = \frac{P}{2L^2}\left[-(L^2 - L_1^2)e_2 + \frac{L^3-L^2L_1+L_1^3-L^3}{L-L_1}(e_2+e_1)\right]$$

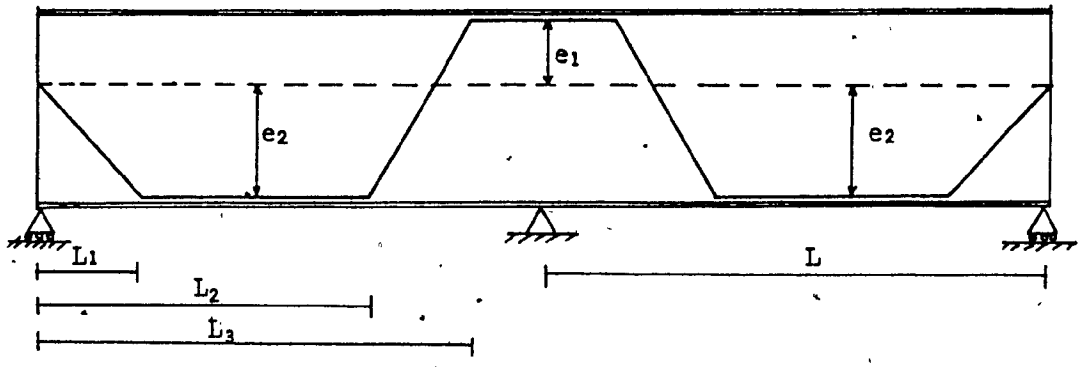

Fig. 27 — General Draped Cable Configuration with $e_3 = 0$.

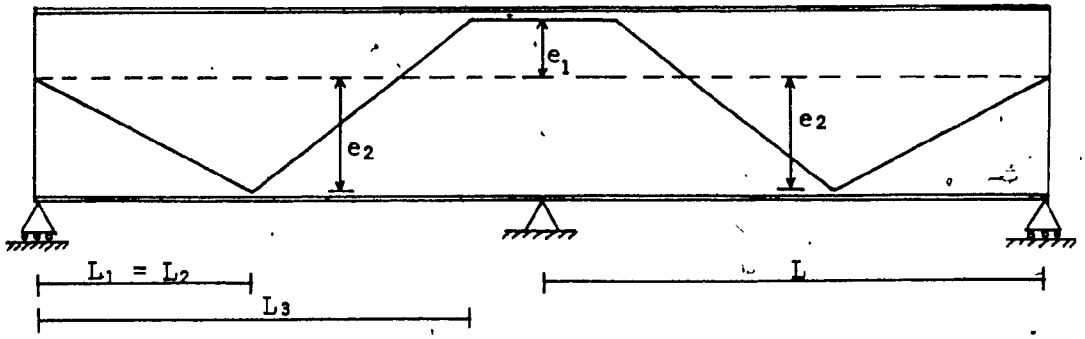

Fig. 28 — General Draped Cable Configuration with $e_3 = 0$ and $L_2 = L_1$.

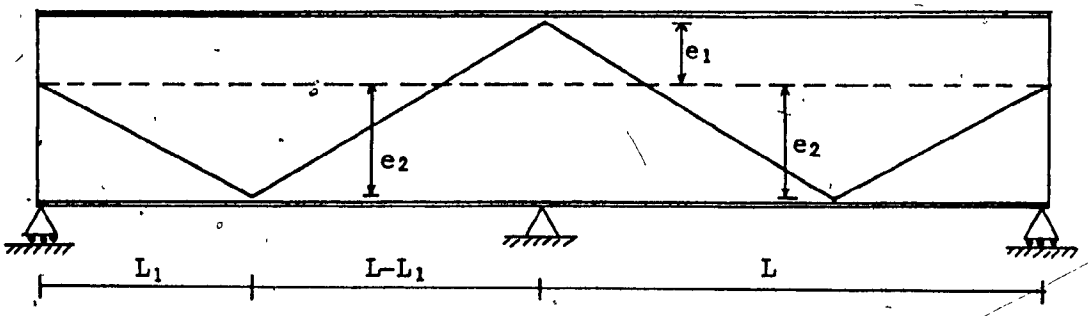

Fig. 28a — General Draped Cable Configuration with $e_3 = 0$ and $L_2 = L_1$ and $L_3 = L$.

$$M_p = \frac{P}{2L^2}\left[-(L^2 - L_1^2)e_2 + \frac{L_1(L_1^2 - L^2)}{L - L_1}(e_2 + e_1)\right]$$

$$M_p = \frac{P}{2L^2}\left[-(L^2 - L_1^2)e_2 - (LL_1 + L_1^2)(e_2 + e_1)\right]$$

$$M_p = \frac{P}{2L^2}\left[-(L^2 - L_1^2 + LL_1 + L_1^2)e_2 - (LL_1 + L_1^2)e_1\right]$$

$$M_p = \frac{-P}{2L^2}\left[(L^2 + LL_1)e_2 + (LL_1 + L_1^2)e_1\right] \quad \ldots\ldots\ldots\ldots\ldots\ldots \quad (2.10)$$

This resulting expression is exactly the same as expression 2.6, calculated by the consistent deformation method. The minus sign arises because a different sign convention was used in deriving the general expression by the Equivalent Load Method.

2.5 Prestressing Moment in Girders with Parabolically Bent Prestressing Cables

Theoretically speaking, parabolic bent cable is the most efficient configuration to use in prestressed continuous bridges because the moment introduced by the prestressing cable has approximately, all along the length of the girder, an intensity proportional to the moment produced by the uniformly distributed dead load of the bridge but with opposite sign. The magnitude of the prestressing moment depends on the amount of cables (prestressing force) and in the location of the cables.

In this parabolic configuration, the prestressing moment counteracts the dead load moment in every location of the whole length of the bridge because the shape of the prestressing moment diagram is similar to the shape of the dead load moment diagram.

In the case of moving live loads, the live load moments are not directly counteracted because they vary with the load position, but by counteracting the dead load more capacity is left in the girder to withstand live load. Capacity that in ordinary design will be only acquired by increasing the size of the cross-section and consequently the weight of the bridge.

In the Khachaturian and Gurfunkel[8] book, "Prestressed Concrete", expressions for continuous prestressed girders with parabolic bent cables are derived. They treat the case of prestressing cable supported by making contact with the concrete throughout the length of the girder. There, the prestressing forces are transmitted to the girder by the pressure exerted by the parabolically bent cable on the surface of contact all along the girder.

This solution of support throughout the prestressing cable is not advantageous to apply in prestressed steel bridges since it is not practical to fabricate a parabolic bed or guide and weld it to the steel girder web in order to support the prestressing cable.

Due to this disadvantage an alternative solution is proposed: to support the prestressing cable on saddles or "hold-downs" located in points in the girder distributed at regular intervals, so that the resulting shape of the cable will approximate the desired parabolic configuration. In fact, the resulting shape of the cable will be a polygon made out of short straight portions of cable following a parabolic pattern. The smaller the segments, the closer the polygon will approximate the parabola.

To illustrate the equivalent load method applied to parabolic cable configuration a numerical example will be worked out in this section instead of deriving a general symbolic expression that would result in extra-lengthy expressions.

So far, constant moment of inertia has been considered in the continuous girders. This example will be still considered with constant moment of inertia all along the girder but later this same configuration will be repeated to illustrate the case of variable moment of inertia.

In Fig. 29, the geometry of the continuous bridge is given (half bridge). It shows also the location of the neutral axis and the saddles (devices holding the prestressing cable).

It should be noted that the shape of the cable over the central support does not approximate the shape of the dead load bending moment diagram, but this shape is preferred because it gives a gradual change in the prestressing moment. Also, with this shape a reduced angle of bent of the prestressing cable is obtained, thus reducing the loss of prestress due to friction on curved cables.

In calculating the prestressing moment the same steps as previous cases are followed. First, the basic moment diagram (statically determinate moment) is plotted. This diagram has the same shape as prestressing cables in the girder.

From this moment diagram, the shear diagram is calculated an then the equivalent loading is ascertained. In this case, the equivalent loading system is a set of concentrated loads (Fig. 30). (Only half of the bridge is shown because of the symmetry).

Now the fixed-end moment in one of the spans is calculated (Fig. 31). Splitting the equivalent loading into its components the fixed-end moment for each component is computed and then by superimposing all the contributions the total fixed-end moment is evaluated (Fig. 31).

Again, because of the symmetry there is no unbalanced moment over the central support and no moment distribution is required. Therefore, the final prestressing moment is the fixed-end moment evaluated in Fig. 31.

Note: all measurements are in inches.

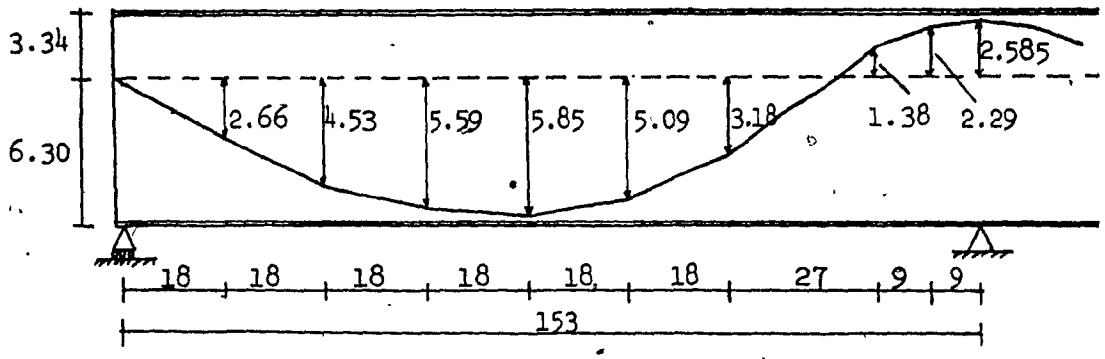

Fig. 29 — Geometry of the Parabolic-polygonal Configuration.

Basic moment:

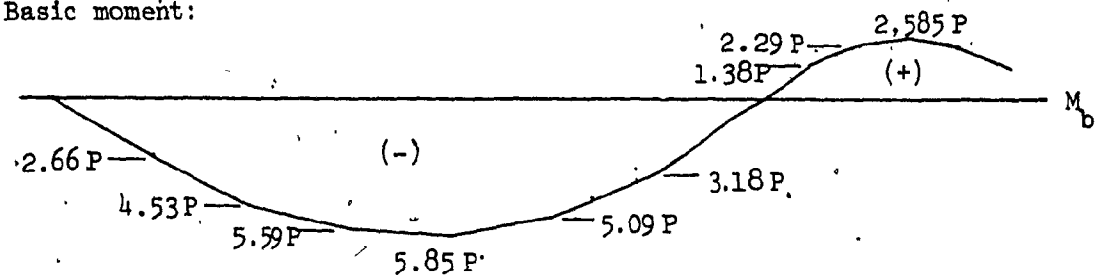

Basic shear:

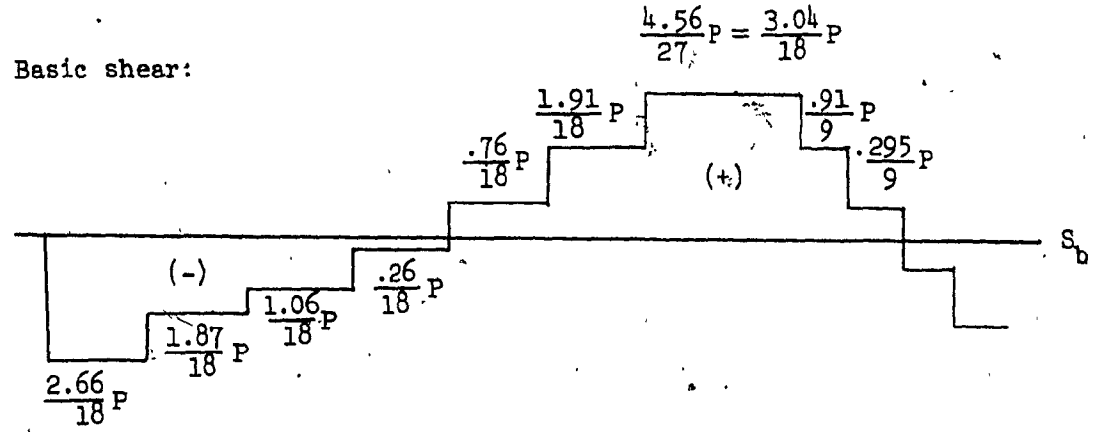

Equivalent load system:

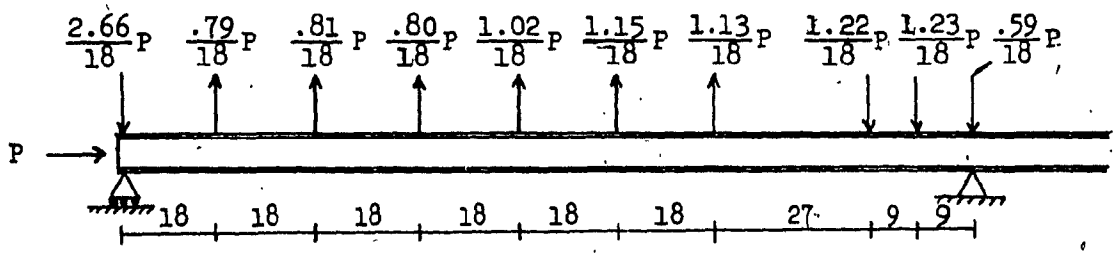

Fig. 30 — Determination of the Equivalent Load System.

Note: all measurements are in inches.

The fixed-end moment is given by the formula:

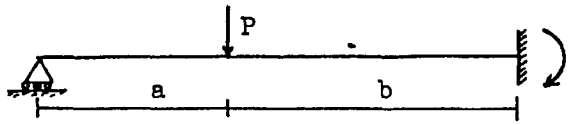

$$M = \frac{Pab}{2L}(L + a)$$

Contributions

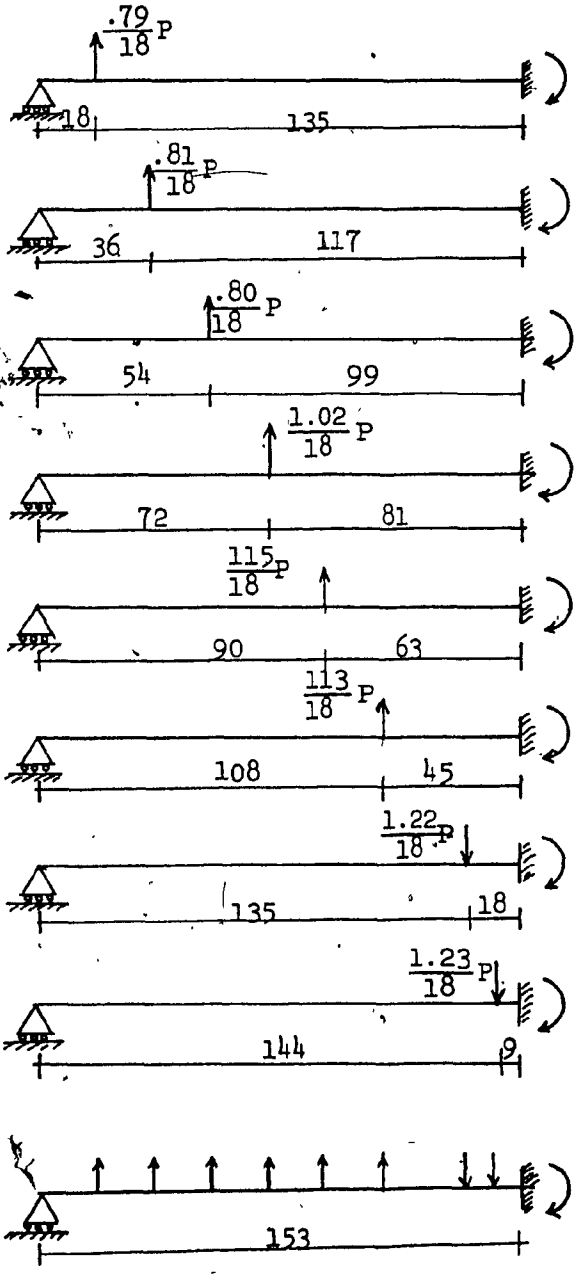

$M = -0.3895\,P$

$M = -0.7652\,P$

$M = -0.0505\,P$

$M = -1.5882\,P$

$M = -1.8802\,P$

$M = -1.7009\,P$

$M = 1.0131\,P$

$M = 0.5618\,P$

$M_b = -5.7996\,P$

Fig. 31 — Evaluation of Superposition of Fixed-end Moment.

If the prestressing moment is desired at any point along the girder, it is necessary to superimpose the secondary moment on the basic moment at the desired point. The final prestressing moment diagram for this example is plotted in Fig. 32.

It has been seen that the secondary moment is originated by the tendency of the girder to bend and have an uplift under the action of the prestressing forces. This uplift is restrained at the supports and therefore causes a reaction at the supports. This reaction alone creates the secondary moment that varies linearly along the girder.

Also as a reminder, we saw that the basic moment is found by multiplying the prestressing force by its corresponding eccentricity about the neutral axis of the cross-section, and that the basic moment diagram has exactly the same shape of the prestressing cable in the girder.

We can see in Fig. 32 that secondary moment is again favourable since it increases the prestressing moment over the middle support where stress due to dead load has its peak. Prestressing moment also helps at the midspans where maximum positive dead load moments exist.

As a verification for this calculation, the final prestressing moment over the support was evaluated using Khachaturian's[9] expressions for support throughout the length of the cable along the girders and it was found to be $M_b = 5.867P$ against $M_b = 5.80P$ in this example. The resulting discrepancy of 1.08% is negligible.

Therefore, it can be concluded that the approximation of using a parabolic polygon configuration supported on saddles is sufficiently valid and that this solution is preferable to the one of support throughout the length of the prestressing cable for prestressed steel bridges because from

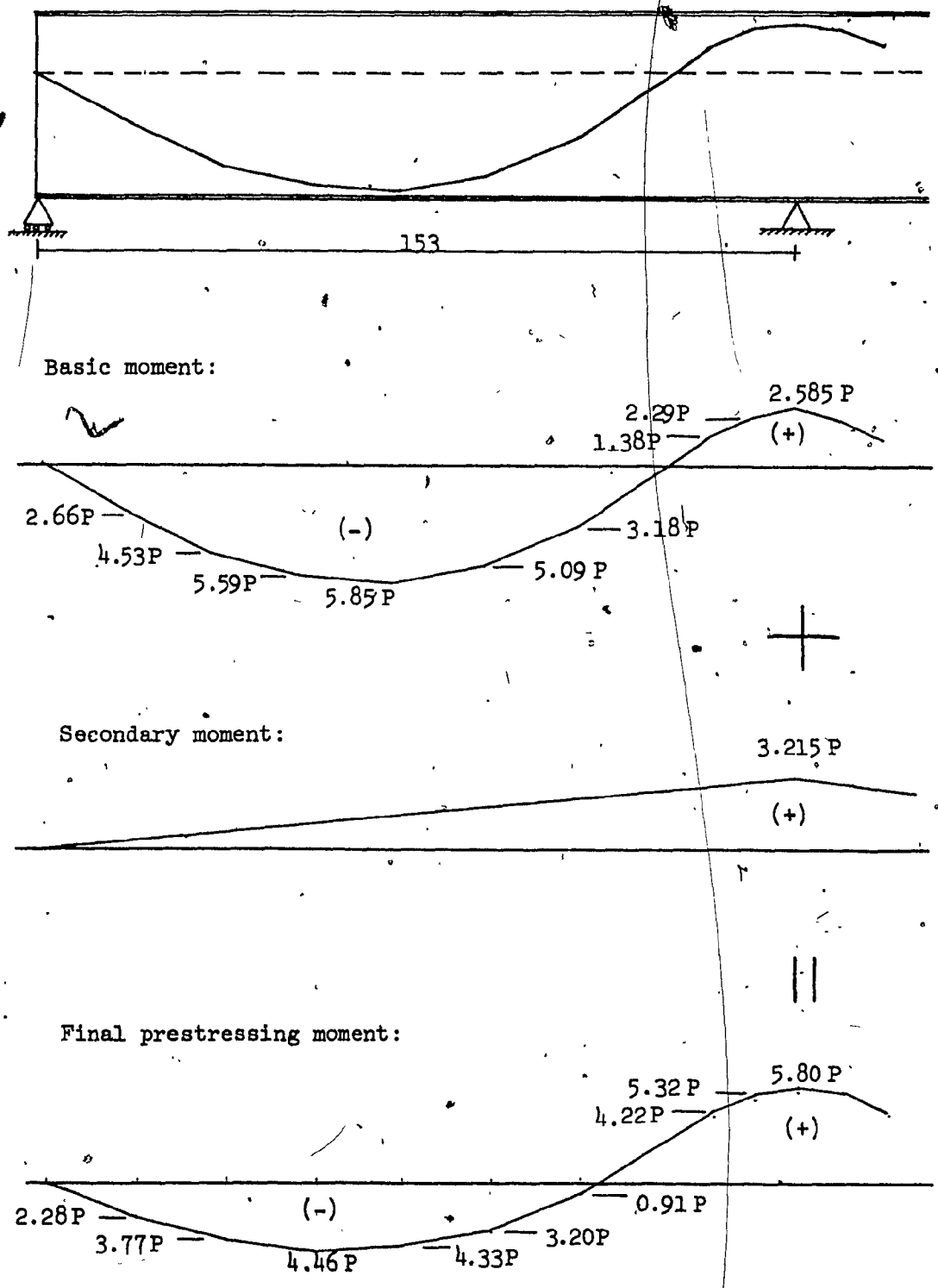

Fig. 32 — Evaluation of the Final Prestressing Moment by Superposition of Basic and Secondary Moments.

the technical point of view, the saddle supported cable has lesser friction between the cable and the supports, and from an economic point of view, overall cost is reduced by the utilization of saddles instead of a "bed" or "guide" all along the girder.

2.6 Analysis of Prestressed Continuous Girder Bridges With Cover Plates

In previous sections prestressing of continuous girder bridges having a constant cross-section was discussed. In this section, a method of analyzing prestressed girder bridges with varying cross-sections will be developed since it could also be convenient to design a prestressed girder bridge having cover-plates in critical zones in order to avoid heavy prestressing.

The equivalent load method can also be used in analyzing continuous girder bridges with cover-plates since the same steps described in previous discussions are followed here. The only variations are to take into account the new rigidity in finding the prestressing moment and to consider the abrupt changes in the neutral axis at the points where the cover-plates start and end.

Again, the basic moment (statically determinate moment) is computed as usual by multiplying the prestressing force by its eccentricity about the neutral axis. In Fig. 33, the geometry of this new example is shown. It can be seen that the geometry is the same as previous examples except for the addition of cover-plates in the zone over the middle support where negative moment due to dead load is critical. This addition of cover-plates is reflected in the switch downwards of the neutral axis in this particular zone.

The resulting basic moment (statically determinate moment) will be sketched in two ways in order to clarify the effects of the abrupt change of the centroid on the moment diagram. The first diagram is shown in the traditional way with the ordinates of the moment at each point referred to a straight axis (Fig. 34). There is a sudden jump in the diagram in the point where there is a change in the cross-section of the girder. In the second diagram (Fig. 34) the discontinuity or abrupt change occurs in the reference axis so that the shape of the diagram does not suffer a sudden jump. Therefore, the shape of this moment diagram resembles the shape of the prestressing cables.

For the sake of clarity and simplicity the basic moment will be split into two ordinary moment diagrams so that the evaluation of the shear forces and equivalent loading is facilitated (Fig. 35).

It can be seen in Fig. 35 that diagram b is the same as basic moment diagram of previous example (Fig. 30) and that the other component of the basic moment (diagram c) is a continuous moment along the zone with the cover-plate. This means that the abrupt downward change of the neutral axis is equivalent to introducing a constant moment. This makes sense because by lowering the neutral axis the eccentricity of the prestressing force was increased in the zone where the cover-plate is located.

For the evaluation of the shear forces the operations are carried out in a reversed manner starting from the basic moment diagram. In this case diagram component b in Fig. 35 is used since the constant moment in diagram c does not originate any shear. Therefore the shear diagram obtained (Fig. 36) is exactly the same as that of previous example (Fig. 30).

The equivalent loading is found from the shear diagram, which in turn, yields the concentrated loads and from component moment diagram c

Note: all measurements are in inches.

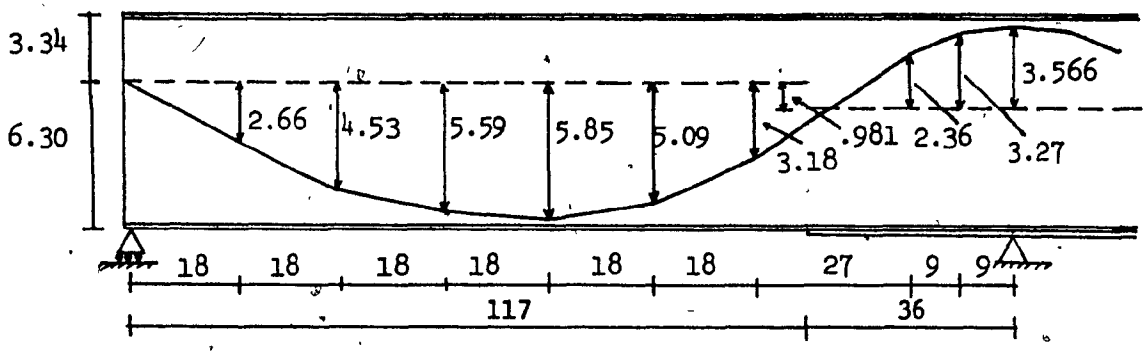

Fig. 33 — Geometry of the Parabolic Configuration in a Continuous Girder with Cover Plate.

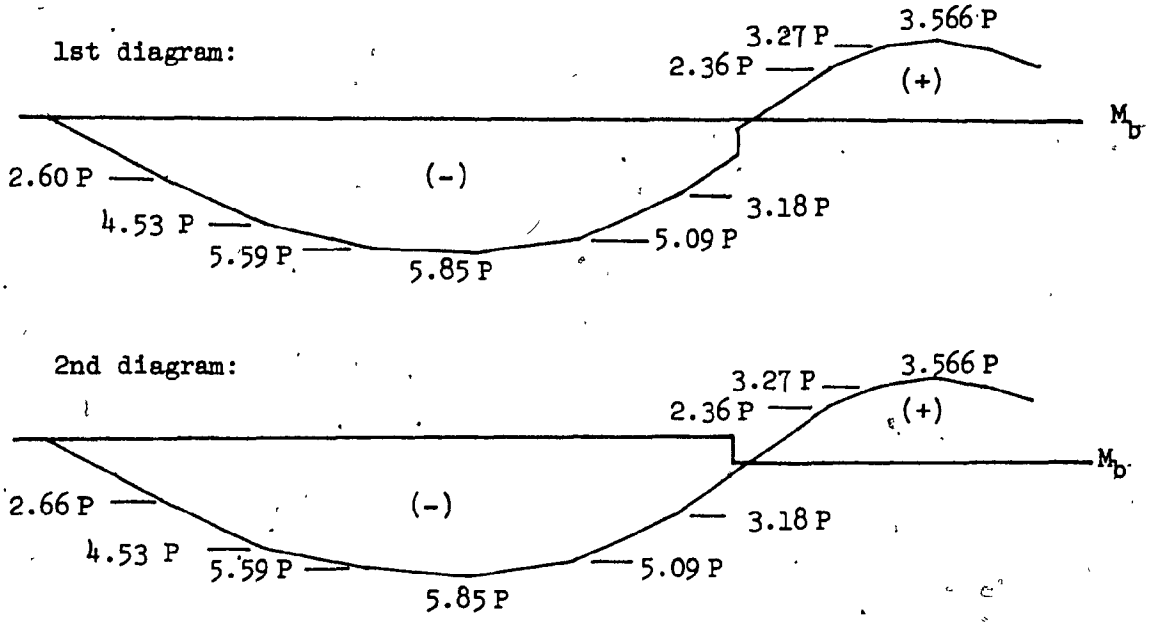

Fig. 34 — Configuration of Basic Moment in Two Ways.

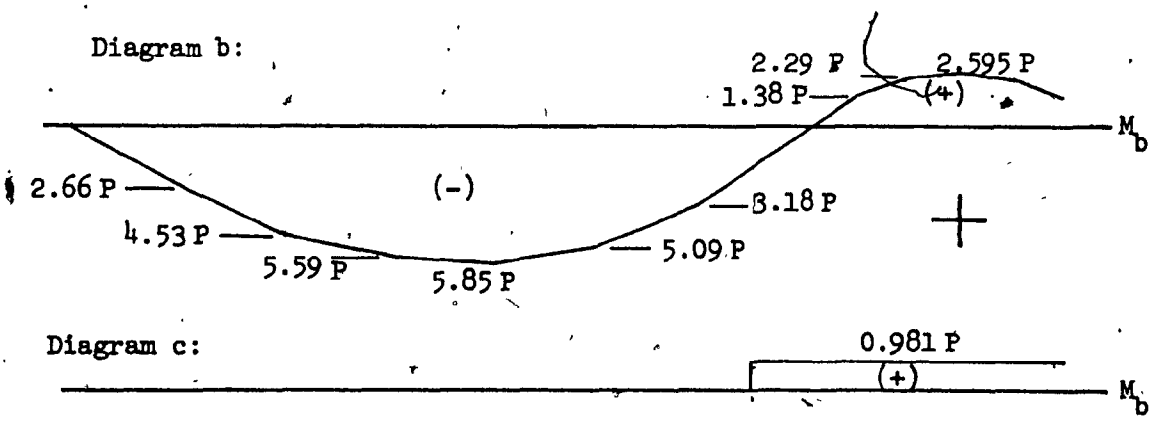

Fig. 35 — Splitting of the Basic Moment Diagram.

that gives the equivalent externally applied moment at the points of change of cross-section (Fig. 37).

Now that the equivalent loading system has been sorted out we can proceed with the evaluation of the final prestressing moment. In previous examples, where the equivalent load method was illustrated, the moment distribution method was employed to find the final prestressing moment in the girder. In this new example the consistent deformation method will be employed since, in the moment distribution method, the evaluation of the fixed-end moments for a beam with different cross-sections requires more lengthy calculations than the evaluation of the end-rotations needed in the solution using consistent deformations.

In the solution of continuous girders with simple supports at the ends by consistent deformations, the fastest and most direct way is by choosing the moment over the supports as redundants. Therefore, in our example, the moment over the middle support is released in order to get a statically determinate girder and then the compatibility equation is set in order to solve the continuous girder (Fig. 38).

For any set of loads in our two-span continuous girder the compatibility equation is (Fig. 38):

$$0 = \tau_{b1} + \delta_{bb} M_b$$

where,

τ_{b1} is the relative rotation at b due to external loads, and

δ_{bb} is a relative rotation at b due to a unit moment at b.

Solving the compatibility equation yields the general expression for the moment over the middle support for any system of loads.

$$M_b = -\frac{\tau_{b1}}{\delta_{bb}}$$

Note: all measurements are in inches.

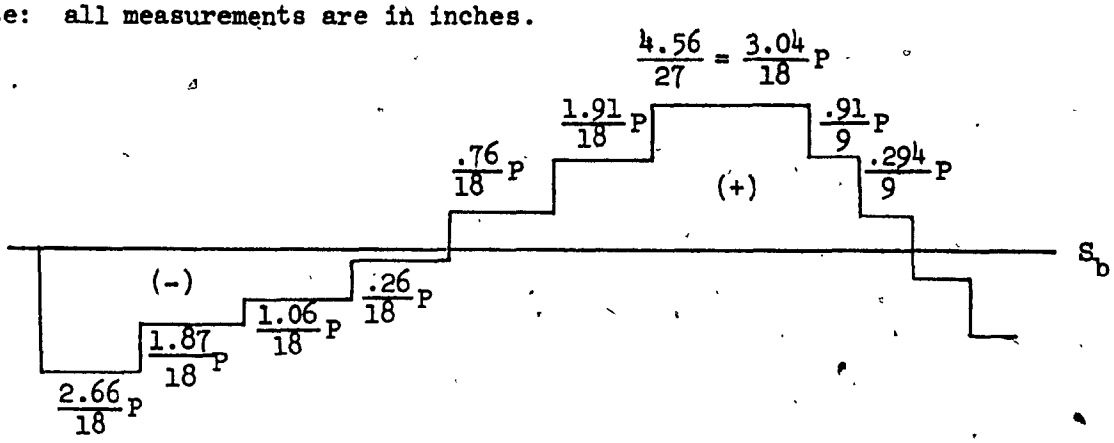

Fig. 36 — Basic Shear Diagram.

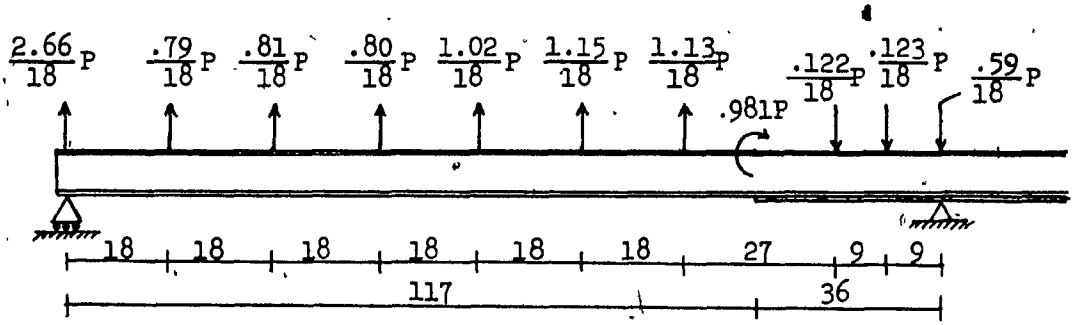

Fig. 37 — Equivalent Loading System.

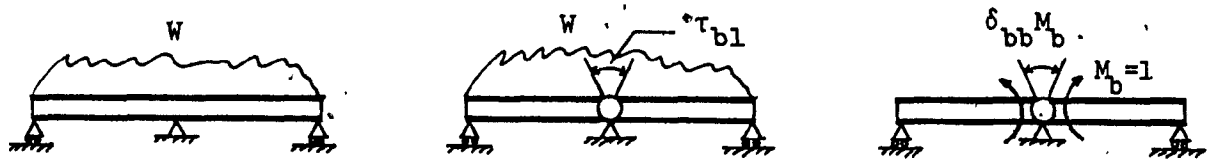

Compatibility equation: $0 = \tau_{bl} + \delta_{bb} M_b$

then $M_b = -\frac{\tau_{bl}}{\delta_{bb}}$

Fig. 38 — Compatibility Conditions.

In our example the system of loads is the equivalent loading already found, consisting of a series of concentrated loads in different locations and an externally applied bending moment. Therefore, formulas for the end-rotations due to a single concentrated load and due to externally applied moments in any location will be developed in this section in order to employ them in this and further examples.

In finding the end-rotations the principle of virtual work is used. The geometry of our example is given in Fig. 39 and the moments of inertia of the two different cross-sections are included as well.

Because of the symmetry of the girder and symmetry of the loads only half of the girder will be considered.

The coefficient δ_{bb} is computed using the virtual work formula

$$\delta_{bb} = \int_0^L \frac{m^2 dx}{EI}$$

where m is the moment along the girder produced by a unit moment applied at the end where the rotation is required (Fig. 40).

Substituting and then solving, we have:

$$1/2\ \delta_{bb} = \int_0^{117} \frac{X^2 dx}{L^2 I_o} + \int_{117}^{153} \frac{X^2 dx}{L^2 K I_o} = \frac{.45771}{E}$$

To find half of the rotation over the middle support ($1/2\ \tau_{b1}$) the virtual work expression is used

$$\tau = \int_0^L \frac{mMdx}{EI}$$

Where M is the moment in the simply supported beam due to the external load, which in this case is a single unit concentrated load.

When the unit load is between the outer end of the girder and

the point where the cross-section changes ($0 < a < 177$) an expression for τ_{b1} is derived from Fig. 41.

$$1/2\ \tau_{b1} = \int_0^a Q\left(1-\frac{a}{L}\right)\frac{x^2}{L}\frac{dx}{I_o E} + \int_0^{36} \frac{Qax'}{L}\left(1-\frac{x'}{L}\right)\frac{dx'}{KI_o E} + \int_{36}^{L-a} \frac{Q_a}{L}x'\left(1-\frac{x'}{L}\right)\frac{dx'}{I_o E}$$

$$1/2\ \tau_{b1} = -1.1921 \times 10^{-5}\frac{Q}{E}a + 2.6635 \times 10^{-1}\frac{Q}{E}a$$

substituting $1/2\ \tau_{b1}$ into the expression for moment M_b, we get:

$$M_b = \frac{\tau_{b1}}{\delta_{bb}} = 2.6045 \times 10^{-5}\frac{Q}{E}a - 5.8192 \times 10^{-1}\frac{Q}{E}a \quad \ldots\ldots\ldots (2.11)$$

$$\text{for } 0 < a < 177.$$

Now, M_b is found for the case when the unit load is in between the point of change in cross-section and support b ($117 < a < 153$), Fig. 42. Setting up and solving in terms of a, we get:

$$1/2\ \tau_{b1} = \int_0^{117} \left(Q - \frac{Qa}{L}\right)\frac{x^2}{L}\frac{dx}{I_o E} + \int_{117}^{a} \left(Q-\frac{Qa}{L}\right)\frac{x^2}{L}\frac{dx}{KI_o K} + \int_0^{L-a} \frac{Qa}{L}x'\left(-\frac{x'^2}{L}\right)\frac{dx'}{KI_o E}$$

$$1/2\ \tau_{b1} = 12.4294\frac{Q}{E} - 0.106998\frac{Q}{E}a - 8.0412 \times 10^{-6}\frac{Q}{E}a^3$$

substituting into the expression for M_b above we obtain:

$$M_b = -\frac{\tau_{b1}}{\delta_{bb}} = -27.1556\frac{Q}{E} - .223377\frac{Q}{E}a + 1.17568 \times 10^{-5}\frac{Q}{E}a^3$$

$$\ldots\ldots\ldots (2.12)$$

$$\text{for } 117 < a < 153.$$

Expressions for the moment at b (M_b) due to an externally applied unit moment at any point along the beam are now developed.

For the case when the unit moment is applied from the beam end to the point of change in cross section ($0 < a < 117$), an expression is developed from Fig. 43a.

This gives:

$$1/2\ \tau_{b1} = \int_0^a \frac{Mx^2}{2}\frac{dx}{EI_o} - \int_0^{36} \frac{M}{L}\left(x' - \frac{x'^2}{L}\right)\frac{dx'}{EKI_o} - \int_{36}^{L-a} \frac{M}{L}\left(x' - \frac{x'^2}{L}\right)\frac{dx'}{EI_o}$$

$$1/2\ \tau_{b1} = -0.26635\ \frac{M}{E} + 3.5764 \times 10^{-5}\ \frac{M}{E}\ a^2$$

and for moment at b we get

$$M_b = .58192\ \frac{M}{E} - 7.8137 \times 10^{-5}\ \frac{M}{E}\ a^2 \quad \ldots\ldots\ldots\ldots\ (2.13)$$

for $0 < a < 117$.

In the same way, M_b is obtained for the case when the load is between the point of change in cross-section and the support b (Fig. 43b).

Working out the expression for M_b, we get:

$$1/2\ \tau_{b1} = \int_0^{117} \frac{M}{L^2} X^2 \frac{dx}{EI_o} + \int_{117}^{a} \frac{M}{L} X^2 \frac{dx}{EKI_o} - \int_0^{L-a} \frac{M}{L}\left(X' - \frac{X'^2}{L}\right)\frac{dx'}{EKI_o}$$

$$1/2\ \tau_{b1} = -0.106998\ \frac{M}{E} + 2.4124 \times 10^{-5}\ \frac{M}{E}\ a^2$$

then:

$$M_b = 0.23377\ \frac{M}{E} - 5.2705 \times 10^{-5}\ \frac{M}{E}\ a^2 \quad \ldots\ldots\ldots\ldots\ (2.14)$$

for $117 < a \leq 153$.

Now that expressions have been derived for the moment at middle support due to a unit concentrated load and an externally applied unit moment, the

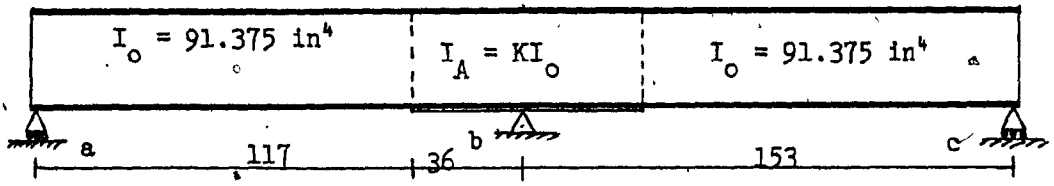

where $K = 1.4825$; then $I_A = KI_o = 135.468$ in⁴

Fig. 39 — Geometry and Properties of Continuous Girder with Cover-Plate.

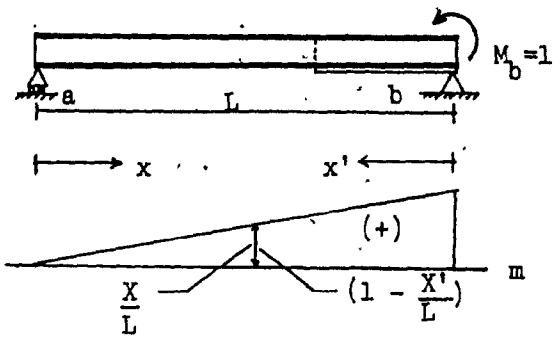

Fig. 40 — Moment in Girder Due to a Unit Moment Applied at b.

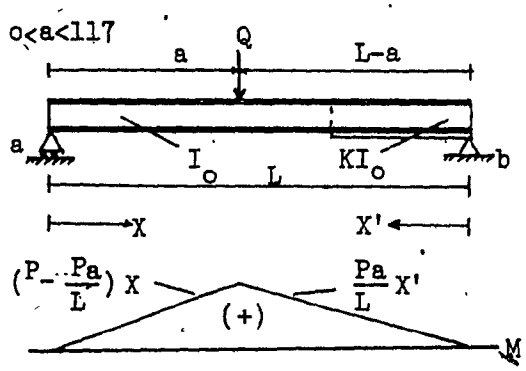

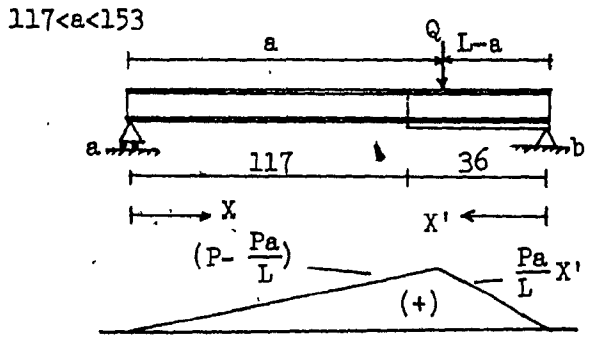

Fig. 41 & 42 — Moment in Girder Due to a Concentrated Load.

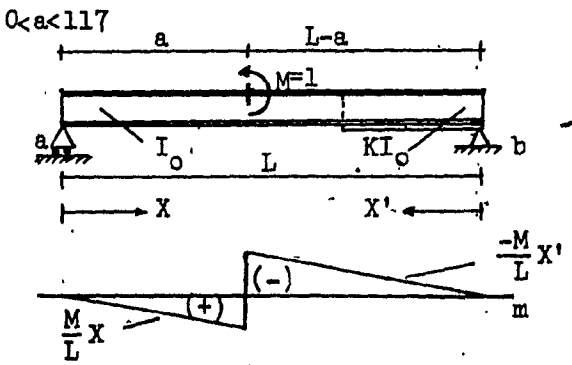

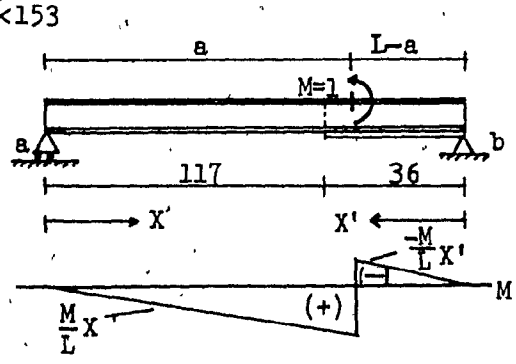

Fig. 43a & 43b — Moment in Girder Due to an Externally Applied Unit Moment.

prestressing moment for the continuous girder bridge with cover-plates under the action of a parabolic bent prestressing cable can be readily evaluated.

The loads shown in the equivalent loading system determined at the beginning of the example (Fig. 37) are now utilized in the computations. Finally, by substituting the numerical values of the various concentrated loads and externally applied moments in the expressions for M_b just derived we get the final prestressing moment over the middle support to be:

$$M_b = 7.2548\ P$$

where P is the force exerted by the prestressing cable (in pounds) and the units of M_b are lb-in.

The final prestressing moment diagram can now be plotted in the same manner as the previous example, but to avoid repetition it is omitted.

Comparing the result obtained in this example for the moment over the middle support ($M_b = 7.2548\ P$) with the one obtained in the previous example of the same continuous girder bridge but with no cover plates ($M_b = 5.80P$), Fig. 32, it can be concluded that the addition of cover-plate makes the prestressing cable originate greater prestressing moment over the middle support; this is to be expected since the rigidity of the continuous girder bridge over the middle support was increased.

Therefore, in design of continuous prestressed girder bridges, it could also be advantageous to add cover-plates in zones over the supports where the critical negative moment exists, in order to make the prestressing cables work more efficiently and at the same time to avoid a very heavy prestressing when a very shallow depth is required in the design of the bridge.

It has to be added at this point of the discussion that expressions 2.11 and 2.12 for moment over the middle support due to a concentra-

ted unit load can also be employed in calculating influence lines for the moment at any point along the continuous girder. Influence lines could be useful in the final stage of design when stresses due to dead load, prestressing and live load have to be superimposed in order to find maximum stress and check the stability of the bridge under design.

As a general conclusion for this chapter, it can be said that evaluation of prestressing moments in continuous girder bridges or even in rigid frame bridges under the action of prestressing forces exerted by high strength cables having any configuration, can be readily tackled by the equivalent load method that proved to be very versatile and fast.

CHAPTER 3

PLANNING OF THE EXPERIMENTAL PROGRAM

In order to confirm the validity of the analytical solution developed in previous chapter, an experimental investigation on a scale model was conducted as a part of this research.

A few experimental studies have been carried out in the field of prestressed steel girder bridges in the United States[10,11] Europe[2,3,9] and South Africa[12], but, to my knowledge, none of them has been applied to continuous girder bridges.

In planning a scale model for the experimental program various considerations have to be made regarding size, materials, fabrication methods for the scale model as well as instrumentation and recording of information during the tests. In the following discussions all of these aspects will be treated.

3.1 PLANNING OF THE MODEL

3.1.1 Size

In deciding on the size of the model two limitations were relevant: the space available for the model in the structural laboratory and the cost of the model itself.

Since the space assigned for the model was 25 feet, a scale reduction factor of 20 was found to be the most suitable for a continuous

girder bridge prototype of 500 ft long (see Appendix A). A smaller factor would have resulted in a model that had been too large, and a greater factor would have yielded a very small model that would be impracticable to work with because of the resulting shallow depth which would make the placement of the prestressing wires and the strain gauges very awkward. It was also considered that in a medium-sized model, reading of the strain would be more accurate than in a small model.

Fabrication tolerances were also taken into account in deciding on a medium-sized model. Detailing and cementing of small models are laborious and critical which increases the cost of fabrication.

Regarding cost, it was found that the difference in cost of materials for a medium-sized model compared to that of a small-sized model was too little to justify the sacrifice in accuracy and the convenience in performing the tests that a medium-sized model provides.

3.1.2 Materials

Three different materials were considered for the model: steel, aluminum and plexiglas.

Steel is the ideal material for the model because it is the same material of the prototype and hence they have the same properties and they behave in the same manner under the action of similar loads.

However, for fabrication of models steel has some disadvantages such as: the difficulty in welding thin and small plate elements that are required for the assemblage of the model; distortions in the model due to the heat generated in the welding process; and the excessive weight of the steel that would make the model very cumbersome to handle.

Aluminum was also considered as an alternative for the model because of its light weight and its low Young's modulus that produces

greater deformations than the steel under a relatively small load. But it was found that distortion also appears after cooling of welding and the material weakens substantially after the heat is introduced during the welding process. All these disadvantages and the high cost of fabrication made this alternative a poor choice for the model.

Plexiglas is a resin material widely used in structural models. It is an easily machinable material. Strong connections can be achieved by cementing the different parts with a bonding solvent. However, creep in plexiglas exists under the action of sustained loads. This is a characteristic very undesirable for modelling but it can be overcome because most of the creep occurs in the first six minutes of application of the sustained load and after which the modulus of elasticity displays little variation.

After studying the pros and cons in the three materials under consideration, plexiglas was chosen because of its ease in fabrication and handling. In order to overcome the problem of creep it was decided to allow the plexiglas to creep until stabilization, after which reading of the strain could be accurately effected. This operation should be repeated in any new variation in loading conditions. The problem of change of properties with the variations of temperature was of no concern because all the tests were to be carried out under constant temperature.

3.2 Design and Description of the Model

3.2.1 Similtude Conditions

The design of the model was made following the principles of similitude outlined in the book by Kinney[12] in order to have a specific relationship between model and prototype so that behaviour and response

of the prototype could be predicted from tests on the model.

In the case of statically loaded structures, as the case considered in our study, the following conditions of similitude should be satisfied: a) all corresponding linear dimensions and linear deflections must be in a constant ratio b) corresponding external loads, internal elastic forces and dead loads must be also in a constant ratio. These constant ratios are called "scale factors" and by applying these scale factors to the dimensions, properties and loads in the prototype, the corresponding dimensions, properties and loads for the model are determined.

From the application of the principles of structural mechanics the conditions of similitude are derived[12] and they are expressed mathematically in terms of the parameters involved and the scale factors.

Similitude in length is given by:

$$k\bar{L} = L \quad \ldots\ldots\ldots\ldots\ldots\ldots \quad (3.1)$$

where k is the scale reduction factor for length and it was previously set as 20 in order to meet the limitations of space and workability. (The dash on the top of the symbol indicates that the parameter refers to the model).

Similitude for Area is:

$$\frac{A}{\bar{A}} = k^2 z \frac{\bar{E}}{E} \quad \ldots\ldots\ldots\ldots\ldots\ldots \quad (3.2)$$

where z is an arbitrary factor introduced to give more flexibility to the design of the model and it will be called "prediction factor". It will be seen later that corresponding thickness fn the elements of the model is not possible to achieve according to the scale factor "k" and that thickness is chosen arbitrarily as convenient or subordinate to the availability of materials. This makes the introduction of the prediction factor necessary.

The relation of moduli of elasticity $\bar{E}/E$ makes provisions for the use of a different material in the model than that of the prototype. The other conditions of similitude to be satisfied are:

Section Modulus: $$\frac{S}{\bar{S}} = k^3 z \frac{\bar{E}}{E} \quad \ldots\ldots\ldots\ldots\ldots\ldots \quad (3.3)$$

Moment of Inertia: $$\frac{I}{\bar{I}} = k^4 z \frac{\bar{E}}{E} \quad \ldots\ldots\ldots\ldots\ldots\ldots \quad (3.4)$$

Deflection: $$\frac{\Delta}{\bar{\Delta}} = k \quad \ldots\ldots\ldots\ldots\ldots\ldots \quad (3.5)$$

Strain: $$\frac{\varepsilon}{\bar{\varepsilon}} = 1 \quad \ldots\ldots\ldots\ldots\ldots\ldots \quad (3.6)$$

Concentrated load: $$\frac{Q}{\bar{Q}} = k^2 z \quad \ldots\ldots\ldots\ldots\ldots\ldots \quad (3.7)$$

Uniformly distributed load: $$\frac{\omega}{\bar{\omega}} = kz \quad \ldots\ldots\ldots\ldots\ldots\ldots \quad (3.8)$$

Bending moment: $$\frac{M}{\bar{M}} = k^3 z \quad \ldots\ldots\ldots\ldots\ldots\ldots \quad (3.9)$$

It should be noted that conditions 3.3 and 3.4 would be automatically satisfied if the scale factor k were applied in all directions in the model but, as mentioned earlier, corresponding thicknesses are impractical to achieve. Therefore, by satisfying conditions 2.2, 2.3, and 2.4, results with no more than 1% error were obtained.[13]

Condition 2.5 for deflection is satisfied if the condition of moment of inertia is satisfied. The contribution of the shear and axial deformation exists in the model under the actions of loads, but generally,

in theoretical computations for practical structures it is not considered since these deformations are negligible compared to bending deformations.

3.2.2 Sectional Properties and Geometry of the Model

In this stage similitude conditions are applied in order to scale down the dimensions of the prototype to find the geometry and properties of the model.

In Appendix A, the design of a two-span continuous bridge is presented. This bridge is used in this study as a prototype. It dimensions and sectional properties are shown in Fig. 75. The steel used in the design of the girders in the prototype is A36 with a modulus of elasticity E = 29,000 ksi.

The mechanical properties of plexiglas are taken from the fabricator's manual.[14] The modulus of elasticity is $\bar{E}$ = 450 ksi and the rupture flexural strength is $\bar{f}_r$ = 16,000 psi but working stresses should not exceed 2,500 psi according to the fabricator's recommendations.

The dimensions of the model are found by scaling down the dimensions of the prototype according to the scale factor k = 20. However, in this model study, it was decided for reasons of workability to utilize a distorted model that would allow the use of a more convenient scale reduction factor in the vertical direction and hence to have a greater depth in the cross-section that would facilitate the installation of prestressing wires and strain gauges. It was found practical to have a depth of 10 inches in the cross-section. The deck of the model was made out of a single plexiglas sheet. The ribs of the deck in the prototype are not reproduced in the model because they can be substituted by using more material in the deck by means of a thick plate. This is a more economical solution that

does not affect the behaviour of the main carrying girder of the model as long as an equivalent sectional area of plexiglas in the model replaces the area of the ribs in the prototype.

In Fig. 44 it is shown the homologous (corresponding) cross-section "A" used in the central portion of the model over the middle support. The breadth of the cross-section is one-twentieth of the breadth of the prototype. The depth is 10 inches for the reasons explained before and the thickness of the plates were chosen arbitrarily seeking only to have the centroid of the cross-section in the same relative position as the cross-section "A" in the prototype. The geometry and the sectional properties are also shown in Fig. 44.

From this cross-section chosen arbitrarily the prediction factor (z) of the model is derived. This prediction factor must be employed in further determinations of homologous quantities in the model in order to be consistent in the design of the model. Therefore, the design of homologous cross-section "B" is not as adaptable. Prediction factor (z) is derived from similitude condition 2.4 for moment of inertia —

$$\frac{I}{\bar{I}} = k^4 z \frac{E}{\bar{E}}$$

$$z = \frac{1}{k^4} \frac{I}{\bar{I}} \frac{E}{\bar{E}} = 5.924$$

The theoretical homologous area for cross-section "A" is found from similitude condition 2.2

$$\bar{A} = \frac{E}{\bar{E}z} \frac{A}{k^2} = 16.35 \text{ in}^2 > \bar{A}_a = 8.83 \text{ in}^2$$

It is seen that the similitude condition for area is not satisfied but the

homologous cross section "A" is accepted providing that corrections in the results are made to make up for this deviation. The corrections to effect are explained in later discussions.

The required moment of inertia for homologous cross section "B" is found from similitude condition 2.4, its determination is accomplished according to the prediction factor (z) previously found. The moment of inertia of cross-section "B" in the prototype is $I_x = 1{,}446{,}352\ in^4$ (Appendix A); therefore, the homologous moment of inertia should be:

$$\bar{I}_x = \frac{E}{\bar{E}z} \frac{I_x}{k^4} = 98.3321\ in^4$$

After several trials a section with the homologous moment of inertia was found but this section had the limitation of not having the centroid in the same relative location as that of the prototype. Consequently, adjustments had to be made to correct the effects introduced by this deviation of the homologous cross-section "B". The geometry and sectional properties are shown in Fig. 45.

The theoretical homologous area for cross-section "B" is:

$$\bar{A} = \frac{E}{\bar{E}z} \frac{A}{k^2} = 14.35\ in^2 > \bar{A}_a = 7.46\ in^2$$

Again, the homologous area is not satisfied, therefore corrections had to be made with the resulting strains in the model so that stresses in the prototype could be accurately predicted.

Once the homologous cross sections A & B are found, the model is designed by scaling down the longitudinal dimensions and the main features of the prototype. Final drawings for the fabrication of model are shown in Fig. 46.

Note: all measurements are in inches.

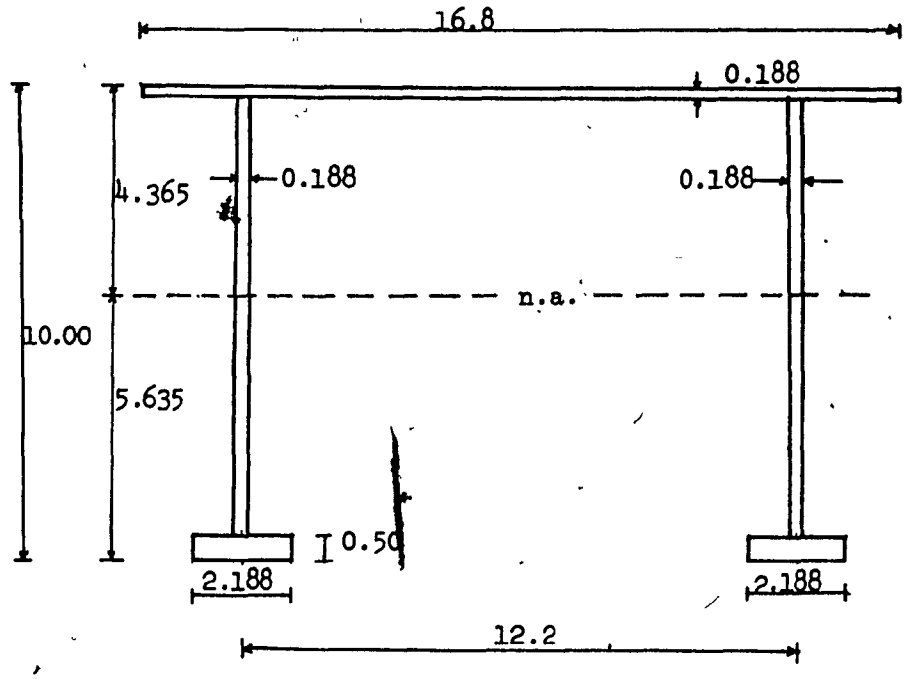

Properties:

$\bar{A}_a$ = 8.83 in^2

$\bar{I}_x$ = 146.998 in^4

$\bar{S}_t$ = 33.677 in^3

$\bar{S}_b$ = 26.087 in^3

Fig. 44 — Geometry and Cross-Sectional Properties of Cross-Section "A".

Note: all measurements are in inches.

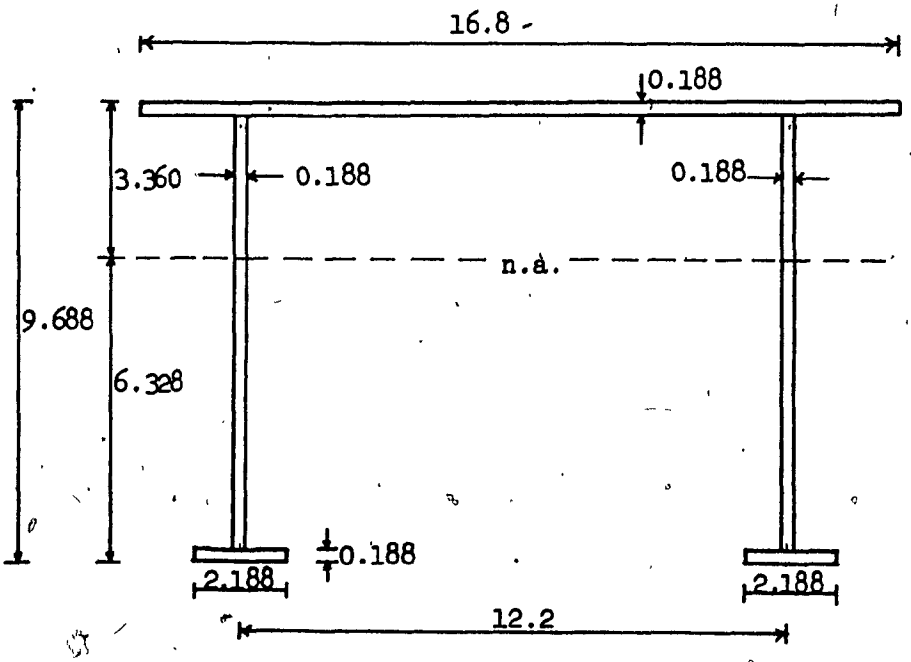

Properties:

$\bar{A}_a$ = 7.46 in^2

$\bar{I}_{xa}$ = 98.336 in^4

$\bar{S}_t$ = 29.267 in^3

$\bar{S}_b$ = 15.540 in^3

Fig. 45 — Geometry and Cross-Sectional Properties of Cross-Section "B".

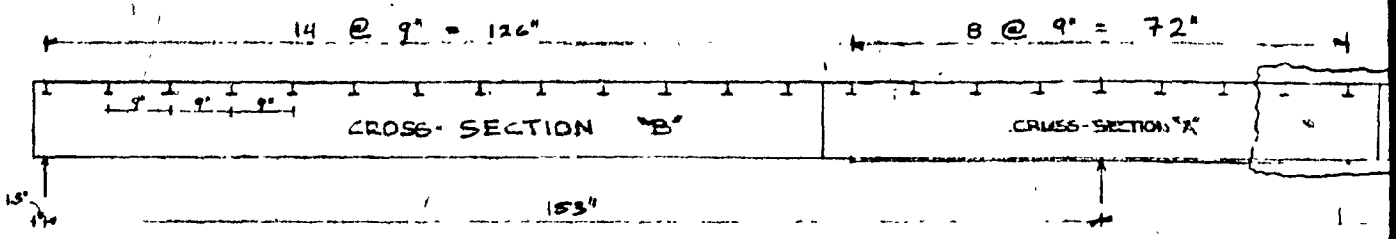

ELEVATION

1 of 1

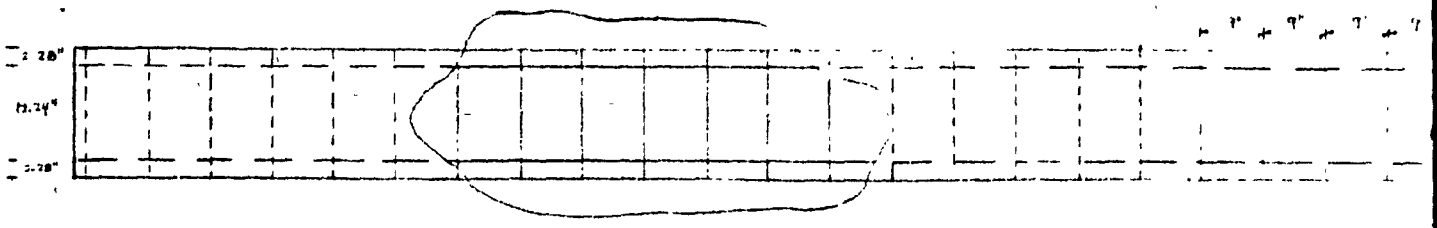

PLAN

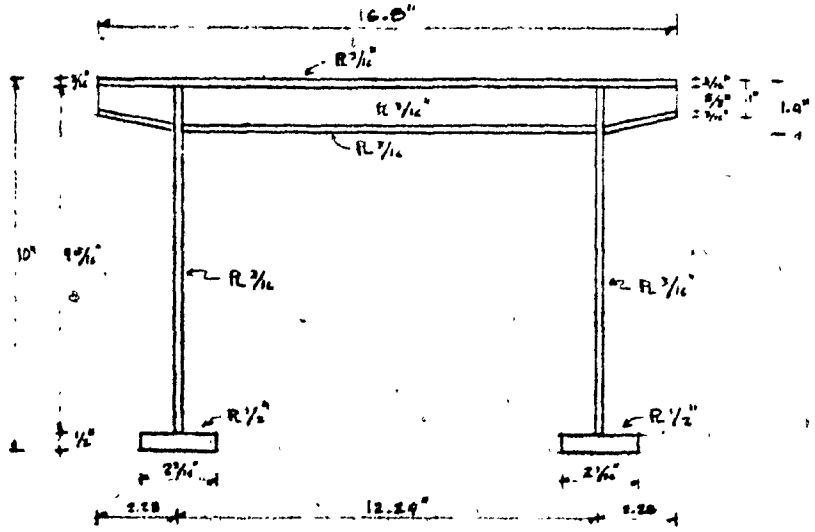

CROSS-SECTION "A"

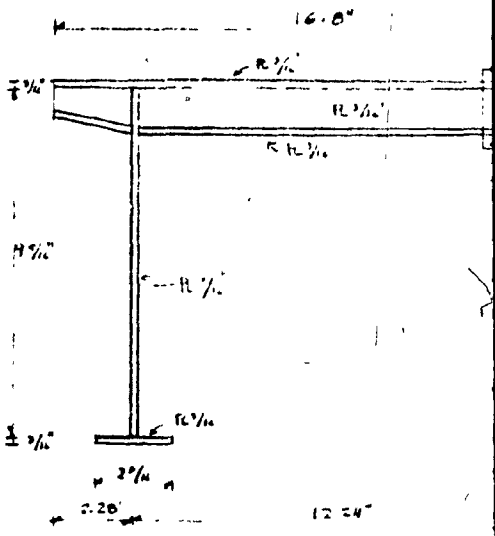

CROSS-SECTION

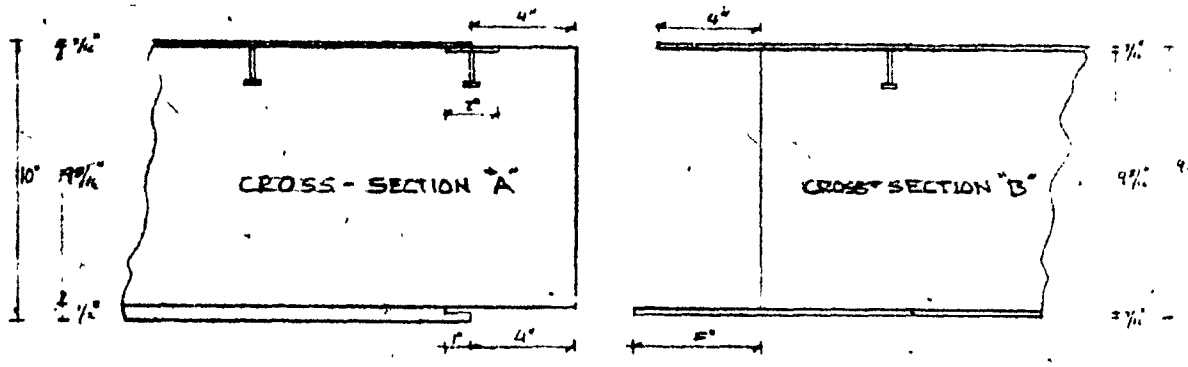

CONNECTION BETWEEN CROSS-SECTION "A" & "B"

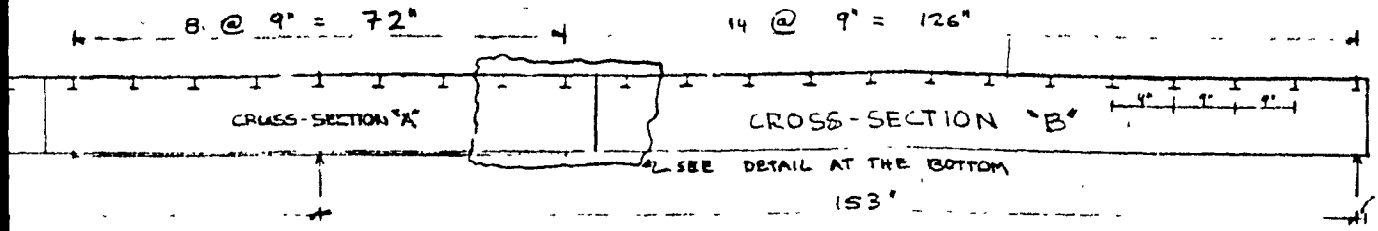

ELEVATION

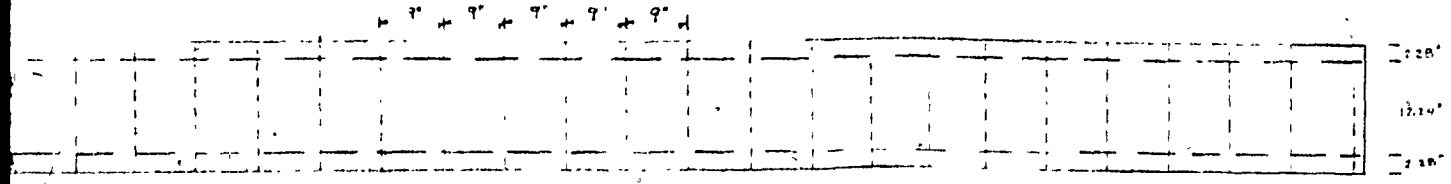

PLAN

1 2of2

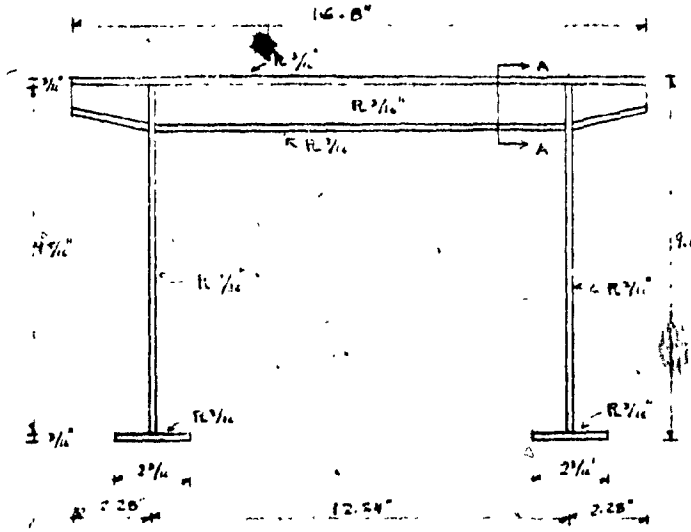

CROSS-SECTION "B"

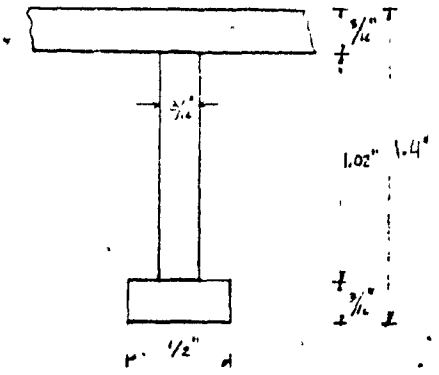

SECTION A-A
FLOOR BEAM

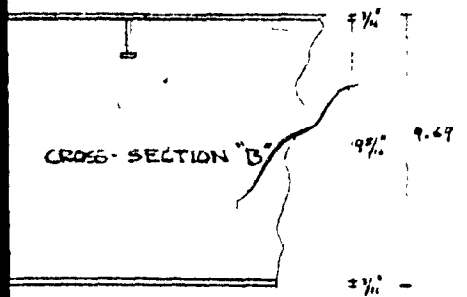

SECTION "A" & "B"

CONCORDIA UNIVERSITY

MODEL IN PLEXIGLASS OF A TWO-LANE CONTINOUS BRIDGE

FIG 46	OSCAR VALENCIA

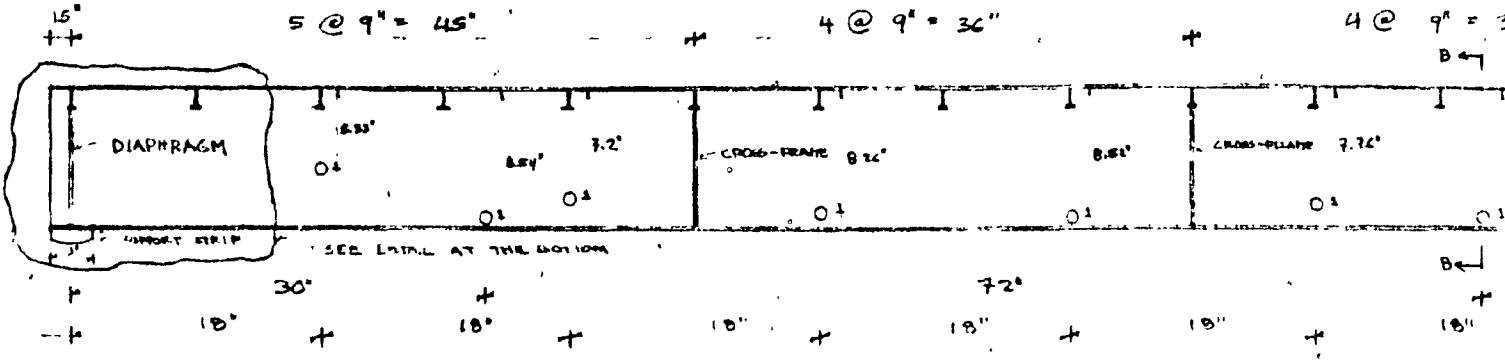

LOCATION OF SADDLES AND CR

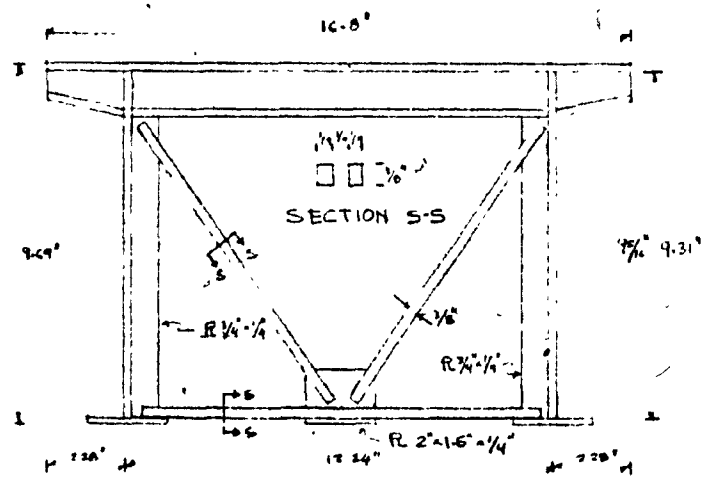

TYPICAL CROSS-FRAME

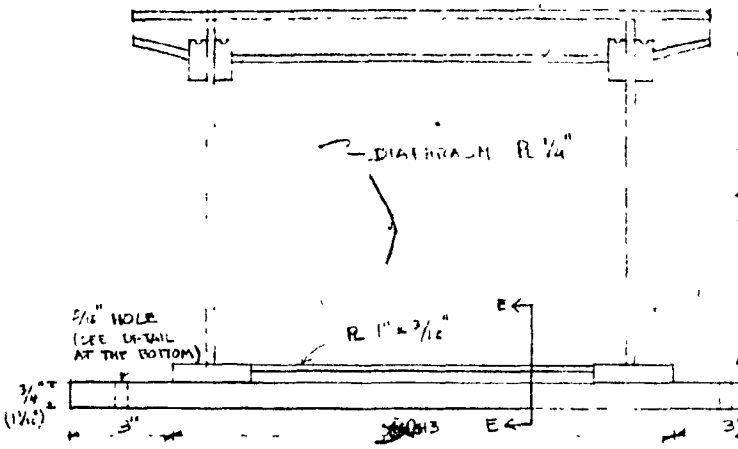

TYPICAL DIAPHRAGM & SECTION C-C

1 of 1

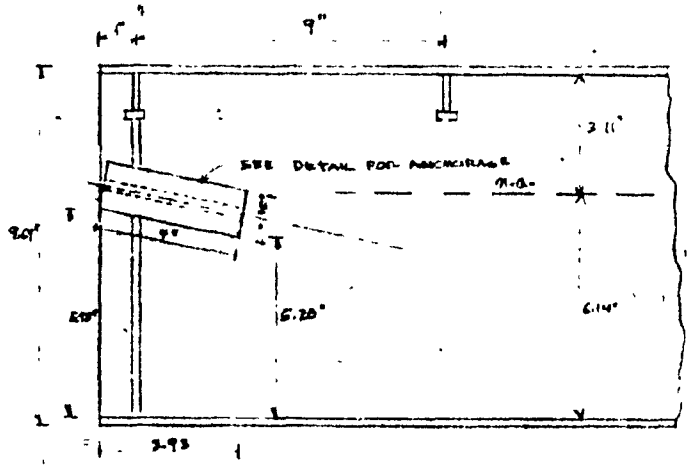

LOCATION OF END ANCHORAGE

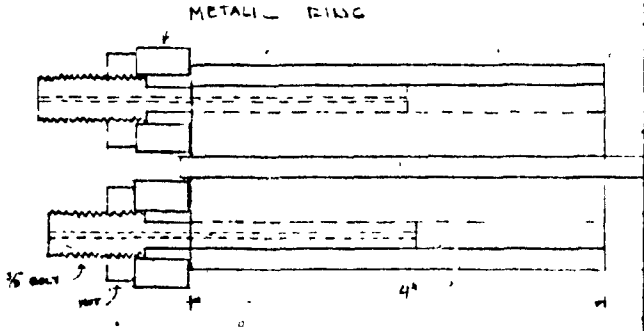

TWIN ANCHORAGE
TOP VIEW

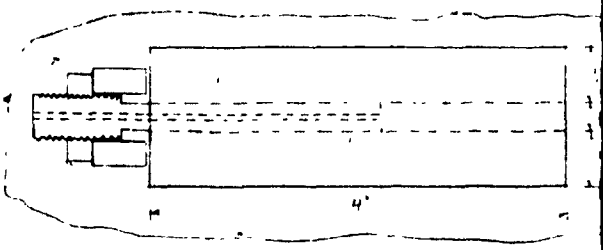

ANCHORAGE
SIDE VIEW

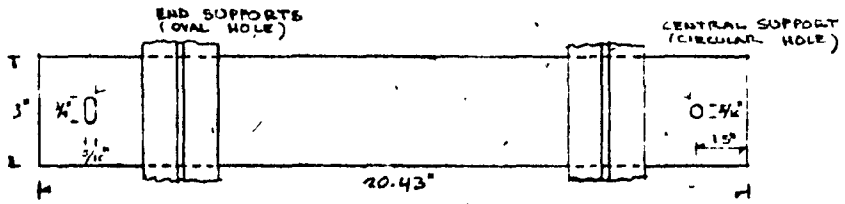

SUPPORT STRIP (PLAN) & DETAIL OF HOLES

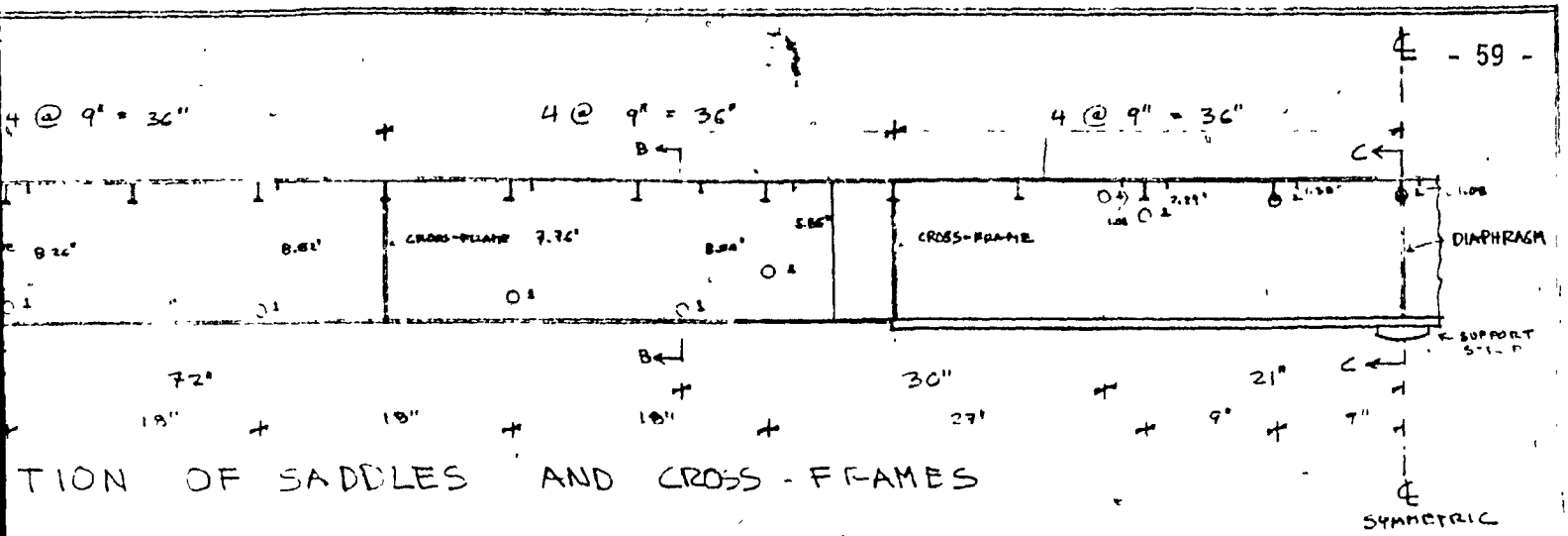

TION OF SADDLES AND CROSS-FRAMES

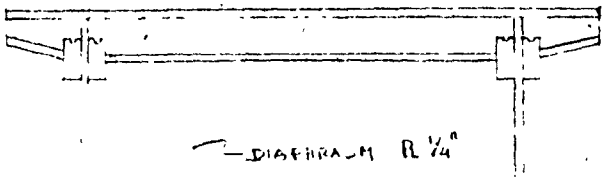

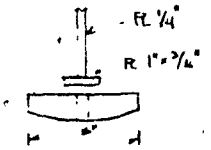

SECTION E-E

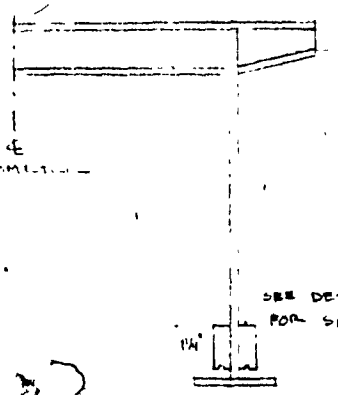

HALF SECTION B-B

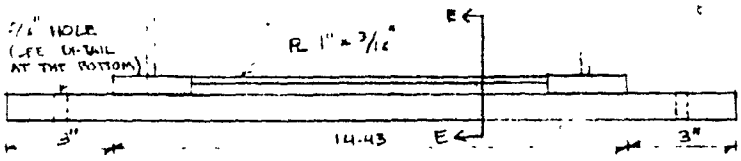

TYPICAL DIAPHRAGM & SECTION C-C

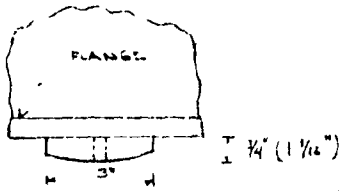

SUPPORT (SIDE VIEW)

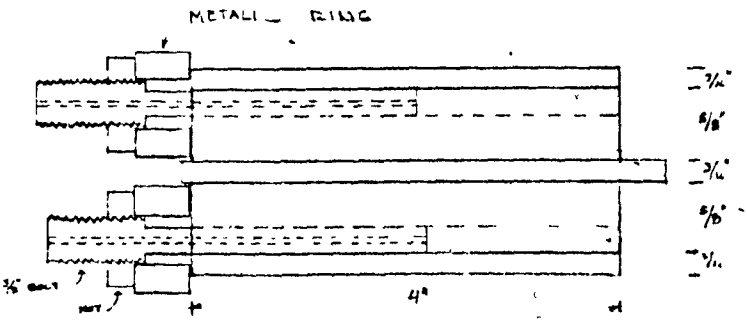

TWIN ANCHORAGE
TOP VIEW

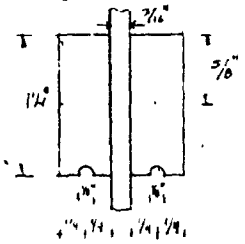

FRONT VIEW

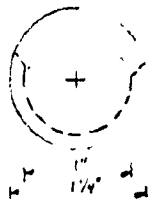

SIDE VIEW

SADDLE

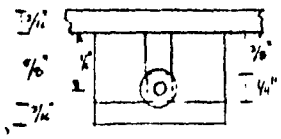

ANCHORAGE
FRONT VIEW

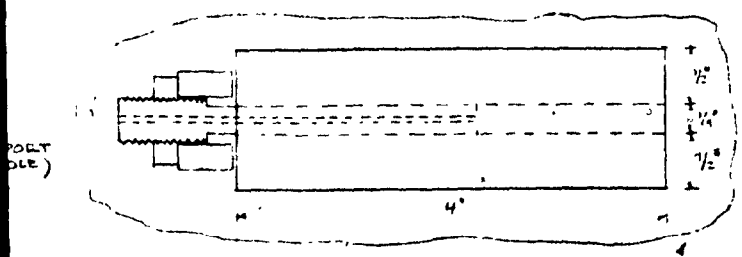

ANCHORAGE
SIDE VIEW

1 2of2

CONCORDIA - UNIVERSITY

MODEL IN PLEXIGLASS OF A TWO-LANE CONTINOUS BRIDGE

FIG. 46 | OSCAR VALENCIA

3.2.3 Prediction of Stresses in Prototype

From the results obtained in the model, homologous corresponding stresses can be ascertained for the prototype by applying certain corrections to the strain readings in the model in order to satisfy condition 2.6 of equal strains in model and prototype. Once this condition is satisfied, the homologous strain is multiplied by the modulus of elasticity (E) of the steel to get the stresses in the prototype. In this manner the transfer from model to prototype is accomplished.

The first step to be made is the separation of axial strain from bending strain, because the strain registered by the strain gauges during the tests is the combination of strain due to bending moment and strain due to axial forces.

This separation of strains is necessary in order to make the corrections to the deviations introduced by the distortion of the model, in other words strain should be resolved into its axial and bending components so that corrections can be made individually as corrections to the axial strain are different from those needed for bending strain.

The method employed in the division of strains is simply that of placing strain gauges in the top and bottom fibers of the cross-section under study. In this way, because of the linearity of strains in the elastic range, the existing distribution of strain is known in that particular cross-section.

In Fig. 47, it is shown how the combined strain is resolved into bending and axial strain. From Fig. 47 we can formulate two relations to express the condition of strains in top and bottom fibers.

$$\bar{\varepsilon}_1 = \frac{c_t}{\bar{d}}\,\bar{\varepsilon}_{be} + \bar{\varepsilon}_a \,, \qquad -\bar{\varepsilon}_2 = \frac{-c_b}{\bar{d}}\,\bar{\varepsilon}_{be} + \bar{\varepsilon}_a$$

Solving for $\bar{\varepsilon}_{be}$ and $\bar{\varepsilon}_a$ we get:

$$\bar{\varepsilon}_{be} = \bar{\varepsilon}_1 + \bar{\varepsilon}_2, \quad \bar{\varepsilon}_a = \frac{\bar{c}_b}{\bar{d}} \bar{\varepsilon}_1 - \frac{\bar{c}_t}{\bar{d}} \bar{\varepsilon}_2 \quad \ldots\ldots\ldots (3.10)$$

where $\bar{\varepsilon}_1$ and $\bar{\varepsilon}_2$ are taken as absolute values regardless they are due to compression or tension.

Now that axial and bending strains have been separated the corrections can be effected individually to axial or bending strains and then, accomplish the transferring of stresses to the prototype.

There are three corrections to be made: one for the variation in depth, another for the shift of the centroid from the homologous location and the other because of the deviation in the theoretical homologous cross-sectional area.

The correction factor for the variation in depth is determined by establishing the relation between the strain in the homologous ideal cross-section and the strain in the actual cross-section of the model (Fig. 48). The strain in the extreme fiber varies correspondingly as the depth changes.

From Fig. 48 a relation is formulated:

$$\frac{\bar{d}}{\bar{\varepsilon}_t + \bar{\varepsilon}_b} = \frac{\bar{d}_a}{\bar{\varepsilon}_{ta} + \bar{\varepsilon}_{ba}}; \quad \bar{\varepsilon}_t + \bar{\varepsilon}_b = \frac{\bar{d}}{\bar{d}_a} (\bar{\varepsilon}_{ta} + \bar{\varepsilon}_{ba})$$

The correction factor is thus the ratio of the depth of the ideal cross-section to the depth of the actual cross-section $\bar{d}/\bar{d}_a$.

To make the correction for the shift of the neutral axis from the homologous location, a relation for the strain in the extreme fiber is established from strain diagrams of Fig. 49a.

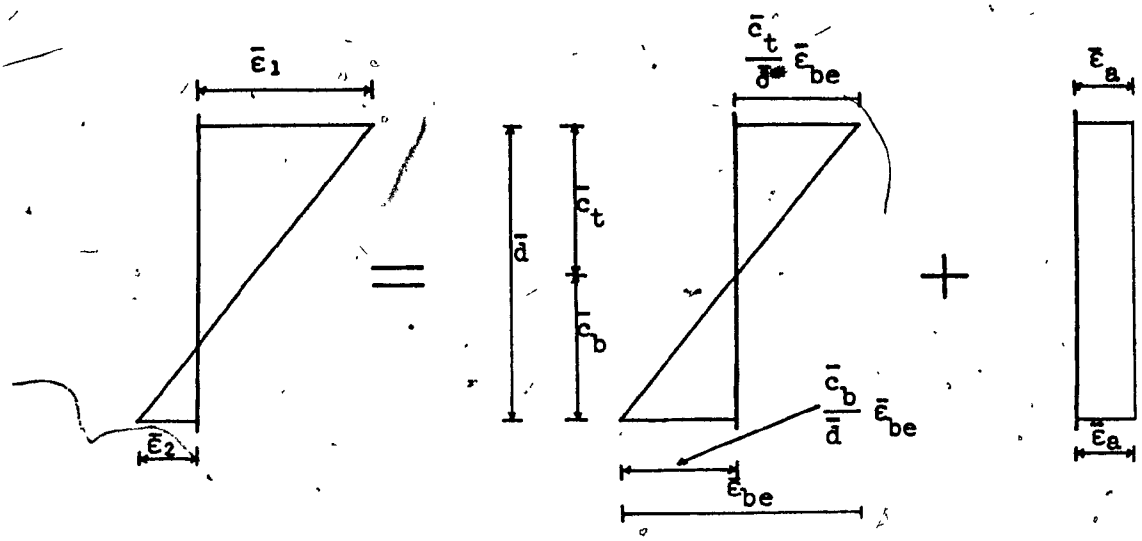

where: $\bar{\varepsilon}_1$ = strain read at the top of the cross-section
$\bar{\varepsilon}_2$ = strain read at the bottom of the cross-section
$\bar{\varepsilon}_{be}$ = bending strain
$\bar{\varepsilon}_a$ = axial strain
$\bar{c}_t$ = distance from centroid to extreme top fiber
$\bar{c}_b$ = distance from centroid to extreme bottom fiber

Fig. 47 — Splitting of Strain Into Its Bending and Axial Components.

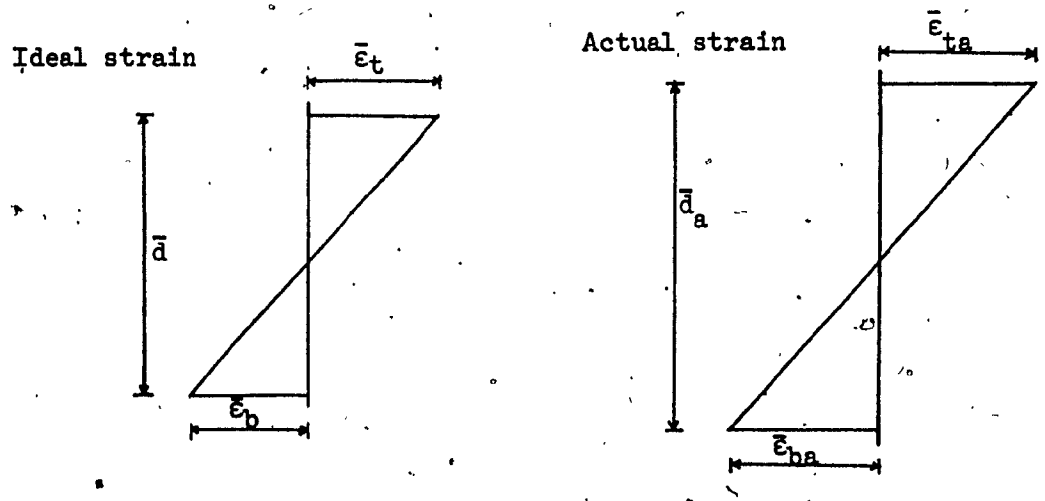

where: $\bar{d}$ = depth of the ideal homologous cross-section
$\bar{d}_a$ = depth of the actual cross-section in model
$\bar{\varepsilon}_t$ = strain at the top in the ideal cross-section
$\bar{\varepsilon}_b$ = strain at the bottom in the ideal cross-section
$\bar{\varepsilon}_{ta}$ = strain at the top in the actual cross-section
$\bar{\varepsilon}_{ba}$ = strain at the bottom in the actual cross-section

Fig. 48 — Strain Diagrams in Ideal and Actual Cross-Sections.

Ideal location of neutral axis:

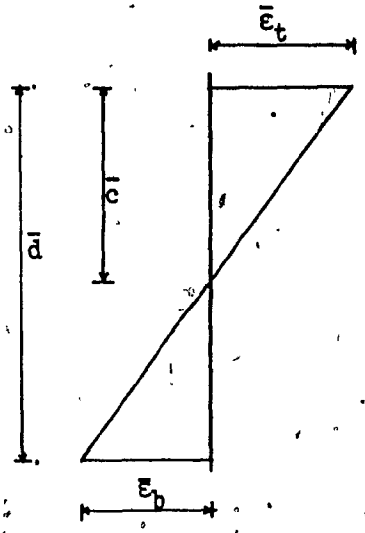

Actual location of neutral axis:

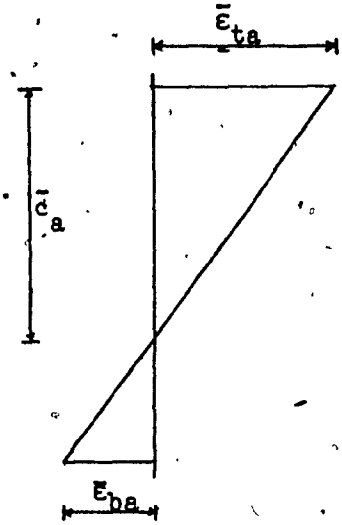

where $\bar{d}$ = depth of homologous cross section

$\bar{c}$ = distance from neutral axis to extreme fiber in homologous cross-section

$\bar{c}_a$ = distance from neutral axis to extreme fiber in actual cross-section

$\bar{\varepsilon}_t$ = strain at the top in ideal cross-section

$\bar{\varepsilon}_b$ = strain at the bottom in ideal cross-section

$\bar{\varepsilon}_{ta}$ = strain at the top in actual cross-section

$\bar{\varepsilon}_{ba}$ = strain at the bottom in actual cross-section

Fig. 49a — Location of Neutral Axis in Ideal and Actual Strain Diagrams.

Since the total strain in the two cross-sections is the same because they have equal depth and moment of inertia, we can write

$$\bar{\varepsilon}_t + \bar{\varepsilon}_b = \bar{\varepsilon}_{ta} + \bar{\varepsilon}_{ba}$$

then

$$\frac{\bar{c}}{\bar{\varepsilon}_t} = \frac{\bar{c}_a}{\bar{\varepsilon}_{ta}} \longrightarrow \bar{\varepsilon}_t = \frac{\bar{c}}{\bar{c}_a}\bar{\varepsilon}_{ta}$$

Therefore, the correction factor for the shift of the neutral axis is the ratio of the distance from the neutral axis to the extreme fiber in the ideal cross-section to the same distance in the actual cross-section $\bar{c}/\bar{c}_a$.

It is possible that the moment of inertia in the actual model may differ from the calculated because of errors due to tolerances in fabrication. Therefore, another correction should be introduced to counteract this possible error. The correction factor in this case is the ratio of the actual moment of inertia to the calculated moment of inertia $\bar{I}_a/\bar{I}$. With this, homologous strains for the theoretical calculated cross-section are determined.

Now that the correction factors have been found the expression for predicting the stresses in the prototype is assembled.

We know that stress in the prototype is equal to the product of modulus of elasticity and the strain, i.e., $f = E\varepsilon_p$. We have seen that in order to satisfy condition (6) of strain, ($\varepsilon_p = \bar{\varepsilon}$) we need to multiply the strain in the distorted model by the different correction factors already defined. So we have that strain in prototype is:

$$\varepsilon_p = \frac{\bar{d}}{\bar{d}_a}\frac{\bar{c}}{\bar{c}_a}\frac{\bar{I}_a}{\bar{I}}\bar{\varepsilon} \qquad \ldots\ldots\ldots\ldots\ldots\ldots\ldots\ldots \quad (3.11)$$

and stresses in prototype (f) can be predicted with the expression:

$$f = \varepsilon_p E_c = \left(\frac{\bar{d}}{\bar{d}_a}\frac{\bar{c}}{\bar{c}_a}\frac{\bar{I}_a}{\bar{I}}\bar{\varepsilon}\right)E \quad \ldots\ldots\ldots\ldots\ldots\ldots \quad (3.12)$$

For the deviation in the homologous cross-sectional area another correction is introduced so that axial stresses can be also predicted in the prototype once axial strain have been separated from bending strains by the method previously explained. The correction factor in this case is the ratio of the actual area in the cross-section to the homologous ideal area $\bar{A}_a/\bar{A}$.

The condition of equal strains $\varepsilon_p = \bar{\varepsilon}$ can now be satisfied and the strain in the prototype is found by multiplying axial strain in the distorted model by the correction factor $\bar{A}_a/\bar{A}$ as follows:

$$\varepsilon_p = \frac{\bar{A}_a}{\bar{A}}\bar{\varepsilon} \quad \ldots\ldots\ldots\ldots\ldots\ldots \quad (3.13)$$

and axial stress can be predicted with the expression:

$$f = E\,\varepsilon_p = E\,\frac{A_a}{\bar{A}}\bar{\varepsilon} \quad \ldots\ldots\ldots\ldots\ldots\ldots \quad (3.14)$$

3.2.4 Loads in Model

A definite relation should exist between the load in the model and the load used in the design of the prototype. This relation is given by the conditions of similitude stated in previous discussions and has to be satisfied so that results obtained in the model could be useful in the prediction of stresses in the actual bridge (prototype).

In our study, the effects of two loads are of interest: the prestressing and the live load. Stresses due to dead load can be evaluated directly in the prototype once the weight of the bridge is known or, in the preliminary stage of design, by assuming an approximate dead load.

In Appendix A, the prestressing force in the prototype was found to be $P = 1{,}344{,}000$ lb., then by using relation of similitude 3.7 for concentrated load $\bar{P} = \frac{P}{k^2 z}$ the prestressing force required in the model is found to be $\bar{P} = 567.1$ lb. However, it was found more practical to use a smaller prestressing force in the model. Therefore, another factor called "slicing factor" (Y) was introduced in order to work with a smaller force on the tests on the model. A prestressing force of $\bar{P} = 200$ lb was chosen arbitrarily to use. Thus, the slicing factor value was $Y = 2.836$. This prestressing force was applied by means of 2 high strength wires of 0.055 in. diameter.

By using a smaller prestressing force than that required, stresses in the prototype obtained through results in the model would be 2.836 times smaller, which is the reduction introduced by the slicing factor (Y). Therefore, in order to get valid results in the prototype, stresses computed with formula 3.12 must be multiplied by the slicing factor (z). Formula 3.12 thus becomes:

$$f = Y\left(\frac{\bar{d}}{\bar{d}_a}\frac{\bar{c}}{\bar{c}_a}\frac{\bar{I}_a}{\bar{I}}\bar{\varepsilon}\right)E$$

For the determination of the homologous live load to be used in the tests, the AASHO[15] HS-20 live load used in the design of the prototype was considered in this calculation. The truck load was chosen in preference to a uniformly distributed equivalent live load on the model since the uniform load would require more preparations for the test; preparations that would not be justified since AASHO gives the choice of using either truck load or equivalent live load. Besides, the truck load represents the actual conditions more closely than the equivalent live load.

Two loading cases were studied: the case of maximum negative moment over the support when both spans are loaded (Fig. 49b) and the case of maximum positive moment at the midspan occuring when only one span is loaded (Fig. 49b).

The load W specified for the truck load is 20 tons or W = 40,000 lb. Therefore, by using expression 3.7 of similitude for concentrated load $\bar{Q} = \frac{Q}{k^2 z}$ and by introducing the slicing factor (Y) already found we get that the homologous weights to be used in simulating the truck load are: $0.2\bar{W}$ = 1.19 lb and $0.8\bar{W}$ = 4.76 lb (see Fig. 49b). These weights must be applied directly on the main girders and not on the transverse beams in order to prevent transverse stresses in the model that would make interpretation of results more complex.

3.3 INSTRUMENTATION

Strain gauges were employed in the measurement of strains in the model during experimentation and they were strategically located so that intensity of bending moment could be known at the most critical points in the model.

Strain gauges were installed by pairs at all the different points to be studied. One strain gauge was placed at the top fiber and the other at the bottom fiber of the same section. This installation by pairs was used so that the values of the strain in the extreme fibers would give the required exact strain distribution in a desired location in order to accomplish the separation of the bending and axial strains at the point under consideration.

Strain gauges were located along one side only in one span of the model. This is possible because of the symmetry of the model and the prestressing wires with respect to the longitudinal and transverse axes.

All measurements are in inches.

Maximum negative moment:

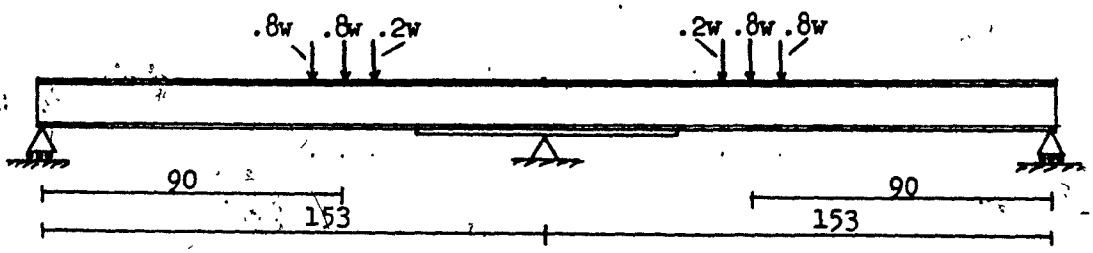

Maximum positive moment:

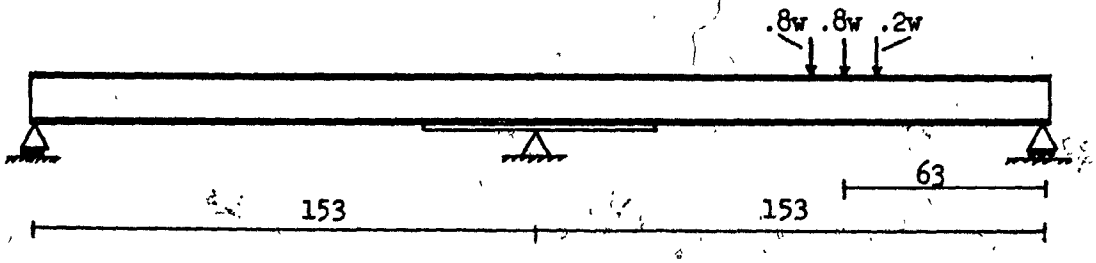

where: $w = 40{,}000$ lb

$\bar{w} = 5.953$ lb

Fig. 49b — Conditions for Maximum Positive and Negative Moments.

In this way, the number of strain gauges required for the tests was considerably decreased.

The strain gauge locations are shown in Fig. 50. It can be seen that they are distributed all along one span and that they are more closely located near the middle support where more attention is put in the design of a continuous bridge because of the critical negative moment produced by the uniformly distributed dead load and the live load as well.

It should be noted that strain gauges are only placed at points in between transverse beams where the cross-section is not affected by any cuts during fabrication. In this way undesired stresses due to holes and cuts are avoided in the tests.

The prestressing force applied by the prestressing wires in the model were measured with a steel load-cell having the shape and dimensions shown in Fig. 51.

Two strain gauges were installed on the flat faces of the load-cell for measuring the existing axial strain. Two gauges were necessary in order to eliminate any possible bending strain that could be introduced in the load-cell by the existence of any small eccentricity. This bending strain would not be eliminated with only one strain gauge placed on face of the load cell because the bending strain in that face would be added to the axial strain, whereas with two opposite strain gauges the bending strain is eliminated when the readings of the two gauges are added because of the opposite sign of the bending strains.

The load-cells were calibrated in the Universal Testing Machine available in the Structural Laboratory, so that the exact axial strain in the load-cells would be known for a specific load even without knowing the cross-sectional area and modulus of elasticity of the load-cell.

Note: all measurements are in inches.

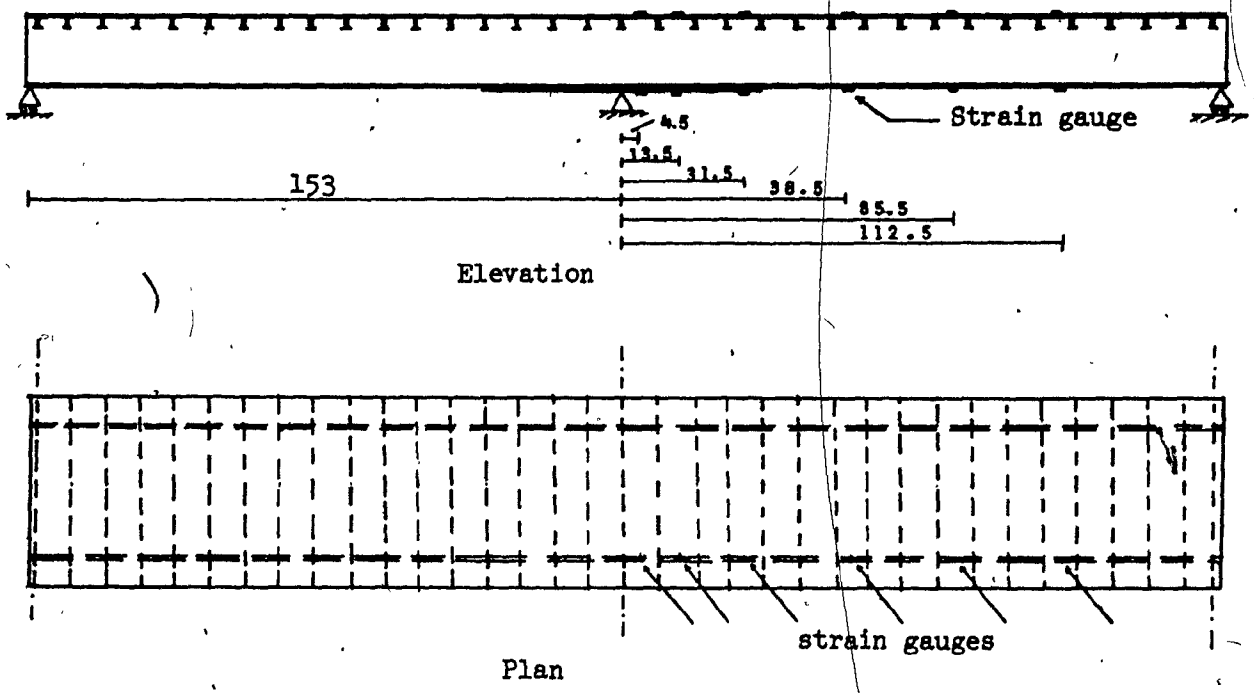

Fig. 50 — Location of Strain Gauges.

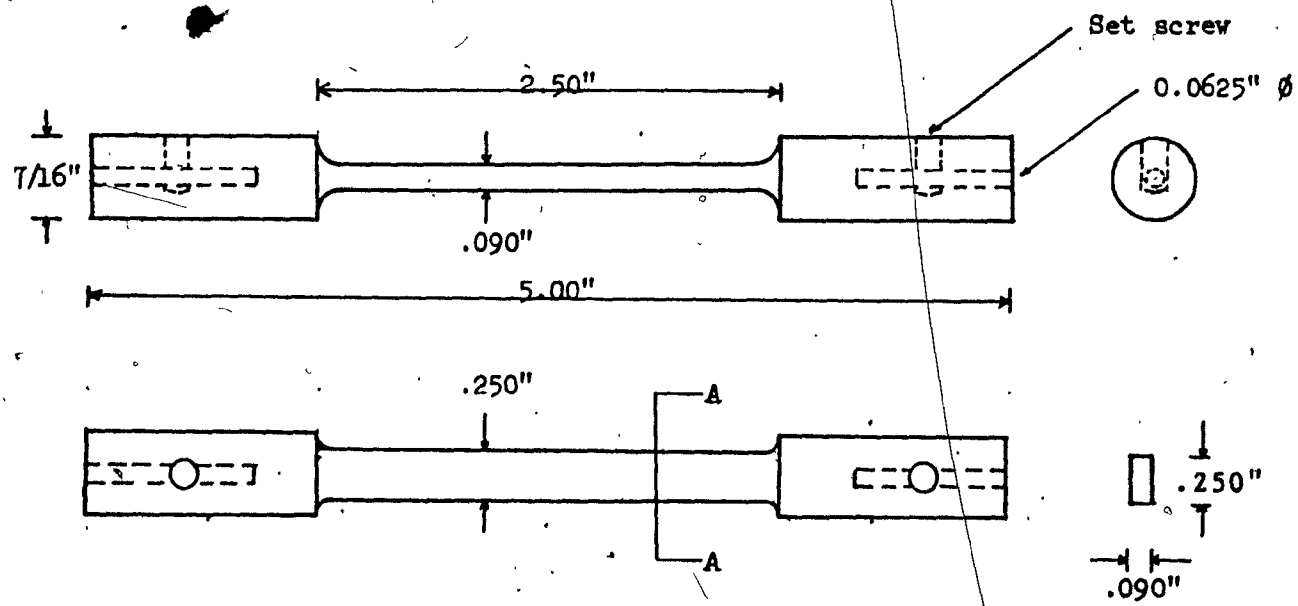

Fig. 51 — Load Cell.

Once the load-cells are calibrated, the corresponding axial strain in the load-cell for the prestressing force required for the tests can be known. In this way, the exact prestressing force is applied to the model and the possibility of introducing an error will be lessened.

For the reading of the strains registered by the strain gauges the Data Acquisition System (Digital Data Logger, B&F Model SY161-6-100-V4-P4) available in the Structural Laboratory, was utilized. This apparatus has capacity for simultaneous reading of 30 independent channels and can perform any reading at any desired time.

CHAPTER 4

EXPERIMENTAL PROGRAM

4.1 FABRICATION DEFECTS AND ADJUSTMENTS

Fabrication of the model was executed according to drawings (Fig. 46) provided to fabricator. For ease of fabrication and transportation, the model was divided into three sections. Once the model was on place in the structural laboratory, it was assembled and cemented permanently and then supported on carefully levelled wooden support stands (Fig. 52).

Measurements of the model were according to the drawings, but it was found that the plate thicknesses did not exactly coincide with those specified in drawings because of existing tolerances in the thickness of plexiglas sheets.

Since it was not feasible at this stage to correct this defect in fabrication, it was decided to use the model in its actual condition but some adjustments would be required for the interpretation of stresses from model to prototype.

After measuring the thickness of the various plate elements in the model at random locations, an average for the thickness of the different elements was determined so that cross-sections made out with average plate thicknesses could be used in computations and in this way minimize

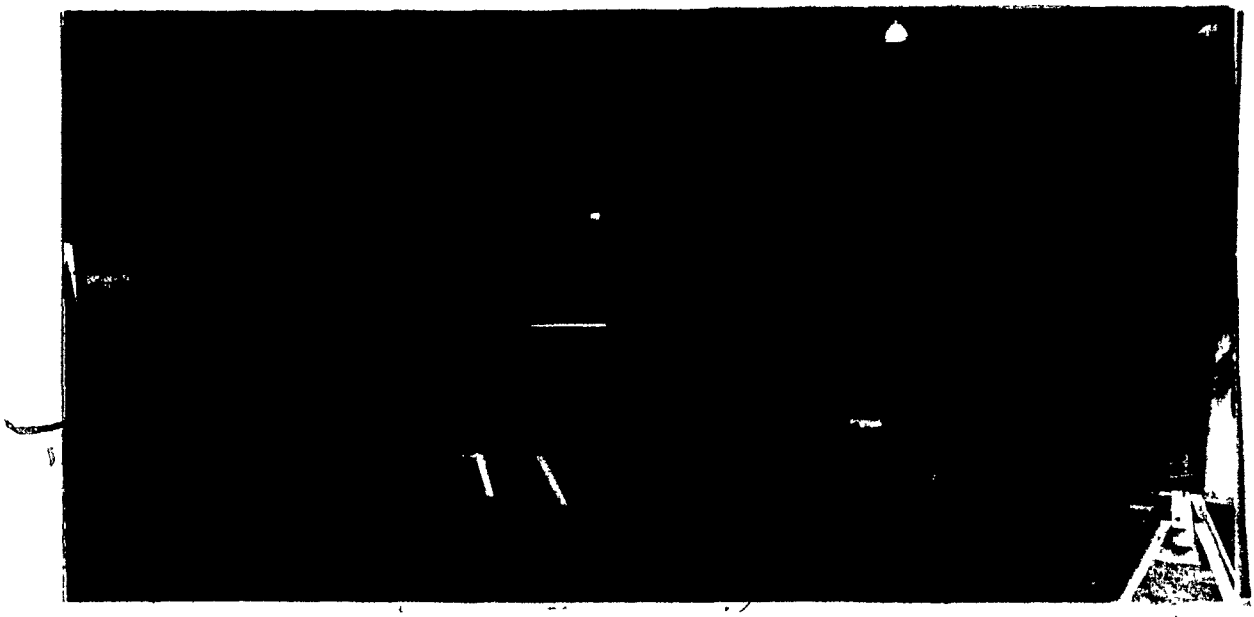

Fig. 52 — General View of Model.

errors. The resulting cross-sections "A" and "B" are shown in Fig. 53, and as can be seen, the properties do not differ much from the properties of the cross-sections originally planned in previous chapter (Figs. 44 and 45).

A new prediction factor and a new slicing factor were determined for the new cross-sections. Using similitude condition 3.4 for moment of inertia $\frac{\bar{I}}{I} = k^4 z \frac{\bar{E}}{E}$, the prediction factor (z) for cross-section "A" was found to be $z = 6.4286$ and for cross-section "B" $z = 6.3755$. The two prediction factors should be the same in order to have exact similitude between model and prototype but they differ in 0.8 per cent. This means that a small error will be introduced in the transferring of stresses from model to prototype. In the computations an average value, $z = 6.402$, was used as a prediction factor.

The value for the slicing factor (Y) for a prestressing load of 200 lb was found to be $Y = 2.6242$.

4.2 Test Set-Up

Six different cable configurations were studied in separate tests. These were chosen as the most likely cable configuration for a practical prestressed continuous girder bridge design. They are shown in Fig. 54 along with the corresponding names to be used in further discussions.

Prestressing force was achieved by stretching high strength piano wire of 0.055 in. diameter placed along the model and anchored at the ends by means of the anchorage devices shown in Fig. 55. It can also be seen in Fig. 55 that screws and nuts were used to apply the tension to the wire. The connection between wire and screw was accomplished by using the clamps shown in Fig. 55.

Note: all measurements are in inches.

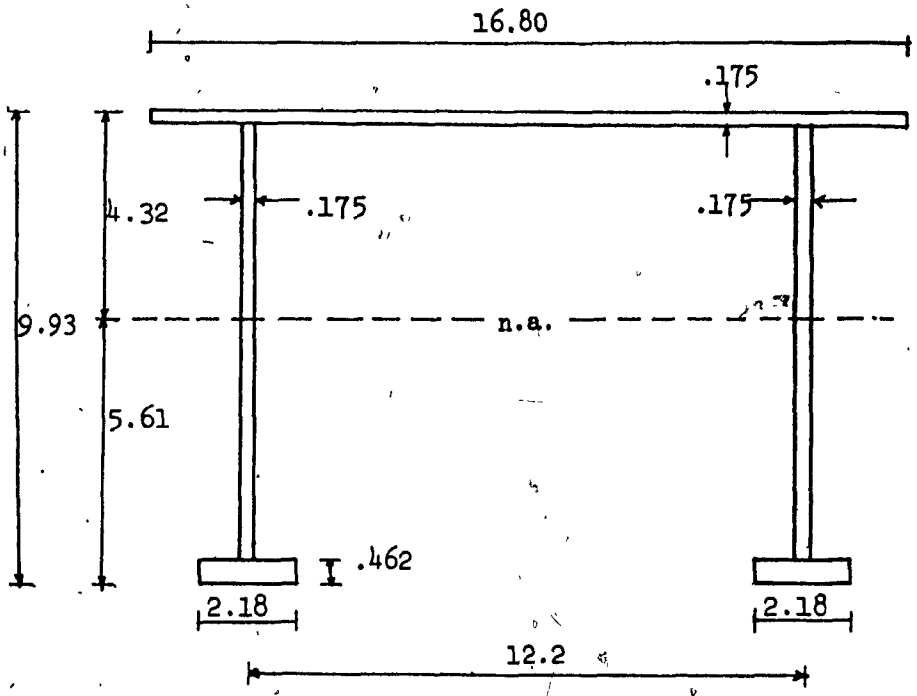

Cross-section "A" (over the central support)

Properties:

$\bar{A}_a = 8.22 \text{ in}^2$

$\bar{I}_{xa} = 135.468 \text{ in}^4$

$\bar{S}_t = 31.352 \text{ in}^3$

$\bar{S}_b = 24.142 \text{ in}^3$

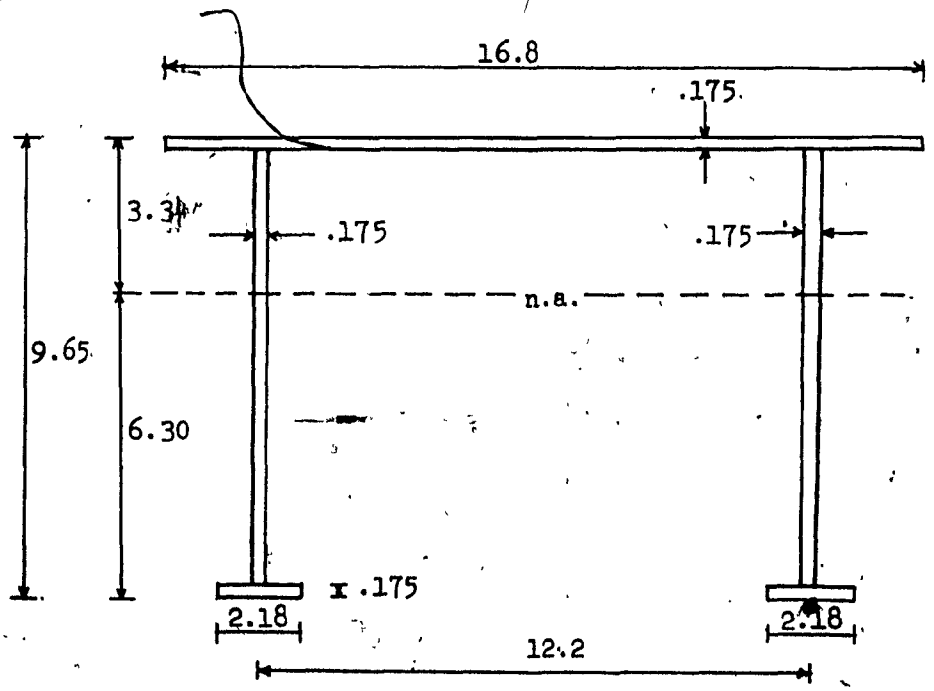

Cross-section "B"

Properties:

$\bar{A}_a = 6.97 \text{ in}^2$

$\bar{I}_{xa} = 91.374 \text{ in}^4$

$\bar{S}_t = 27.354 \text{ in}^3$

$\bar{S}_b = 14.493 \text{ in}^3$

Fig. 53 — Actual Geometry and Sectional Properties of Cross-Sections in the Model.

Note: all measurements are in inches.

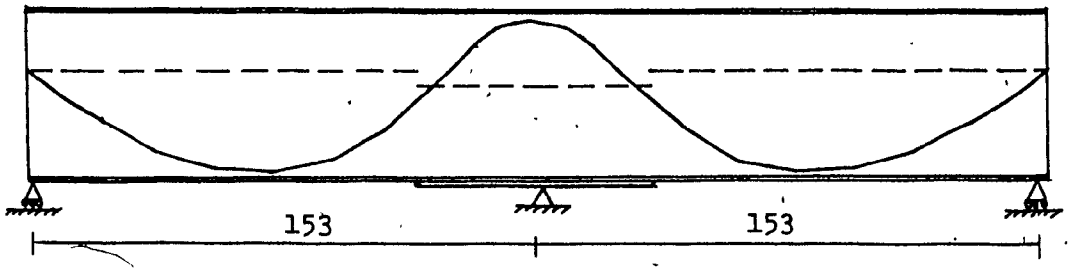

Parabolic configuration

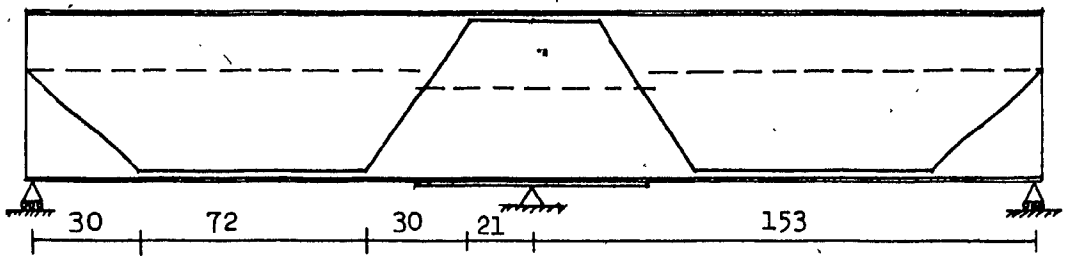

Trapezoidal configuration

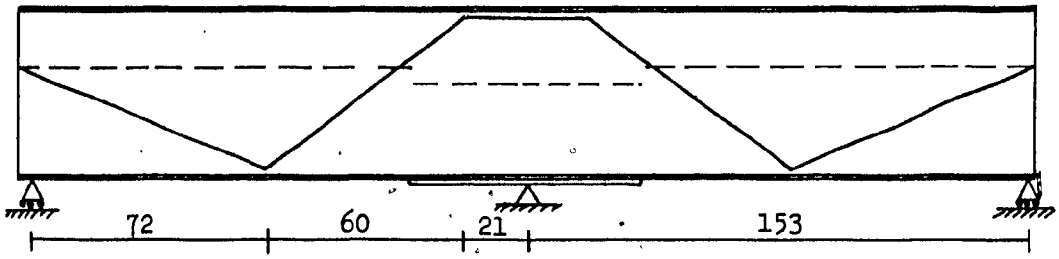

Trapezoidal-triangular configuration

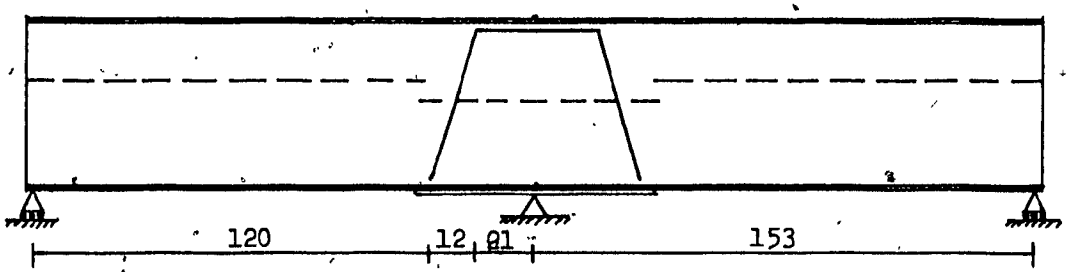

Draped segmental configuration

Fig. 54 — Cable Configuration Under Study.

by the Data Acquisition System.

These undesirable strains could not be prevented but awareness of their existence and their magnitude was necessary to account for them where applicable. It was decided to leave the first false strain due to the heat in the strain gauge in the final reading of strains since its oscillation pattern was difficult to determine and the false strain introduced was negligible in comparison with actual strain in the model due to loads.

The second undesirable strain due to fluctuations in temperature produces only axial strain in the model that can be isolated from the bending strain in the way explained in the previous chapter.

But, because of this introduction of temperature strain in the model the evaluation of the axial compressive strain due to the prestressing force had to be sacrificed. In this way, the results were limited to the determination of bending strains that in the case of girders are the most important.

4.3 Test Procedure

Before the application of any load on the model, all strain gauge channels were set to zero level of strain. This means that the level of strain existing in the model under no-load conditions was considered as a point of reference. The prestressing force was then gradually applied by the wires into the model by tightening the nuts at the end of the anchorage devices.

Once the total prestressing force was fully applied, a time of seven minutes was allowed to elapse in order to let the creep of the plexiglas to stabilize. The reading of the strain in all the strain gauges was

then taken. These results thus obtained are the strains due to prestressing alone. They are necessary to determine the behaviour of the model under prestressing and thus to obtain the actual prestressing moments in the model.

The concentrated truck loads were next applied, and again, allowing the plexiglas to creep for seven minutes. This operation was repeated twice; once for the condition of maximum negative moment with truck loads at 0.6L on both spans and the other for the condition of maximum positive moment with truck loads at 0.4L on one span only. These results are necessary for determining the behaviour of the model under live load. Superposition of the different loads acting on the bridge was used to obtain the final total stress in any desired location.

Since the results obtained in the first test with the truck load acting on the prestressed model matched closely the analytical results (Table 5.2) it was decided to shorten all the subsequent tests by studying only the behaviour of the model under prestressing forces exclusively.

The test procedure previously described was first made in trial tests using four prestressing wires in the trapezoidal configuration with a prestressing force of 100 lb. each. Two of the wires were in the inner part of the two webs, the other two were in the outer part of the webs. Another test was performed in the same trapezoidal configuration but only the two outside wires were employed with the same prestressing force of 100 lb. per wire. The results obtained in the second test were exactly half of the values in the first test, which proved that it was not necessary to place prestressing wires in pairs at each side of the web to avoid the excentricity produced by a single cable in only one side of each web. One cable or bunch of cables in only one side of each web can be readily used

because the transverse moment introduced by the asymmetry is negligible. Fig. 62 illustrates the location of the wires in both tests.

Because of the points described above it was decided for reasons of simplifying the tests to perform all the subsequent tests with only the two outside wires.

All subsequent tests were carried out satisfactorily and results agreed very closely with the analytical results of the formulas derived in Chapter 2. All tests were performed a second time in order to verify the results obtained in the first test and when a blunder was evident in one of the tests a third test was performed immediately after.

In the following chapter, a comparison of the analytical and experimental results is presented, along with comments and conclusions about the six different cable configurations studied in the experimental part.

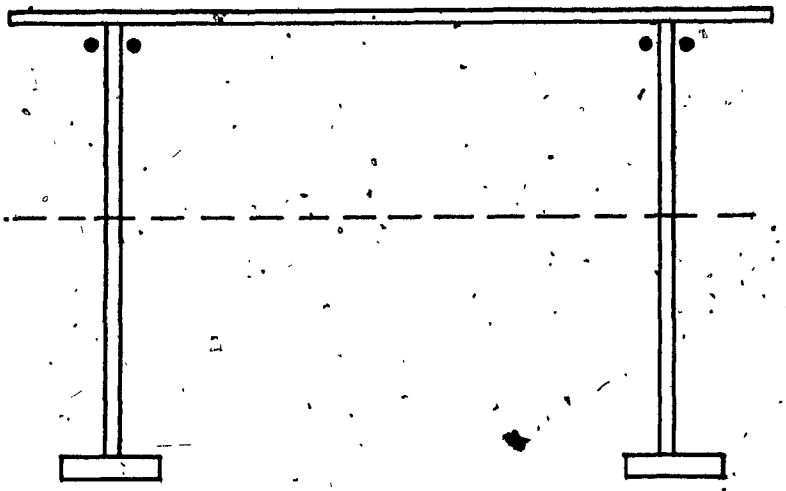

Four Wire Set-Up

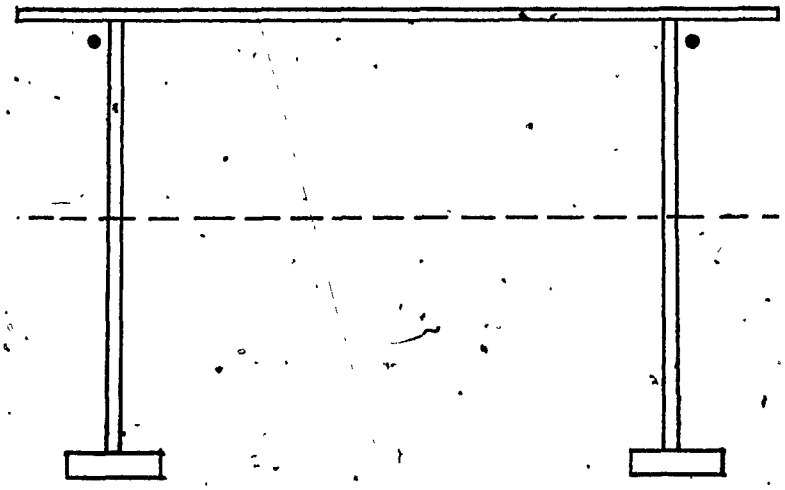

Two Outside Wire Set-Up

Fig. 62 — Four and Two Wire Set-Ups.

CHAPTER 5

TEST RESULTS AND CONCLUSIONS

5.1 PARABOLIC WIRE CONFIGURATION

Results obtained from the parabolical wire configuration were employed for the purpose of transferring the stresses from model to prototype. For the other five wire configurations considered in the experimental part of this research, conclusions will be drawn directly from the strains and bending moments obtained in the model. As stated before, this was possible because the model behaves exactly as a full scale bridge since the model was designed according to the principles of similitude outlined in Chapter 3, having as a prototype the actual bridge designed in Appendix A.

Fig. 63 shows the wire configuration explained in Chapter 2 and the locations where the strain were recorded.

Table 5.1 presents the bending strains obtained in the test. These strains are utilized in transferring the stresses to the prototype (minus sign indicates compressive strains). Bending strains were separated from axial strains by using expression 3.10 in Chapter 3. In the same table the comparison of the analytical and experimental bending moments as well as the deviation existing in the experimental results with respect to theoretical results are also presented. At the top of the table

Note: all measurements are in inches.

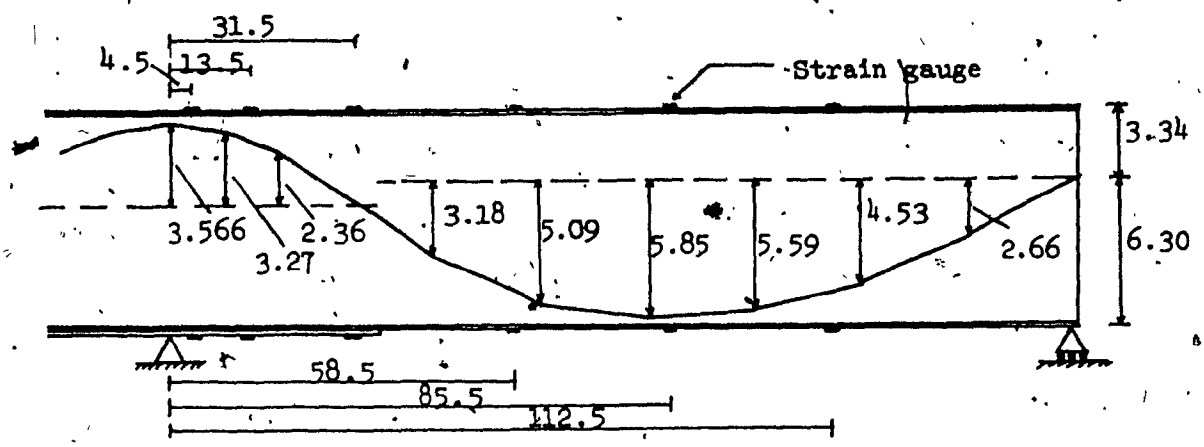

Fig. 63 — Parabolic Configuration and Strain Gauge Location.

Table 5.1 — Results for Parabolic Configuration.

Location of point under study: Distance to Central Support	4.5"	13.5"	31.5"	58.5"	85.5"	112.5"
Experimental results; prestressing force P = 200 lb						
Bending strain at top (millionths)	-96.7	-83.5	-40.9	40.9	69.3	63.0
Bending strain at bottom (millionths)	125.4	108.5	53.1	-77.1	-130.7	-118.9
Experimental moment (lb-in)	1363	1178	577	-503	-853	-776
Analytical results; prestressing force P = 200 lb						
Secondary moment (lb-in)	716	673	586	456	326	195
Basic moment (lb-in)	684	563	-16	-923	-1157	-959
Prestressing moment (lb-in)	1400	1236	570	-467	-832	-764
Deviation of experimental results						
Deviation (%)	-2.6	-4.7	-1.3	+7.7	+2.5	+1.6

the location in the model of the different sections under consideration is shown.

It can be seen in Table 5.1 that the experimental results agree very closely with the analytical results computed in the example of section 2.6, Chapter 2, for the parabolic configuration. This, therefore, validates the mathematical model developed in Chapter 2.

Table 5.2 shows the bending strains for the condition of maximum negative moment due to truck loads on the prestressed model. It also indicates strains for the condition of maximum positive moment when the truck load is in one span only. The table also shows the bending moment obtained from these experimental results and this is compared with the analytical bending moment obtained by superimposing the moment due to prestressing plus the moment originated by the truck load above. We can see that the results agree closely verifying experimentally that, in the design stage, the superposition of stresses due to the different loads acting on a prestressed girder bridge is valid.

Stresses in the prototype were derived from strains measured in the model with expression 3.15 derived in Chapter 3. They are presented in Table 5.3. This table shows the stresses at the top and bottom fibers at the different homologous locations in the bridge girder. These stresses are due to the prestressing force alone and due to truck loads plus prestressing force. Corresponding bending moments are included in the table as well.

5.2 Trapezoidal Wire Configuration

This configuration is shown in Fig. 64. We can observe that it is composed of straight portions of wire forming trapezoidal shapes. One

Table 5.2 — Results for Tests With Truckloads Applied to the Model Prestressed With the Parabolically Bent Wires.

Location of point under study						
Distance to Central Support	4.5"	13.5"	31.5"	58.5"	85.5"	112.5"
Experimental results for condition of maximum negative moment						
Bending strain at top (millionths)	-54.8	-52.6	-31.3	15.9	46.1	49.2
Bending strain at bottom (millionths)	71.2	68.4	40.7	-30.1	-86.9	-92.8
Experimental moment (lb-in)	773	743	442	-196	-567	-605
Analytical results by superposition (maximum negative moment)						
Moment due to truck load (lb-in)	-636	-485	-182	262	310	186
Prestressing moment (lb-in)	1400	1236	570	-467	-832	-764
Total moment (lb-in)	764	751	388	-205	-522	-578
Experimental results for condition of maximum positve moment						
Bending strain at top (millionths)	-81.8	-76.1	-44.4	10.4	21.1	38.1
Bending strain at bottom (millionths)	106.2	98.9	57.6	-19.6	-39.9	-71.9
Experimental moment (lb-in)	1154	1074	626	-128	-260	-469
Analytical results by superposition (maximum positive moment)						
Moment due to truck load (lb-in)	-278	-175	30	337	602	406
Prestressing moment (lb-in)	1400	1236	570	-467	-832	-764
Total moment (lb-in)	1122	1061	600	-130	-230	-358

Table 5.3 — Stresses in Prototype Determined by Transferring Results Obtained in Tests on Model.

Location of point under study						
Distance to central support	4.5"	13.5"	31.5"	58.5"	85.5"	112.5"
Transferred stresses due to prestressing alone						
Bending stress at top (lb/in^2)	-5430	-4689	-2297	2187	3892	3538
Bending stress at bottom (lb/in^2)	6993	6050	2961	14608	-7812	-7107
Prestressing moment (k-in)	183100	158400	77520	-67580	-114600	-104200
Transferred stresses due to prestressing plus truck load (max. negative moment)						
Bending stress at top (lb/in^2)	-3077	-2954	-1758	850	2465	2631
Bending stress at bottom (lb/in^2)	3971	3814	2270	-1799	-5194	-5547
Bending moment (K-in)	103900	99860	50420	-26380	-76170	-81340
Transferred stresses due to prestressing plus truckload (max. positive moment)						
Bending stress at top (lb/in^2)	-4593	-4273	-2493	556	1128	2037
Bending stress at bottom (lb/in^2)	5922	5515	3212	-1171	-2384	-4297
Bending moment (K-in)	155000	144400	84090	-17180	-34970	-63020

straight portion is located at the top of the girder over the middle support. This portion counteracts the critical dead load moment over the central support. At midspan there is another straight portion counteracting the maximum negative moment.

The test was satisfactorily carried out and results are shown in Table 5.4. It can be seen that the comparison of experimental and analytical moment at the various locations shows very close agreement which confirms again the validity of the mathematical model.

This trapezoidal cable configuration would be preferable than the parabolic shape in an actual design of a prestressed girder bridge because it requires a fewer number of saddles (cable supports) to give the required shape to the prestressing cable. Also, the prestressing moment obtained with a trapezoidal configuration counteracts efficiently the dead load moment all along the bridge. At the same time, it can be observed from Table 5.9, where the six configurations of the experimental part are compared, that the trapezoidal configuration gave the highest positive moment over the middle support with same cable eccentricity at that location. This occurs because the secondary moment has a favourable sign and higher value in the trapezoidal configuration than in the others.

5.3 Trapezoidal - Triangular Wire Configuration

This configuration has a similar shape to the case before except for the straight portions of the wire missing at the bottom (Fig. 65). This configuration was studied because it required less saddles than the trapezoidal and could be employed in designs where only the dead load negative moments are critical.

Note: all measurements are in inches.

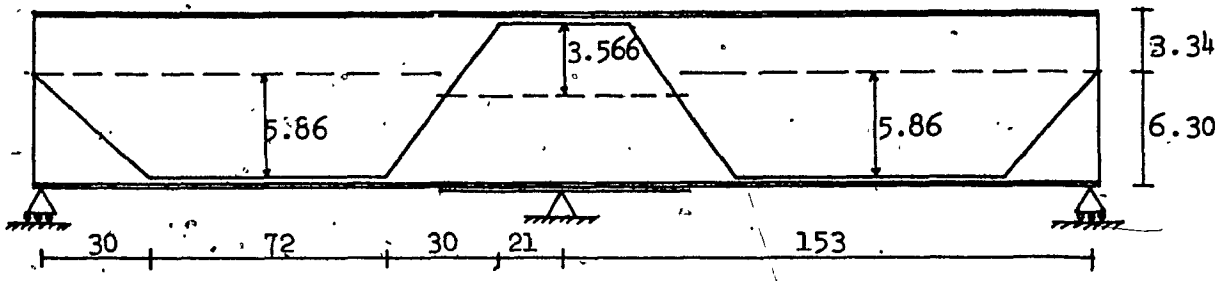

Fig. 64 — Trapezoidal Wire Configuration.

Table 5.4 — Results for Trapezoidal Configuration.

Location of point under study

Distance to central support	4.5"	13.5"	31.5"	58.5"	85.5"	112.5"

Experimental results; prestressing force P = 200 lb

Bending strain at top (millionths)	-103.3	-98.5	-51.2	54.9	67.3	77.7
Bending strain at bottom (millionths)	141.2	135.6	70.1	-109.8	-133.4	-154.3
Experimental moment (lb-in)	1535	1473	761	-716	-870	-1006

Analytical results; prestressing force P = 200 lb

Secondary moment (lb-in)	807	758	660	514	367	220
Basic moment (lb-in)	713	713	122	-1172	-1172	-1172
Prestressing moment (lb-in)	1520	1471	782	-659	-805	-952

Deviation of experimental results

Deviation (%)	+1.0	+0.1	-2.7	+8.7	+8.0	+5.7

Test results are presented in Table 5.5. It can be seen again that the resulting experimental bending moment agrees closely with the analytical moment.

If the results obtained in this test are compared with the results in the previous case of trapezoidal configuration (Table 5.4), it can be remarked that the prestressing moment over the middle support has diminished by about 50%. This is not very advantageous because the middle support is the location where the counteracting prestressing moment is needed at the most. Therefore, it can be said that savings gained by reducing the number of saddles in the triangular-trapezoidal configuration were offset by the great loss in efficiency and also not much was gained by the decrease in length of the prestressing cable. Consequently, it would be preferable in an actual design to use the trapezoidal configuration.

5.4 Draped-Segmental Wire Configuration

This is a new variation of the trapezoidal configuration. It consists of a segmental wire with a trapezoidal shape, located in the zone of negative dead load moment over the support (Fig. 66). In this alternative an economic and efficient solution is sought for the case of continuous girder bridges with critical negative moment over the supports. Fig. 66 shows a rational approach to location of the wire. In this instance wire is provided only where it is needed for the dead load negative moment, thus cutting down the length of the prestressing cable substantially.

The test was repeated 3 times in this case as some of the results did not agree with the analytical values. The discrepancies in the three tests were not consistent, but appearing in different locations in each test. This suggests that an error was introduced by the measurement sys-

Note: all measurements are in inches.

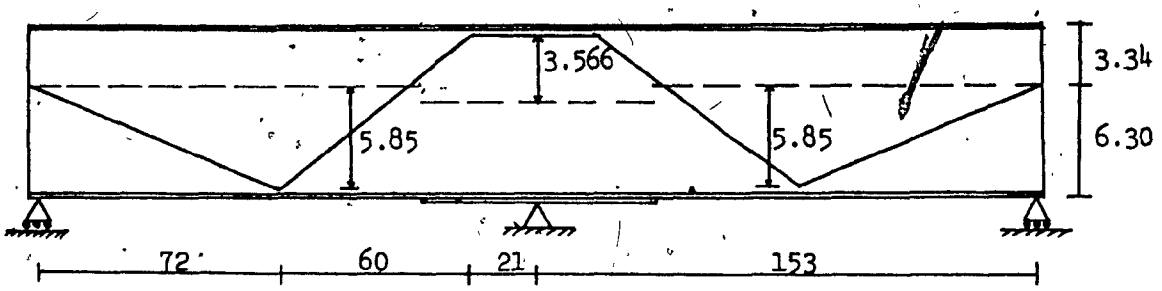

Fig. 65 — Trapezoidal-triangular Wire Configuration.

Table 5.5 — Results for the Trapezoidal-triangular Configuration.

Location of point under study

Distance to Central Support	4.5"	13.5"	31.5"	58.5	85.5"	112.5"

Experimental results; prestressing force P = 200 lb

Bending strain at top (millionths)	-73.1	-70.9	-47.9	27.7	78.6	49.2
Bending strain at bottom (millionths)	94.9	92.1	62.2	-52.3	-148.4	-92.8
Experimental moment (lb-in)	1031	1000	675	-341	-968	-605

Analytical results; prestressing force P = 200 lb

Secondary moment (lb-in)	306	287	250	195	139	83
Basic moment (lb-in)	713	713	390	-537	-1097	-658
Prestressing moment (lb-in)	1019	1000	640	-343	-958	-575

Deviation of experimental results

Deviation (%)	+1.2	0.0	+5.4	-0.5	+1.0	+5.3

tem. This error was magnified because the strain in those particular locations is very low and this causes the error to appear enlarged. Therefore, the error was disregarded and the test results were considered valid (Table 5.6).

There was one point in the model where the disagreement was consistently high in the three tests. That was the point located at 31.5 inches from the support almost coinciding with the starting point of the prestressing wire. Since it was the only result consistently off and everything else was in agreement with the theory it may be concluded that the mathematical model developed in this study does not give accurate results in the zone close to the starting of the wire.. This is to be expected since stresses in the vicinity of concentrated loads cannot be evaluated with simple theory but require special analysis. However, the evaluation of those stresses is not within the scope of this research.

5.5 Segmental Wire Configuration

This alternative consists of a straight segment of wire located in the zone of dead load negative moment over the central support (Fig. 67). This alternative is an attempt to find a more economical and rational solution for the cases of continuous girder bridges where the negative dead load moment governs the design, as for example, for the case of multiple-equal-span-girder bridge.

Again, some of the results were off in the tests but they were disregarded because the discrepancy did not appear in the same location in all cases, and as was explained in the test before, the machine induced error is amplified in the results because of the low level of strain in the part of the model where these discrepancies occurred. Whereas, in

Note: all measurements are in inches.

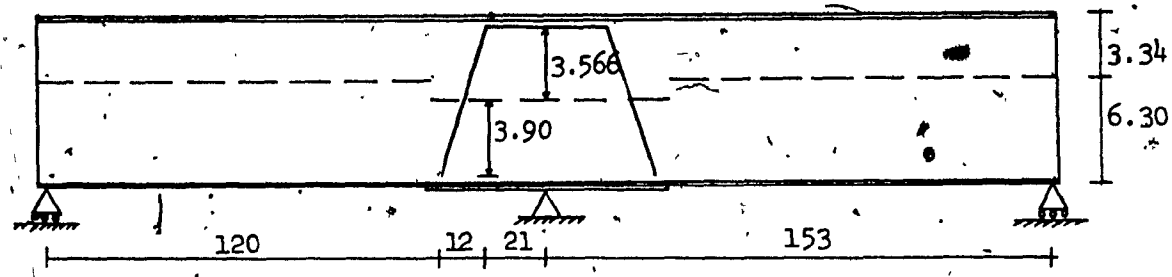

Fig. 66 — Draped-Segmental Wire Configuration.

Table 5.6 — Results for Draped-Segmental Configuration.

Location of point under study

Distance to Central Support	4.5"	13.5"	31.5"	58.5"	85.5"	112.5"

Experimental results; prestressing force P = 200 lb

Bending strain at top (millionths)	-34.8	-37.4	39.2	12.5	8.3	5.5
Bending strain at bottom (millionths)	45.2	48.6	-50.9	-23.5	-15.7	-10.5
Experimental moment (lb-in)	491	528	-552	-154	-102	-68

Analytical results; prestressing force P = 200 lb

Secondary moment (lb-in)	-215	-202	-176	-137	-98	-59
Basic moment (lb-in)	713	713	-593	0	0	0
Prestressing moment (lb-in)	498	511	-769	-137	-98	-59

Deviation of experimental results

Deviation (%)	-1.4	+3.2	-28.2	+12.1	+4.6	+16.2

locations such as the middle part of the model where prestressing strains are relatively high the problem did not arise (Table 5.7).

As in the draped-segmental configuration in last test results, strains in the vicinity of the anchorage of the prestressing wire do not obey the mathematical model of Chapter 2 because of the concentrations of stresses and because the prestressing force is just being introduced in the web. This implies that St. Venant's principle is applicable here. The determination of the length required for uniform distribution of the stresses is not within the scope of this research. Besides, knowledge of this length in the design is not vital, as one can always placee the anchorage in zones where bending and shear stresses are low.

It can also be noticed in the same Table 5.7 that the counteracting positive prestressing moment over the support has a low value compared to the trapezoidal configuration (Table 5.4) for the same prestressing force of 100 lb. per wire (the moment in the segmental is almost one quarter of the trapezoidal). This occurs because the secondary moment in the segmental alternative has unfavorable effects over the middle support. This secondary moment (-) has opposite sign to the basic moment and the same sign as the negative dead load moment that we are seeking to counter. Whereas in the trapezoidal configuration (Fig. 64) the secondary moment has favourable effects over the middle support because as was seen in Chapter 2, the prestressing cable located at the bottom of the girder tends to bend the girder upwards and the middle reaction prevents this lift, causing a positive moment (tension at the bottom fiber).

Even if we compare this segmental alternative with the draped-segmental wire configuration (Table 5.6) we can notice that the value of the prestressing moment over the central support in the segmental config-

Note: all measurements are in inches.

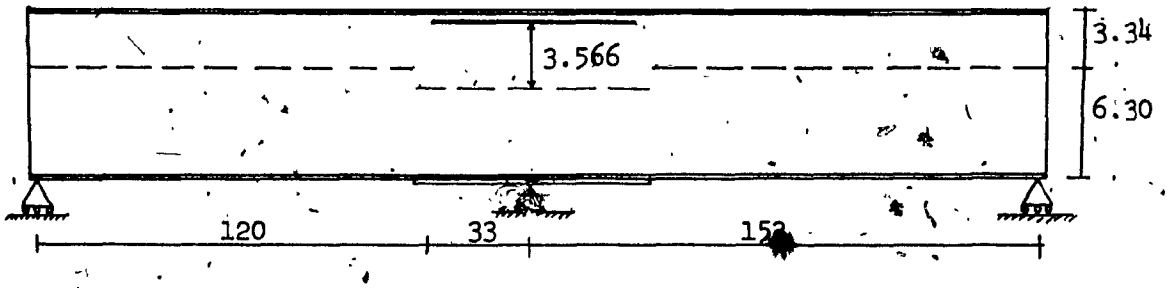

Fig. 67 — Segmental Wire Configuration.

Table 5.7 — Results for Segmental Configuration.

Location of point under study

Distance to Central Support	4.5"	13.5"	22.5"	31.5"	58.5"	85.5"	112.5"

Experimental results; prestressing force P = 200 lb

Bending strain at top (millionths)	-28.7	-30.5	-27.8	-3.5	15.2	12.1	6.9
Bending strain at bottom (millionths)	37.3	39.6	36.2	4.5	-28.7	-22.9	-13.1
Experimental moment (lb-in)	405	430	393	49	-188	-149	-85

Analytical results; prestressing force P = 200 lb

Secondary moment (lb-in)	-329	-309	-289	-269	-209	-149	-90
Basic moment (lb-in)	713	713	713	713	0	0	0
Prestressing moment (lb-in)	384	404	424	444	-209	-149	-90

Deviation of experimental results

Deviation (%)	+5.3	+6.2	-7.5	-88.9	-10.3	0.0	-4.8

uration was diminished to 77 percent of value in the draped-segmental configuration. Therefore, it can be said, that by draping the prestressing wire in the former example a smaller unfavorable secondary moment was achieved (222 lb-in against 339 lb-in in the segmental alternative).

Final conclusions cannot be drawn until a comparative study of the six alternatives under consideration is made at the end of this chapter. In such a study, the ratio, in each configuration, of the prestressing moment over the middle support to the total length of wire utilized will be compared. At that time, the efficiency of the different cable configurations are determined and recommendations for the application of the various configurations given.

5.6 Double-Segmental Wire Configuration

In this arrangement segmental wires were used at different locations maintaining a symmetrical pattern as all the cases tested before (Fig. 68). Here it was sought to place segmental wires in the zone of negative dead load moment over the middle support at the top of the girder and in zones of positive dead load moment at the bottom of the girder at the midspan. It should be mentioned that the prestressing force in the wires at the midspan (50 lb per wire) was one half of the prestressing force in the wire over the middle support (100 lb per wire).

For this arrangement, as in the previous alternatives involving segmental wires, the test results agree closely with the analytical results (Table 5.8) except in the area close to the commencement of the prestressing wire for the reasons previously explained. Unfortunately, strain could not be measured in the vicinity of the anchorage of the wires located at

Note: all measurements are in inches.

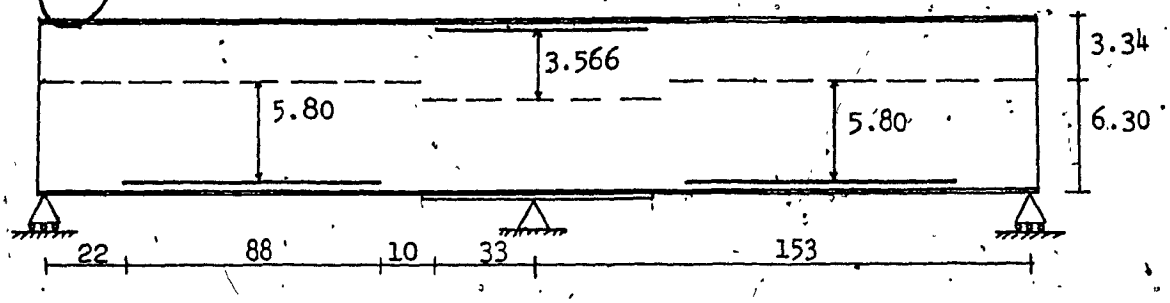

Fig. 68 — Double Segmental Wire Configuration.

Table 5.8 — Results for Double-Segmental Configuration.

Location of point under study

Distance to Central Support	4.5"	13.5"	22.5"	31.5"	58.5"	85.5"	112.5"

Experimental results; prestressing force P = 200 lb

Bending strain at top (millionths)	-63.5	-60.9	-58.3	-20.0	40.2	44.0	46.4
Bending strain at bottom (millionths)	82.5	79.1	75.7	26.0	-75.8	-83.0	-87.6
Experimental moment (lb-in)	895	859	822	282	-494	-541	-571

Analytical results; prestressing force P = 200 lb

Secondary moment (lb-in)	182	171	160	149	116	83	50
Basic moment (lb-in)	713	713	713	713	-580	-580	-580
Prestressing moment (lb-in)	895	884	873	862	-464	-497	-530

Deviation of experimental results

Deviation (%)	0.0	-2.8	-5.8	-67.3	+6.6	+8.9	+7.7

the bottom, so that the deviation observed at the top segmental wire could be ratified.

In Table 5.8, it can be seen that the addition of prestressing wires at the midspans, besides counteracting the positive moment, helps to increase the prestressing moment over the central support where it is needed the most in order to offset the critical dead load negative moment.

If we compare the results obtained in this test with those in the previous one (Table 5.7), we can see that the prestressing moment in the double-segmented configuration over the middle support is 2.3 times as large as in the former case with only a segmental wire over the central support.

However, it is not possible to formulate general conclusions about which of the six alternatives is the most appropriate one for the design of a prestressed continuous steel girder bridge because it is necessary to consider other factors involved in design such as: number of spans, length of the spans, cost of saddles, cost of prestressing cable, cost of anchorage, type of girder to be employed in the design of the bridge, type of deck and perhaps availability of materials. Therefore, it is up to the designer to decide which cable configuration is best suited to the particular conditions of the bridge project.

5.7 Comparison of Results and Conclusions

It was seen in the recent tables for the six different cable configurations under study that the resulting prestressing moment has such a different value in each configuration even with equal prestressing force in all the wires that we realize that the cable configuration is a

very important factor involved in the design of a prestressed girder bridge. We also noticed that the length of wire employed in each configuration was different for each case. The trapezoidal configuration was the alternative that required the greatest length of wire but at the same time this was the alternative where the largest prestressing moment over the middle support was obtained.

However, the comparison of the magnitude of prestressing moments does not give a clear criterion for choosing the most suitable cable configuration in the design of a prestressed girder bridge. Therefore, we have to compare our six cable configurations on a different basis. This comparison is effectively achieved with the help of the ratio between the prestressing moment at the middle support to the length of the cable. This ratio will be called in future discussions the "coefficient of efficiency" (C.E.).

In this way, we will be able to judge which cable configuration produces the best results in counteracting the critical negative dead load moment with the least of prestressing cable length.

Of course it is possible to have cases of girder bridge design where the positive moment is of importance but more emphasis has been placed on counteracting the negative moment because in most girder bridge projects, it is the negative moment that governs the design.

In Table 5.9, the coefficient of efficiency (C.E.) for the six cable configurations is computed for a point at the central support and for a point at the midspan located 85.5 in. from the central support.

We can see in the Table 5.9 that the cable configuration most suitable for counteracting the negative moment is the draped-segmental one but at the same time this is the configuration that counteracts the

dead load positive moment the least efficiently. It should be remarked that this prestressing moment existing at the midspans is just the secondary moment produced by the prestressing wire over the middle support since there is no prestressing wire at the midspan in the draped-segmental configuration (Fig. 66).

It can also be seen in the same Table 5.9 that even though the parabolic and trapezoidal configurations have the highest prestressing moment at the middle support they have a relatively low coefficient of efficiency (C.E.). This is because they utilize a great length of prestressing wire.

The double-segmental arrangement (Fig. 68) has a high coefficient of efficiency (C.E.) for both locations under consideration but the number of anchorages required is greater than in any other configuration, a factor that diminishes the appeal for this alternative in a prestressed girder bridge design.

From the comparison of results presented in Table 5.9, it can be concluded that in a prestressed bridge project where the negative dead load moment governs the design, the draped-segmental configuration gives the optimal results because it gives relatively high prestressing moment over the middle support with a very short length of cable. This solution is also recommended because it requires a set of only two saddles for each prestressing cable against six in the parabolic case. The number of anchors required for the draped-segmental solution is the same as in any other configuration.

Fig. 69 illustrates the way the draped-segmental configuration would be applied in the solution of a multi-equal-span prestressed girder bridge.

Table 5.9 — Comparison of Results for the Six Configurations.

CONFIGURATION	LENGTH	Negative Moment over Central Support			Positive Moment at 85.5 in.		
		PREST. MOMENT	C.E.	%	PREST. MOMENT	C.E.	%
Parabolic	307.75	1451.0	4.72	67.4	-831.5	2.70	83.7
Trapezoidal	309.46	1544.6	4.99	71.3	-805.2	2.60	80.6
Triangular-Trapez.	307.65	1028.2	3.42	47.8	-957.9	3.11	96.5
Draped Segmental	70.26	491.6	7.00	100.0	-97.8	1.38	42.8
Segmental	66.00	374.6	5.68	81.0	-149.4	2.26	70.1
Double Segmental	154.00	901.0	4.85	83.6	-497.1	3.23	100.0

$$C.M. = \frac{\text{Prestressing Moment}}{\text{Length of Prestressing Cable}}$$

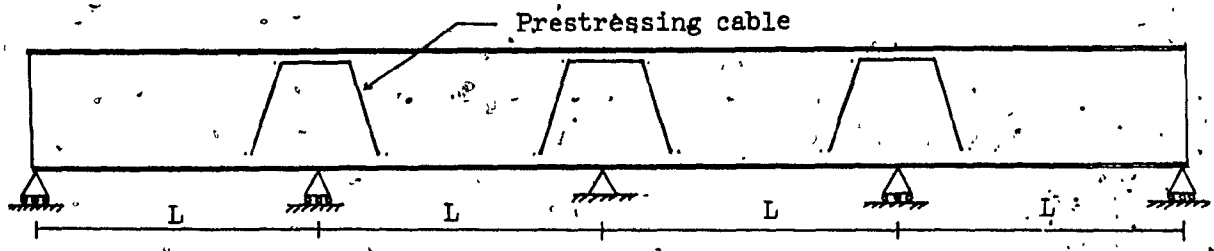

Fig. 69 — Prestressed Solution for a Multi-Span Girder Bridge Using Draped Segmental Cable.

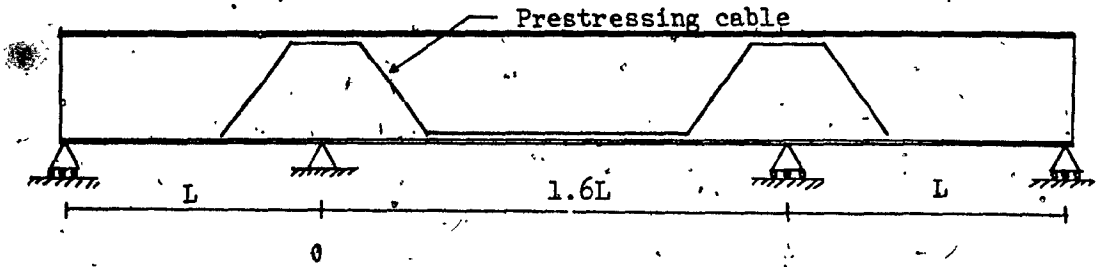

Fig. 70 — Prestressed Solution for an Unequal Three-Span Girder Bridge Using a Trapezoidal Cable Configuration.

In the case of bridges with unequal spans where the positive dead load moment in the longest span is almost as high as the negative dead load moment over the adjacent supports, the trapezoidal configuration is recommended (Fig. 70). If the positive moment has a higher value, then it will be necessary to help the trapezoidal configuration with a segmental cable along the zone of positive moment. Fig. 70 shows how the trapezoidal configuration would be applied in a three-unequal-span prestressed continuous girder bridge.

As a part of the conclusion, it can also be said that in projects in which the prestressing cable in the external face of the girder webs is not desirable for aesthetical reasons, then, the utilization of prestressing cables can be placed exclusively in the internal face of the girder webs, so that the prestressing cable remains hidden.

It can also be added here that the parabolic configuration, because of the great number of saddles (cable supports) required, is not advisable since similar results can be achieved with the trapezoidal configuration that utilizes a smaller number of saddles.

CHAPTER 6

PRACTICAL APPLICATIONS

The use of prestressing of steel structures is not widely used in North America. This probably stems from the fact that prestressed steel has not been commercialized and therefore contractors believe that the technique does not offer any economical advantage to be worth even studying the utilization of prestressed steel structures as an alternative in the preliminary phase of design.

So far, in the few existing applications of prestressed steel, the use of commercial prestressing systems for concrete has proved to be feasible[3,7,16,17] and some savings were achieved. It is believed that not until a prestressing manufacturing company starts producing a prestressing system specially conceived for steel structures, that bridge designers and contractors will advocate the use of prestressed steel to any large degree. In the meantime, the available commercial prestressed concrete systems will have to be adapted in the design of new bridges involving prestressed steel.

In this research work a comparative design of a steel bridge using the conventional approach and the prestressed approach was performed. In the first part, the bridge was designed by the conventional approach using non-prestressed plate girders. In the second part prestressing was introduced and the cross-sectional area was reduced in order to have the cross-

section working at full capacity. Substantial decrease in weight was achieved by prestressing and the depth of the cross-section was appreciably reduced.

In this example, a trapezoidal configuration was utilized. The reason of this choice was to achieve savings of material all along the girder. As known from the conclusions in the last chapter (Fig. 77), the trapezoidal configuration gives high prestressing moments both over the central support and the midspans and therefore both positive and negative dead load moments are counteracted efficiently.

The geometry of the alternatives for the bridge under study are presented in Fig. 71. The location of the prestressing cable in the prestressed alternative is shown as well. The type of live load used in the design was the AASHO[15] equivalent truck load HS-20.

The cross-section was made up of two plate girders working in conjunction with an orthotropic steel deck with closed ribs. Fig. 72 shows the cross-sections used in the conventional alternative and Fig. 73 shows the ones used in the prestressed solution of the bridge.

In the prestressed alternative ten one-inch diameter high-strength prestressing cables were used. The location of the cables is presented in Fig. 71.

The total weight of the bridge for the non-prestressed solution was found to be W_{non} = 1121 Kips, and for the prestressed alternative was W_p = 946 Kips. The total length of cable required in the prestressed design was L = 5137 ft. weighting W_c = 10.5 Kips. It can be seen from figures above that a saving of 175 Kips of steel was achieved in the prestressed design which represents a reduction in weight of 15.6 percent or put it in a different way, the conventional design was 18.5 percent heavier than the

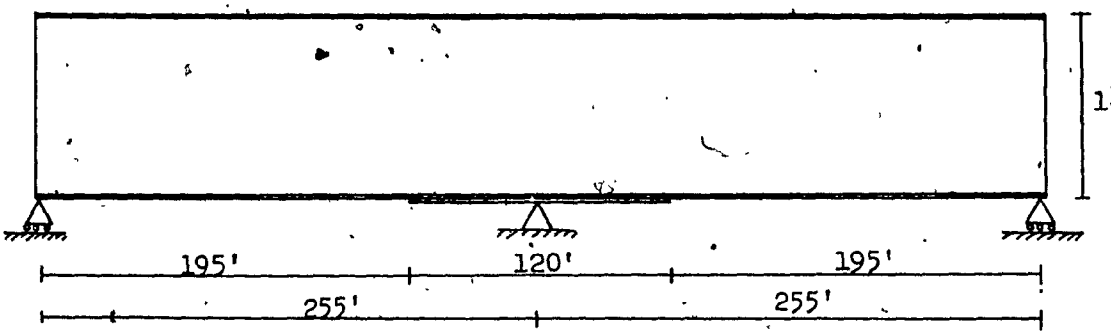

Geometry of the Conventional Solution.

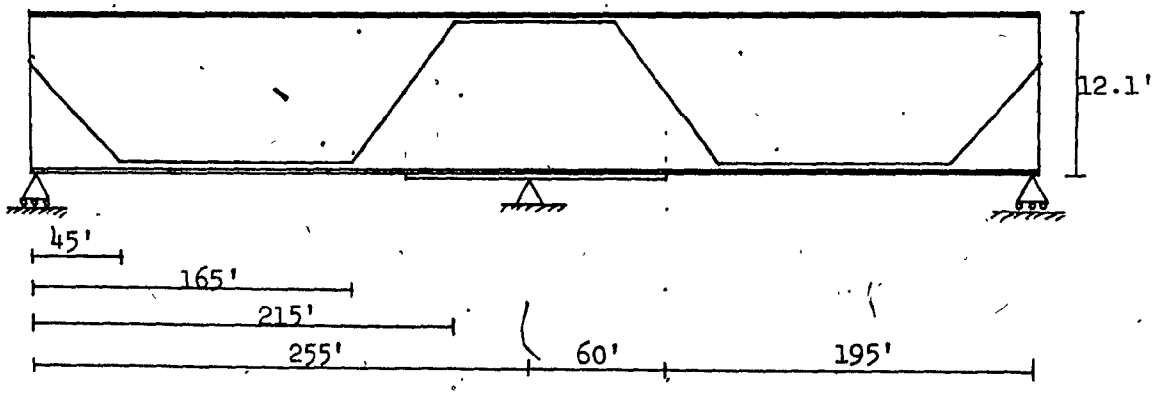

Geometry of Prestressed Solution.

Fig. 71 — Geometry of Conventional and Prestressed Solutions for a Continuous Two Span Steel Bridge.

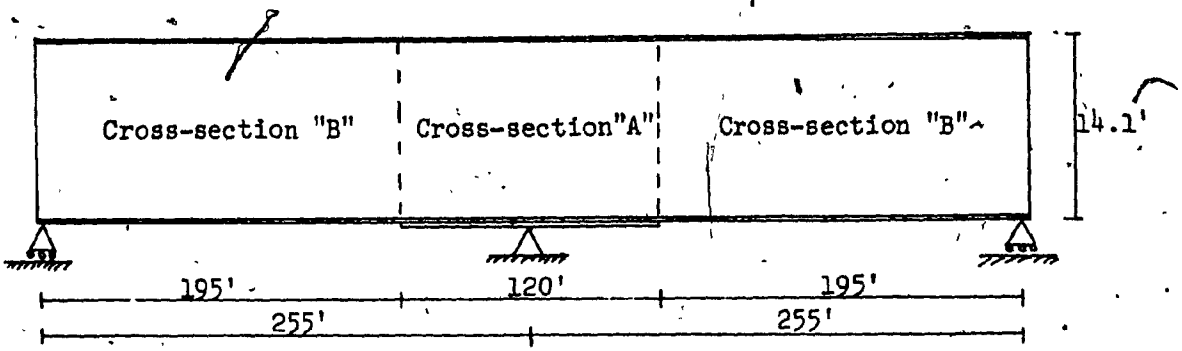

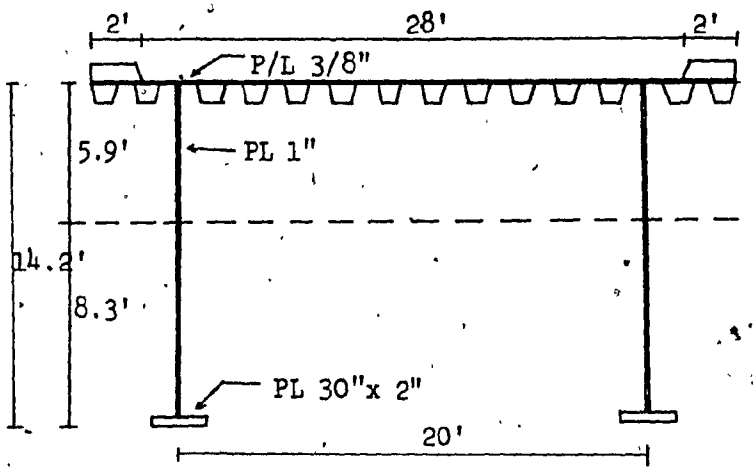

Cross-section "A"

Properties:
A = 691.7 in^2
I_x = 3,114,225 in^4
S_t = 43,686 in^3
S_b = 31,428 in^3

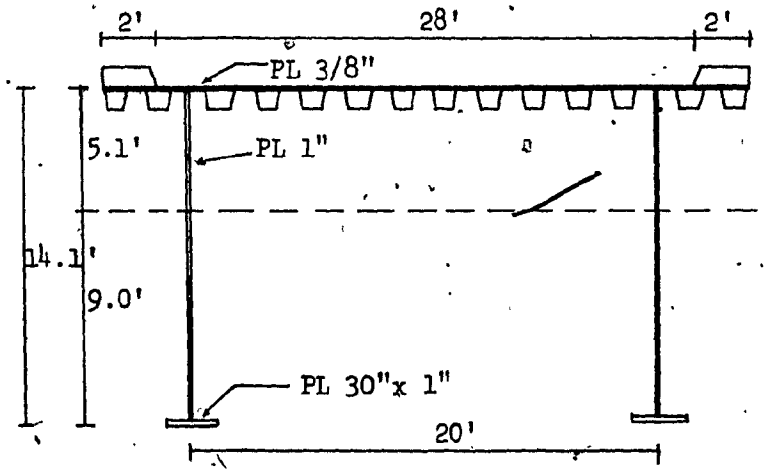

Cross-section "B"

Properties:
A = 631.7 in^2
I_x = 2,475,646 in^4
S_t = 39,980 in^3
S_b = 23,039 in^3

Fig. 72 — Cross-Sections in Conventional Alternative.

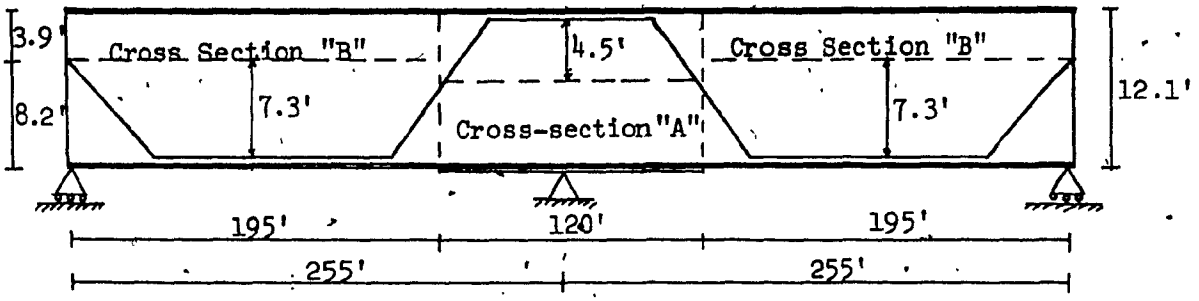

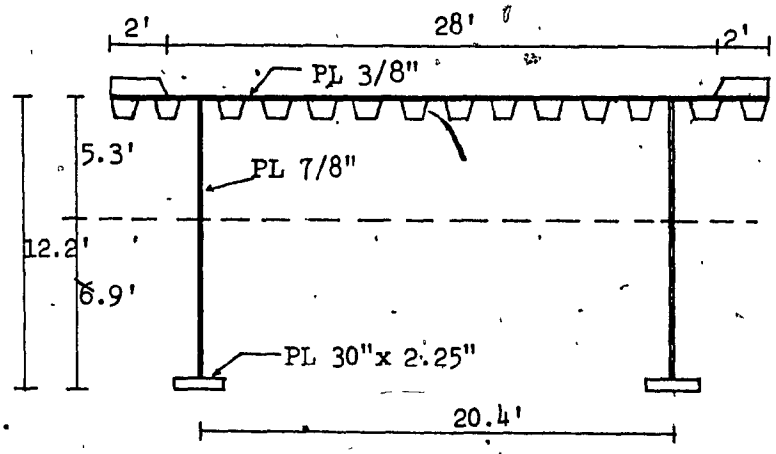

Cross-section "A"

Properties:

$A = 601.2\ in^2$
$I_x = 2,162,172\ in^4$
$S_t = 33,764\ in^3$
$S_b = 26,180\ in^3$

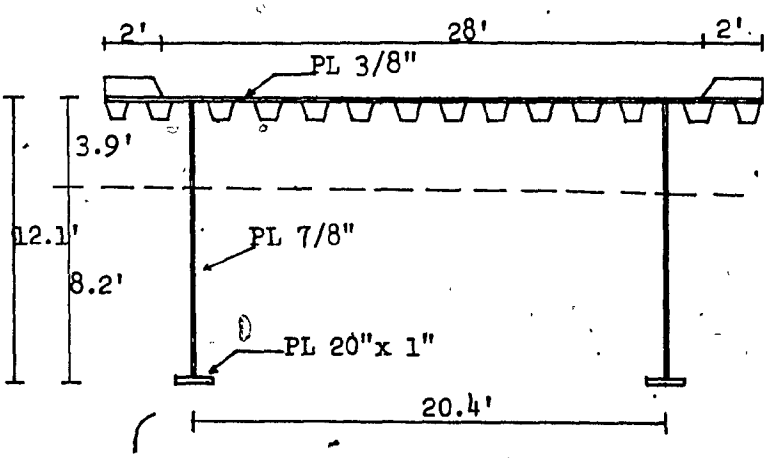

Cross-section "B"

Properties:

$A = 527.7\ in^2$
$I_x = 1,446,352\ in^4$
$S_t = 30,941\ in^3$
$S_b = 14,664\ in^3$

Fig. 73 — Cross-sections in Prestressed Alternative.

prestressed alternative.

It can be concluded that substantial reduction in weight can be achieved in a prestressed steel girder bridge design and that appreciable reduction in the depth of the girder can be made possible by introducing prestressing to the conventional girder bridge design. These two factors make the use of prestressed steel appealing in the design of new bridge projects.

As for the anchorage of the prestressing cables it is suggested to adapt in the prestressed steel bridge any of the available commercial post-tensioning anchorage system which best suit the conditions of the project. The Post-Tensioning Manual[18] describes the most usual anchorage systems used in today's post-tensioning concrete design.

Fig. 74 shows the anchorage systems deemed to be adaptable to a prestressed steel bridge project. It can be seen that these anchorage systems are made of a steel plate to which the prestressing cable is anchored by means of conical wedges that grip the cable into a hole in the steel plate after tension is applied to the cable. The connection between the anchorage system and the steel girder would be accomplished by welding the steel plate of the anchorage to properly stiffened support elements provided in the steel girder.

It is hoped that the prestressed steel girder bridge technique will soon gain some acceptance among contractors and designers and then a more suitable prestressing system will be developed by a prestressing firm in order to make popular the use of prestressing in steel bridges in North America.

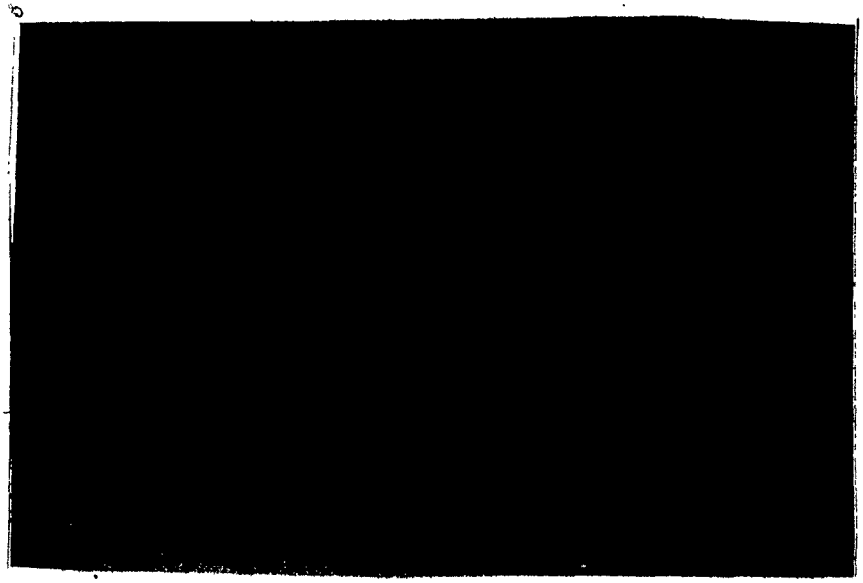

Atlas Prestressing Corporation System

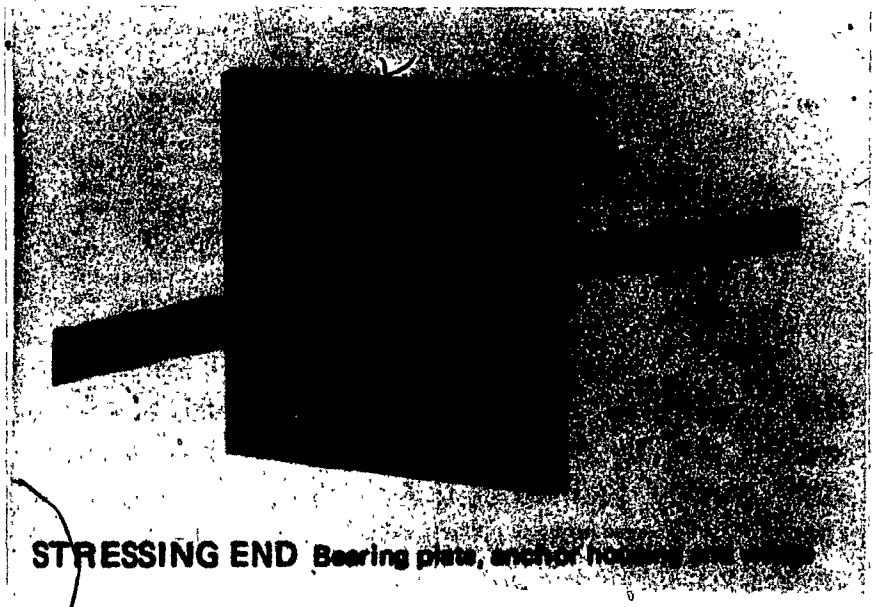

Stresssteel Monostrand System

Fig. 74 — Suggested Anchorage Systems to be Adapted in a Prestressed Steel Girder Bridge Project.

REFERENCES

1. Wenk, H. "Reconstruction of the Western Lane of the Motor Road Bridge at Mountabaur", Demag News, No. 137, pp. 1-9.

2. "Willstress System Experimental Bridge", Acier Stahl Steel, No. 2 - 1961, pp. 80-83.

3. Finn, E.V., Needham, F.H. "The Use of Prestressed Steel in Elevated Roadways", The Structural Engineer, Jan. 1964, pp. 5-18.

4. "Prestressed Steel Makes a Bridge", Engineering News Record, Nov. 1964, pp. 24-27.

5. "Prestressing Steel Stringers Reduces Bridge Weight by 25%", Engineering News Record, Oct., 1961, pp. 32-33.

6. Hadley, H.M., "Steel Bridge Girders with Prestressed Composite Tension Flanges", Civil Engineering, ASCE, May 1966, pp. 70-72.

7. "Mexico Opens New Rail Line to the Pacific", Engineering News Record, Dec. 1961, pp. 30-34.

8. Khachaturian, N., Gurfinkel, G., "Prestressed Concrete", McGraw Hill, 1969.

9. Knee, D.W. "The Prestressing of Steel Girders", The Structural Engineer, October 1966, pp. 351-353.

10. Tochaček, M., Amrhein, F.G., "Which Design Concept for Prestressed Steel?" AISC Engineering Journal, Jan. 1971, pp. 18-30.

11. Reneker, W.D., Ekberg, C.E. "Flexural Fatigue Tests of Prestressed Steel I-Beams", Journal of the Structural Division, Proceedings ASCE, April 1964, pp. 131-151.

12. Kinney, J.S. "Indeterminate Structural Analysis", Addison-Wesley Pub. Co., 1957.

13. Lazar, B.E. "Model Investigations of Cable Stayed Bridges", Thesis, Sir George Williams University, Faculty of Engineering, August 1970, pp. 17-30.

14. Rohm and Haas. Plexiglas Acrylic Plastic Sheet, Mechanical Properties, PL-783c, June 1973, Philadelphia, Pa.

15. "Standard Specifications for Highway Bridges", The American Association of State Highway Officials, Eleventh Edition, 1973.

16. "Prestressed Steel Girders Carry Prestressed Concrete Floor", Engineering News Record, March 1964, pp. 24-25.

17. "Prestressed Steel Makes a Bridge", Engineering News Record, Nov. 1964, pp. 24-26.

18. Post-tensioning Institute, "Post-tensioning Manual", Second edition, first printing, 1976, pp. 37-132.

19. Subcommitee 3 on Prestressed Steel of Joint ASCE-AASHO, Committee on Steel Flexural Members, "Development and Use of Prestressed Steel Flexural Members", Journal of the Structural Division, Proceedings ASCE, Sept. 1968, pp. 2033-2060.

20. Zielinski, Z.A., Przeprawy tras Swietokrzyskiej i Lazienkowskiej - Praca 24 (Swietokrzyska and Lazienkowska River Crossings, Project 24) Inzynieria i Budownictwo No. 11/12/1961 - Description of awarded competition design of two long span bridges, (in Polish).

21. Zielinski, Z.A., O sprezeniu konstrukcji stalowych (Prestressed Steel Structures), Inzynieria i Budownictwo, No. 7/1954, (in Polish).

22. Zielinski, Z.A., Dwa przklady zastosowania w Polsce sprezania do wyzmocnienia istiejacych konstruckji (Two examples of uses of post-tensioning for strengthening of existing structures in Poland), Inzynieria i Budownictwo, No. 1/1956, (in Polish).

23. Douglass, M.M. "Structural Analysis", Lecture Notes, 1976, Concordia University, Montreal.

24. Troitsky, M.S. "Cable-Stayed Bridges: Theory and Design", London, Crosby Lockwood Staples, 1977.

25. Skaff, S.I., "Prestressing in a two-Bay Frame with Pinned Supports", Master's thesis, Concordia University, Montreal, Nov. 1972.

26. Vaugham, J. "Strain Measurement", Bruel & Kjaer, October 1975.

APPENDIX A
DESIGN OF THE PROTOTYPE

A two span continuous prestressed steel girder for two traffic lanes was designed in order to be used as a prototype for the design of the plexiglas model.

The bridge is prestressed by means of 10 one-inch diameter high strength cables with a total prestressing force of P = 1344 Kips. The arrangement given to the prestressing cable has a trapezoidal shape as shown in Fig. 75.

The design criterion followed was that of superimposing all the stresses due to the different loads acting on the bridge (prestressing included) and then checking that the total stresses were within the limits prescribed by AASHO.[15] Different cross-sections were tried in order to find an optimum cross-section working at full capacity in zones of maximum positive and negative moments. The cross-sections utilized are shown in Fig. 76 along with their properties. These cross-sections would be overstressed by about 20% if the prestressing had not been introduced in the design.

An orthotropic steel deck working in conjunction with the plate girders was used. The deck ribs are closed type ribs as shown in Fig. 76. The floor beams in the deck system are spaced every 15 feet.

AASHO[15] specifications were followed in the design of all the components of the bridge.

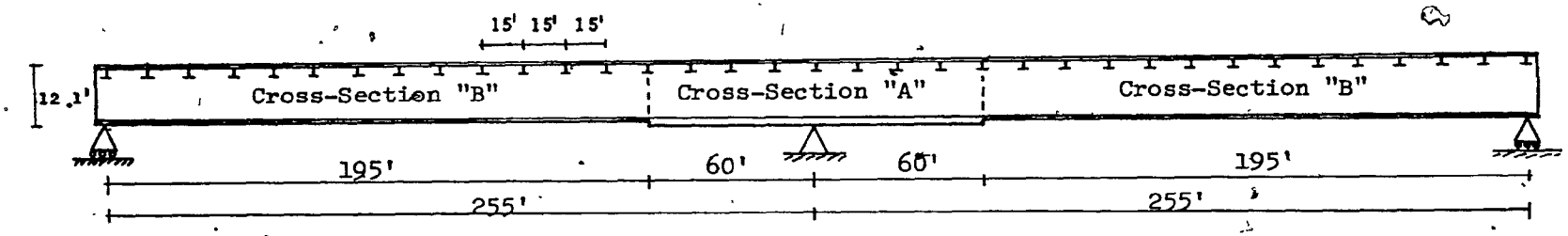

Elevation

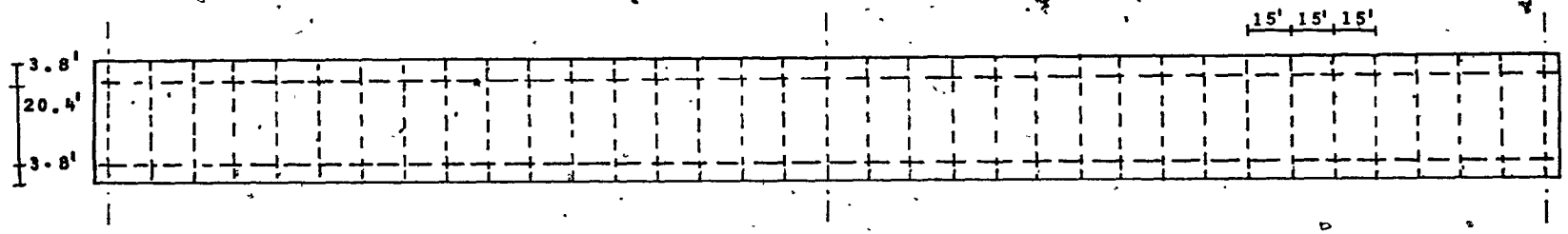

Plan

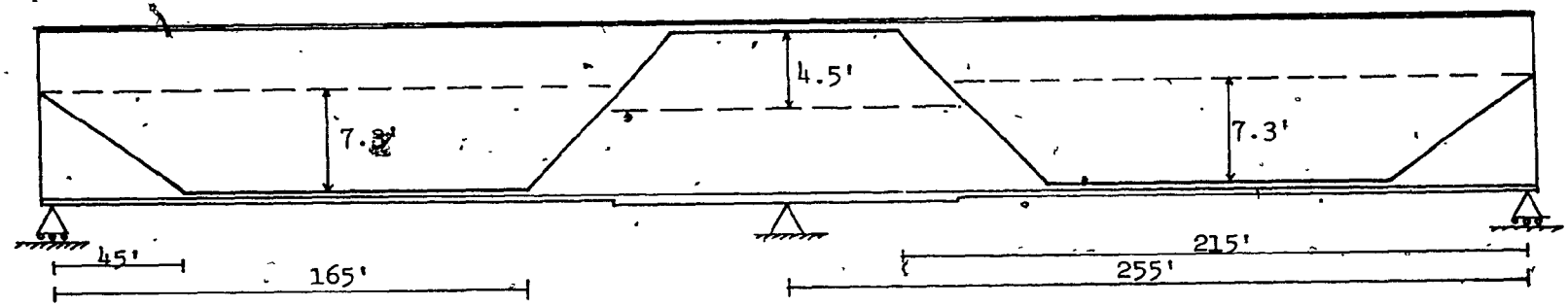

Elevation (shape of the prestressing cable).

Fig. 75 — Geometry of the Bridge.